Zeitschrift: IABSE reports = Rapports AIPC = IVBH Berichte
Band: 81 (1999)

Rubrik: Session B: Material and construction

Concrete Model Code for Asia : Report of the Working Group on Materials and Construction

Somnuk TANGTERMSIRIKUL
Department of Civil Engineering,
Sirindhorn International Institute
of Technology, Thammasat
University, Patumthani, Thailand

Anura NANAYAKKARA
Department of Civil Engineering,
University of Moratuwa,
Maharagama, Sri Lanka

Shigemitsu HATANAKA
Department of Architecture,
Mie University Mie, Japan

Boonchai STITMANNAITHUM
Department of Civil Engineering,
Chulalongkorn University,
Bangkok, Thailand

Takafumi NOGUCHI
Department of Architecture,
University of Tokyo,Tokyo, Japan

Yew Chaye LOO
Faculty of Engineering and Applied Science,
Griffith University, Queensland, Australia

Summary

This paper summarizes the activities of a working group for materials and construction set up under the International Committee on "Concrete Model Code for Asia". The activities commenced from the survey on situation of construction industry, concrete technology and concrete code in many countries in Asia. Then, discussion on the proper characteristics of the Model Code for Asia, the drafting of a framework and the drawing up of a tentative draft of the Model Code was conducted. Considering the features on which special cares should be taken in making an unified model code in the region, the Model Code was characterized by the conceptual phrases and divided into 6 chapters, and the table of contents of each chapter was arranged in similar manner except for Chapter 1 General and Chapter 2 Basic Requirements. The code was drafted into 3 levels of document. Level 1 document provides all essential requirements for each chapter whereas detail explanations are provided as commentary in Level 2 document. Level 3 document will be show examples of code application.

1. Introduction

1.1 Background

Concrete has been playing and will do a major role as an essential material for construction in Asia. As the global environmental problems and economic crisis come into Asian concern, it is inevitable to reduce the exploitation of natural resources, reduce the disposal of waste from

removed structures and reduce the cost from repair and maintenance of the infrastructures. While concrete is an excellent material considered useful for structures, it has a disadvantageous point of difficult recyclability and not being maintenance-free. It is, therefore, necessary to build concrete structures with high durability. With the recent active inter-activity in construction industries in Asia as a background, Japan Concrete Institute set up a Research Committee on "Concrete Model Code for Asia" in 1992 to study the present situation of construction industry, concrete technology and code used in different countries, and to carry out some preliminary groundwork towards the establishment of the Code [1]. After two years of the survey on the above subjects, a framework of Concrete Model Code for Asia was proposed in Tokyo in April 1994 by the committee. Then in December 1994 during the Bangkok meeting, three working groups namely Design WG, Materials & Construction WG and Maintenance & Management WG were formed. The firstly formed working group on materials and construction first consisted of ten members from Australia, Indonesia, Japan, Philippine, Sri Lanka and Thailand. The working group has been discussing on policy, basic idea, format, etc. of the Code as well as drafting and revising the Code since then. During drafting and revision, comments were also obtained from respondents from China, India, Singapore, etc.

1.2 Performance-Based Concept of the Code

The changes in the codes from prescriptive specifications to performance-based provisions are currently proceeded around the world. This concept is adopted to the model code for Asia too [2,3,4]. According to the performance-based code, the concrete structure are supposed to be designed based on required performance of the concrete structure throughout the service life. The structure and components are designed to fulfill their functions with respect to load carrying capacity, stability, serviceability and durability throughout their design life. The materials are evaluated by the resisting performance to the chemical, physical, mechanical, biological attacks as well as their combination attack regarding the durability, and are evaluated by mechanical properties such as strength and the modulus of elasticity relevant to the stress in structural aspect. In regard of the durability of concrete, there seem to be few properties recognized as performance or few test methods are established as standards for the recognized performance, and so such specifications as water to cement ratio, cement content, etc. are adopted as indexes of resistant properties at present. Since the water to cement ratio that develop the identical resistant property varies with the proportion of the ingredients, types of cement and admixtures used, specifying water to cement ratio may not lead to the concrete as required in the performance-based code. Accordingly, the performance-based model code requires to make close connections between actions and concrete resistant properties and to prescribe the resisting performance according to the required life. On the other hand, concrete cover is determined taking both the environmental conditions and the resisting performance of concrete into consideration. It is determined depending on not only the durability but also the fire resistance, the safe transmission of bond forces, the adequate compaction of concrete, etc.

2. Activities of WG on Materials and Construction

2.1 Survey on Concrete in Asia

Investigations in Asian countries were made by asking each member in the member countries to prepare a report. The reports included both the state of code and standard specification relating to concrete works used in the country and the circumstances of construction industries such as the share in GDP or GNP of construction, the cement production and consumption, the materials used, the role of professional bodies, the consultants and contractors and the automation. According to the reports received from the members from different countries, the followings are clarified as features on which special cares should be taken in making an unified model code in the region.

- Most countries have, in general, adopted the available codes such as British and ACI codes with certain modifications to suit the local conditions.
- There are wide differences in the climatic and environmental conditions.
- There are wide differences in the construction industry, level of technologies, labor circumstance and types of materials.

Due to the mentioned differences among Asian countries, it was decided that the code would comprise of 3 document levels. Level 1 is the main text which includes the fundamental provisions prescribing only the performance and functional requirements. Level 2 is the descriptive details of the main text in commentary form. Level 3 is the example of adoption of the model code to national code, depending on situation of each country.

2.2 Format of Part 2: Materials and Construction

The Model Code for materials and construction was divided into 5 chapters; 1) General, 2) Essential Requirements, 3) Formwork, 4) Reinforcement, 5) Concrete 6) Prestressed Concrete. Each table of contents for Chapter 3, 4, 5 and 6 were arranged to have the similar composition as listed below.

1. Scope
2. Basic requirements
3. Materials
4. Workmanship
5. Quality control and assurance
6. Records

2.3 Progress of Drafting Part 2 : Materials and Construction

The first draft of "Chapter 4 Concrete" was presented at Jakarta meeting in March 1996 by Thailand group and a discussion was held focusing on performance-based provision. The revised Chapter 4 and the first drafts of "Chapter 2 Formwork" and "Chapter 3 Reinforcement" were circulated at Dalian meeting in October 1996. Many arguments were presented about the meaning of "Model" and a discussion was held about the format of the code. At the Hyderabad meeting in March 1997, the first draft of Chapter 5 Prestressed Concrete was circulated together with the first revision of Chapter 2, 3 and the second revision of Chapter 4. At the Haki meeting in August 1997, the revised versions of Chapter 3, 4, 5 and 6 were discussed for preparation of

the final revision ready for the working group meeting in EASEC-6, Taipei whereas Chapter 1 and 2 were assigned to be drafted. At EASEC-6, Taipei in January 1998, the level 1 and level 2 drafts were proposed and discussed. It was proposed that the test methods should be included and some example of level 3 document should be given in the next meeting in Singapore. In August 1998, the meeting in Singapore was held at the National University of Singapore. The revised level 1 and level 2 drafts including the test methods were discussed. It was proposed here that the level 3 document be introduced at the IABSE Colloqium, Phuket, Thailand in March 1999.

3. Content of Draft of Model Code for Asia

The draft of "Materials and Construction" in Model Code for Asia is briefly introduced below. The introduced draft includes provisions for materials, workmanship, quality control and assurance and records of works for formwork, reinforcement, concrete and prestressed concrete. All 3 levels of document consist of the same chapters and subtitles.

Chapter 1 General

This chapter gives the scope of the code which states the attempts to introduce a guideline for being adopted to establish the national code based on local condition of each country in Asia. The content of this chapter also includes definitions of terms, notations and units used in the model code.

1.1 Scope
1.2 Definition
1.3 Notation
1.4 Units

Chapter 2 Essential Requirements

This chapter explains the basic requirements for materials, construction team and workmanship, quality control and assurance and records.

2.1 General
2.2 Materials
2.3 Construction Team and Workmanship
2.4 Quality Control and Assurance
2.5 Records

Chapter 3 Formwork

3.1 Scope
3.2 Basic requirements for formwork
3.3 Materials
3.4 Design of formwork
    3.4.1 Loads in formwork design
    3.4.2 Deformation
3.5 Workmanship
    3.5.1 Erection of formwork
    3.5.2 Formwork removal
3.6 Quality control and assurance
3.7 Records

Chapter 4 Reinforcement

4.1 Scope
4.2 Basic requirements for reinforcement
4.3 Materials
    4.3.1 General
    4.3.2 Material properties

6.5.1 Quality control and inspection during concrete casting
6.5.2 Quality control and inspection during prestressing transfer
6.5.3 Quality control and inspection during transportation and erection
6.6 Records

4. Concluding Remarks

The unsettled subjects are still left regarding some standard test methods for the materials and some quantified specification of the performance of concrete for level 3 document.

5. References

1. Research Committee on Concrete Model Code for Asia (1994), Report of Research Committee on Concrete Model Code for Asia, Japan Concrete Institute

2. Noguchi, T., Yamazaki, J., Uomoto, T. and Ohtsuka, K. (1995) "Model Code for Materials and Construction of Concrete Structures," *Proceedings of the EASEC-5, Building for the 21st Century*, Gold Coast, Australia, July 25-27, Vol. 3, pp.2345-2350

3. Noguchi, T., Tangtermsirikul, S., Nanayakkara, A., Austriaco, L. R. and Loo, Y. C. (1997) "Model Code for Concrete Materials and Construction Ensuring High Durability of Concrete Structures," *Proceedings of the International Conference on Maintenance & Durability of Concrete Structures*, March 4-6, JNT University, Hyderabad, India, pp.174-179

4. Tangtemsirikul, S., Noguchi, T., Nanayakkara, A., Tanzo, W., Austriago, L. R. and Loo Y. C. (1998), "Report of the Working Group on Materials and Construction (Concrete Model Code for Asia)", *Proceedings of the 6th East Asia-Pacific Conference on Structural Engineering & Construction*, 14-16 January 1998, National Taiwan University, Taipei, Taiwan, pp. 767-772

Alternatives for River Sand

S.M.A. Nanayakkara
Senior Lecturer
University of Moratuwa
Sri Lanka

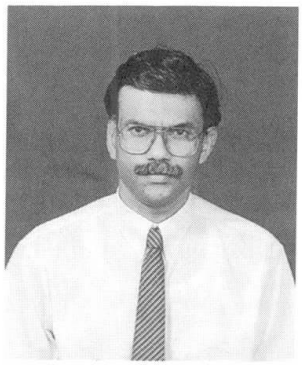

S.M.A. Nanayakkara, born in 1958 received his B.Sc. Eng. Degree from University of Moratuwa in 1982 and D.Eng from University of Tokyo in 1990. He is a Senior lecturer attached to the Dept. of Civil Engineering, University of Moratuwa.

Summary

Offshore sand, dune sand and land based sand have been identified as alternatives for river sand. Experimental investigations have been carried out to find their physical and chemical properties and properties of concrete made with these alternatives. It was found that all the offshore sand samples tested comply with the chloride limitation for normal reinforced concrete with OPC. However, it does not comply with that for prestressed concrete. In addition, it was found that chloride content of dune sand is extremely low and can be used for concrete without washing. The compressive strength results show that the concrete made with all three alternatives is as good as the concrete made with river sand.

1. Introduction

River sand is the most widely used fine aggregate in Sri Lanka. The average annual demand for sand is around 5 million cu.m and by the year 2000, the demand would be 9.6 million cu.m[1]. Due to large scale and uncontrolled river sand mining, there are environmental problems such as riverbank collapses, salt-water intrusion and coastal erosion. Because of these environmental problems, there is a necessity to reduce river sand mining especially at harmful locations. In order to restrict river sand mining, it is necessary to introduce some alternatives for river sand to meet the demand for sand. A few river sand alternatives such as offshore sand, dune sand, quarry dust and land based sand have been identified and some of these are already in use for various purposes. Out of the four identified alternatives, the quarry dust is widely used as a partial replacement of sands in concrete and other various applications. The properties of quarry dust and its performance are known to a greater extent. However, the other three alternatives are less known in Sri Lanka as alternatives for river sand specially for concrete. Therefore the experimental investigation is mainly focused on properties of offshore sand; dune sand and land based sand and their suitability for concrete.

2. Experimental Investigation

The physical properties of sand such as specific gravity, particle shape, particle size distribution, fine dust content were determined based on relevant British Standards[2]. The following tests were also carried out, based on relevant British Standards.

1. *Shell content*: BS 812:Part 106:1985 [3] describes the method for determining the shell content in coarse aggregate. This method was adopted for shells greater than 5 mm. Shell content in fine aggregate was determined by modifying the method given in the literature by Chapmen et al[4]. In this method, a representative oven dry sample of about 50 g is accurately weighed and standard hydrochloric acid solution is added to dissolve shells (calcium carbonate). Addition of hydrochloric acid is continued until there is no further reaction. The residue of the sand sample is carefully washed and the oven dried weight is obtained. The percentage loss of weight of the sample indicates approximately the shell content in the sample.
2. *Salt contamination (water soluble chlorides)* : Chloride content was measured using a method for determination of chloride content in drinking water [5]. In the case of offshore samples, a wet sample was used after draining the excess water under gravity to obtain the highest possible chloride content. About 500 g of the sample was weighed and placed in a bottle; 500 ml of distilled water was added and the sample was agitated in a shaker for 24 hrs. The filtrate was tested to determine the chlorides in the sand sample.
3. *Compressive strength of concrete*: Since the main objective of the investigation is to find out the suitability of the selected alternatives for concrete, properties of concrete made with offshore sand, dune sand and land based sand were obtained. The standard mix proportion for grade 20 concrete given in ICTAD specifications[6] was used in this test. The slump and compressive strength at 7 days and 28 days were obtained.

3. Sand Samples

3.1 Offshore sand

As an island surrounded by the sea, Sri Lanka has access for considerable amounts of offshore sand deposits, existing mainly in the continental shelf area. In Sri Lanka, offshore sand has been used in beach nourishment and land filling work. Offshore sand samples were collected from locations in the western reaches of the continental shelf close to Ratmalana, Wadduwa and Negombo. These locations are about 1 km to 6 km from the shoreline and at a depth of about 14 m. Some samples were collected from Muthurajawela area since offshore sea sand was used to fill that area.

3.2 Dune sand

In Sri Lanka, dunes exist along the north-west coast between Chilaw and Kalpitiya, across Mannar island and the Pooneryn peninsula, along the north-east coast between Pulmoddai and Point Pedro and in the south-east coast from east of Ambalantota to Timitar[7]. Six dune sand samples were collected from Puttalam and Chilaw Districts.

3.3 Land based sand

Soil samples were collected from the Kosgama, Puwakpitiya, Bulathsinhala and Horana areas. Sand was extracted from these soil samples by washing manually. A steel wire mesh of 0.3 mm was used to extract sand from the soil in case of soil from Kosgama and Puwakpitiya and washed water was allowed to settle in order to obtain the clay. Sand extracted from these two soil samples were tested to obtain physical and chemical properties as well as the properties of concrete made with those sands. Sand from other soil samples was extracted using a 0.075 mm square mesh and only the composition of soil and particle size distribution of sand were obtained.

4. Test Results

4.1. Specific gravity and particle shape

Table 1 gives the specific gravity of the offshore sand, dune sand and land based sand samples tested. It can be seen that the specific gravity of dune sand is higher than that of the offshore sand and land based sand because dune sands are composed of quartz grain with a relatively high proportion of heavy minerals[7]. The water absorption is fairly low except for one land based sample. Although there is no clear-cut relation between the strength of concrete and the water absorption of aggregate used, the pores at the surface of the particle affect the bond between aggregate and the cement paste, and may thus exert some influence on the strength. And also it can be seen from the results given in Table 1 that the clay, silt and dust content(i.e. amount of materials passing through 75μm sieve) of offshore sand as well as dune sand is less than 3%, which is the limit given in BS 882 [8] for clay, silt and dust content in sand. Clay, silt and dust content of land based sand samples depends on the efficiency of washing. Since thorough washing was carried out, clay, silt and dust content in washed land based sand is very low.

Table 1 - Physical properties of river sand alternatives

Sample		Specific gravity (SSD)	Water absorption (%)	Clay, silt and dust content(%)	Particle shape
Offshore sand	Muturajawela	2.68	0.30	-	Rounded Irregular
	Ratmalana	2.75	0.20	0.42	
	Wadduwa	2.66	0.14	0.47	
	Negombo	2.71	0.10	0.39	
Dune Sand	Daluwa	2.78	0.23	0.3	Irregular
	Sinnapadu	2.89	0.29	0.64	
	Chilaw	2.78	0.32	0.9	
Land based sand	Kosgama	2.68	0.78	1.6	Angular
	Puwakpitiya	2.67	0.12	0.07	

4.2. Sieve Analysis

Figures 1, 2 and 3 show the grading curves for the offshore, dune and land based sand samples tested respectively. It can be seen that most of the samples fall into the overall limits specified in BS 882 [8]. It can be noted that particle size distribution of offshore sand samples vary from the coarser zone C to the finer zone F, whereas all dune sand samples fall into finer zone F. The particle size distribution of land based sand is in the coarse zone C and there is a deficiency in very fine particles in the samples from Puwakpitiya and Kosgama. This is because of the use of a coarse mesh (0.3 mm) in the separation of sand from these two soil samples. Since large

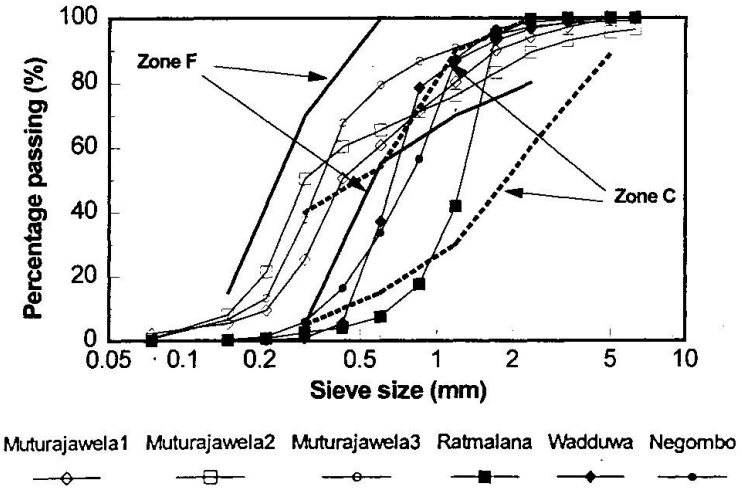

Fig.1 Particle size distribution of offshore sand

quantities of sand were needed for other tests such as strength properties of concrete, a coarser mesh was used to separate sand. The use of a finer mesh like a 0.075 mm square mesh is not practical in large scale washing because it is a time consuming process to separate very fine particles from clay manually. And also it was found that most of the soil samples contain sand around 50% (by wt) (i.e. particles less than 5 mm) and also a fairly high percentage of clay (i.e. about 40% by wt. of soil). However, it is important to note that grading alone is not a governing factor to reject aggregates as blending and/or adjustment of the coarse to fine aggregate ratio are possible remedies.

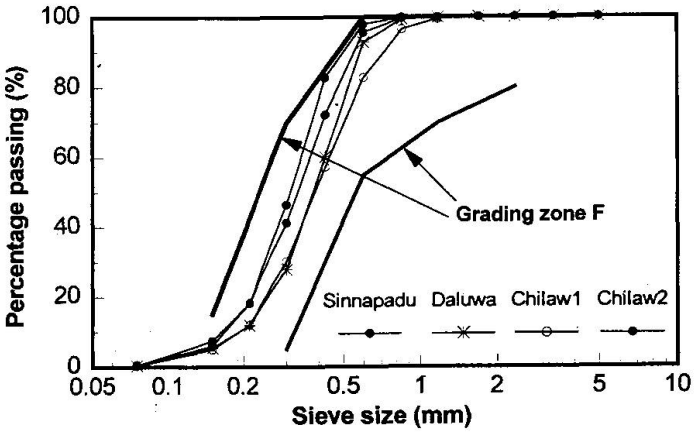

Fig.2 Particle size distribution of Dune sand

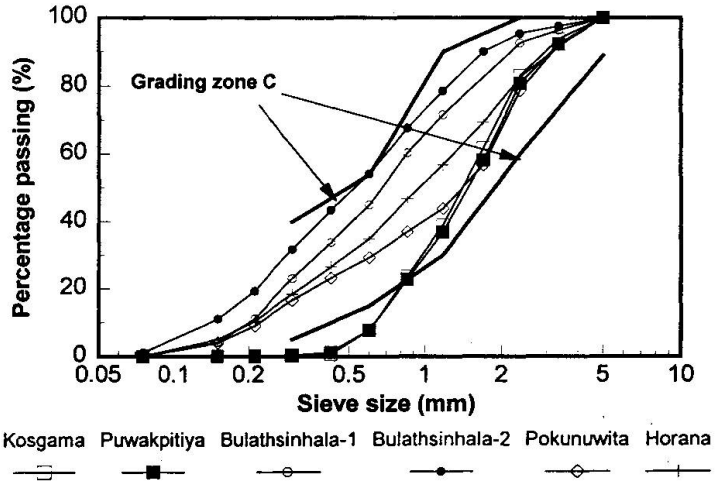

Fig.3 Particle size distribution of Land based sand

4.3. Shell Content

The shells larger than 5 mm was found to be in the range of 0.6% to 5.3% for offshore sand samples. The shell content of the fraction less than 5 mm was found to be in the range of 6.5% to 39.0%. There were no shells in the dune sand. The BS 882[8] gives no limits for shells in sand, but limits shell content to 20% by weight in 10-5 mm aggregate and to 8% by weight in sizes above 10 mm. The presence of a large shell content has no adverse effect on strength but workability of concrete made with aggregates having large shell contents is slightly reduced[9].

4.4. Chloride Content

The chloride content of offshore sand and dune sand is given in Table 2. The samples taken from Muthurajawela show very low chloride content because that sand was exposed to rain for over a year and salt must have been washed away. Similarly dune sand also shows very low chloride content because these dune sands have got accumulated over very long periods and salt deposits on the sand must have been washed away by rain water.

Table 2 - Chloride content in offshore sand and dune sand

	Offshore sand			(Offshore sand)		Dune sand		
	Wadduwa	Ratmalana	Negombo	Mutu-1	Mutu-2	Daluwa	Sinnapadu	Chilaw
Chloride Content(%)	0.14	0.13	0.14	0.001	0.001	0.0004	0.0005	0.0009

Mutu – Muthurajawela

Table 3 - Limits for chloride ion in British Standards

Type of concrete	Mandatory limit for concrete to comply with BS8110:1985-Table 6.4 (wt % of cement)	Guidance limit for aggregate* in BS 882:1983 Table 8 Appendix C (wt % of aggregate)
Prestressed concrete	0.1	0.02
Concrete with SRPC	0.2	0.04
Concrete with OPC	0.4	0.06

* The combined aggregates, i.e., coarse and fine aggregate combined in the proportion to be used in concrete.

Table 4 - Equivalent values of chloride content limits

Grade	Mix proportion (kg/m^3)			Maximum total chloride content in concrete expressed as a % of Cl^- by *mass of sand*		
	C	S	G	Prestressed concrete	Concrete with SRPC	Concrete with OPC
20	350	788	962	-	0.066	0.155
25	390	765	935	-	0.076	0.178
30	430	743	908	0.029	0.087	0.202

C – Cement, S – Sand, G – Coarse agg.

BS 8110 [10] and BS 882 [8] specify the limits for total chloride ion content in concrete and aggregate respectively as given in Table 3. The limits on the chloride content of aggregates given in BS 882 are for guidance only, since they assume that only aggregates contribute to the chloride content of the concrete. In practice, however, cement and admixtures contain small amounts of chloride and allowance may need to be made for this by a corresponding reduction in the permissible levels of chloride in aggregates. Table 4 shows the above limits (i.e. BS 8110 limits) converted to equivalent values expressed as a percentage of chloride ions by mass of fine aggregate, based on the prescribed mixes for ordinary structural concrete given in ICTAD specifications for Building works[6]. When calculating the maximum chloride content in Table 4 , it is assumed that chloride ions are contributed by fine aggregate and cement only. In addition, the chloride content of cement is assumed to be at the maximum of the typical range of 0.01~ 0.05% for OPC[11]. From Table 4, it can be noted that all the offshore sand samples tested comply with the requirement for normal reinforced concrete with OPC. However, it does not comply with that for prestressed concrete. In any case, it is better to wash offshore sand, but it is not necessary to do so in the case of dune sand.

4.5 Compressive Strength of Concrete

Table 5 shows the workability and the 7 day and 28 day compressive strength of a standard 1:2:4 concrete mix (quantities per cubic meter of concrete: cement – 320 kg, sand – 0.44 m^3 , coarse agg. – 0.88 m^3 , w/c – 0.55)[6] with river sand, offshore sand, dune sand and land based sand. It can be seen from the results that the compressive strength of concrete made with all the alternatives for river sand is as good as the strength of concrete made with river sand. Furthermore, concrete with dune sand gave the highest strength as well as workability. However, all mixes,

Table 5 - Properties of concrete made with various types of sand

Sample		Workability	Compressive strength(N/mm^2)	
		Slump(mm)	7 day	28 day
River sand		20	19.5	28.2
Offshore sand	Ratmalana	collapse	19.4	25.8
	Negombo	10	18.4	24.1
	Muturajawela	20	17.6	26.0
Dune sand		25	20.3	29.8
Land based sand	Puwakpitiya	0	16.9	27.4
	Kosgama	3	15.7	26.0

including the mix with river sand, displayed generally low workability. The mixes with land based sand gave zero slump, which may be due to a deficiency in fine particles or due to the angularity of particles.

5. Conclusions

It was found that all offshore sand samples tested comply with chloride limitation for normal reinforced concrete with OPC. However, it does not comply with that for prestressed concrete. Grading of offshore sand varies from fine to coarse. Offshore sand can be used even without washing for production of concrete with OPC for normal RC structures. After washing, it can be used even for prestressed concrete because washing will lower the chloride content to a very low level. Since chloride content in dune sand is very low, it can be used for any type of concrete. The quality of the land-based sand depends on the type of soil and method of washing. Sand obtained from this method is suitable for works where coarse sand is required. The compressive strength results show that the concrete made with all three alternatives is as good as the strength of concrete made with river sand.

Acknowledgments

The author gratefully acknowledges the financial support given by the Central Environmental Authority of Sri Lanka. The author also wishes to thank Prof. Priyan Dias and Dr. Asoka Perera for their valuable assistance given for this study.

References

1. National sand study for Sri Lanka: Phase one Vol. 1 and 2, Netherlands Economic Institute and Delft Hydraulics, Colombo, Sri Lanka, April 1992.
2. BS 812: 1975, "Method for sampling and testing of mineral aggregates, sand and fillers", British Standards Institution, London.
3. BS 812:Part 106:1985, "Method for determination of shell content in coarse aggregate", British Standards Institution, London.
4. Chapmen, G.P., Roeder, A.R., "Sea-dredged sands and gravel", The quarry managers' journal: Institute of quarrying transaction, July 1969, pp. 251-263.
5. American Public Health Association, " Standard Method for Examination of Water and Wastewater", 16th Edition, American Public Health Association, Washington, 1985.
6. Institute of Construction Training and Development, " ICTAD Specification for Building Works", Colombo, 1980.
7. Swan, B: Sand dune in the humid tropics: Sri Lanka, Zeittschrift fur Geomorphologie, 1979.
8. BS 882:1983, " Specification for aggregate from Natural sources for Concrete", British Standards Institution, London.
9. Neville, A.M., " Properties of Concrete", Pitman Books Limited, London, 1981.
10. BS 8110: Part 1:1985," Structural use of Concrete", British Standards Institution, London.
11. Lee, T.P. and Sym, R.: The precision of the method for determining the chloride content of cement recently proposed for BS 4550, World Cement, 1986.

Modeling of Temperature Rise in Concrete Using Fly Ash

Prabir Kumar SARKER,
PhD Student, School of Civil Engineering, Curtin University of Technology, Australia,
Former Graduate Student, School of Civil Engineering, Asian Institute of Technology, Thailand

Pongsak JITVUTIKRAI,
Graduate Student, Department of Civil Engineering, Sirindhorn International Institute of Technology, Thammasat University, Thailand

Somnuk TANGTERMSIRIKUL,
Associate Proffessor, Department of Civil Engineering, Sirindhorn International Institute of Technology, Thammasat University, Thailand

Toshiharu KISHI,
Assistant Professor, School of Civil Engineering, Asian Institute of Technology, Thailand

Summary

This paper proposes models for thermal conductivity and specific heat of hardening concrete and the material parameters of different types of fly ashes to determine the temperature rise in concrete. Thermal conductivity of hardening concrete is computed based on the volumetric ratio and the respective thermal conductivity values of the ingredients. Similarly, the specific heat model is based on the weight fractions and respective specific heat values of the ingredients. In the fly ash model, the reference heat rate and thermal activity of different types of fly ashes are expressed as functions of their CaO content. Temperature rise values in concrete specimens and a mat footing are computed using the proposed models and compared with the measured results. Good correlation among the analytical and test results is obtained.

1. Introduction

When water is added to cement, an exothermic reaction takes place causing a temperature rise in concrete after mixing. As the thermal conductivity of concrete is comparatively low, it acts like an insulator and heat produced inside mass concrete can not dissipate easily. At the same time, the exterior surface looses some heat. As a result, a temperature difference is developed between the exterior surface and the interior of the mass. This temperature difference causes internal tensile stress in mass concrete. When the tensile stress exceeds the tensile strength of concrete at that age, concrete structures, especially with external restrains, experience cracks. These cracks in the early age of concrete affect the durability and shorten the life span. So some means are required to control the temperature rise in concrete. Among other means, one effective method is to reduce the cement content of concrete by replacing it with fly ash [1]. Kishi and Maekawa [2] proposed a multi-component hydration model for blended cement with blast furnace slag and fly ash. This paper proposes a modification of the fly ash component of their model considering the difference of hydration heat produced by different fly ashes for their chemical compositions [1]. As the temperature rise in concrete is also a function of its thermal conductivity and specific

heat, models are proposed here to predict these thermal coefficients at different stages of hydration [3].

2. Assumptions of the models

The following assumptions are made in proposing the models for thermal coefficients and material parameters of fly ash:

1. Linear combination rule is used in computing the thermal coefficients of concrete.
2. The changes of total volume and unit weight of concrete during hydration are assumed to have negligible effect on thermal properties of concrete.
3. For non air-entrained concrete, as the thermal conductivity of air is very small as compared to those of other ingredients, it is neglected in computing the heat conductivity of concrete.
4. As the weight fraction of air is very small as compared to those of the other ingredients, it is neglected in computing the specific heat of concrete.
5. Volume of air remains unchanged during the hydration.
6. Volume decrease of the hydration product during hydration is neglected.
7. The material parameters of fly ash are expressed as functions of its CaO content.

3. Thermal coefficients of concrete

3.1 Thermal Conductivity

As the hydration reaction proceeds, the amount of free water in concrete reduces with an increase in the amount of hydrated product and concrete converts gradually from a fresh state to plastic and hardened states. So the thermal conductivity of concrete increases with time, especially in early age. The thermal conductivity of concretes with different mix proportions and containing different types of materials are also different. Here a model is proposed to compute the heat conductivity of concrete at different ages based on the volumetric ratio and thermal conductivity of the individual components of concrete, namely coarse aggregate, fine aggregate, cement and water. The volumetric ratio of fly ash as a cement replacing material is also considered. As coarse aggregate, fine aggregate and air are inert, their volumetric ratio and heat conductivity remain constant throughout the hydration. But the volume of unhydrated cementitious material (eg. cement and fly ash) and free water reduces and the amount of hydrated product increases with time. Considering these factors, the following equations are proposed to determine the heat conductivity of concrete during the hydration process.

$$Z(t) = n_g z_g + n_s z_s + n_{fw}(t) z_w + n_{uc}(t) z_c + n_{ufa}(t) z_{fa} + n_{hp}(t) z_{hp} \tag{1}$$

$$n_{uc}(t) = \left(1 - dh_c(t)\right) n_{c0} \tag{2}$$

$$dh_c(t) = \frac{Q_{3A}(t)}{Q_{3A\max}} \rho_{3A} + \frac{Q_{AF}(t)}{Q_{AF\max}} \rho_{AF} + \frac{Q_{3S}(t)}{Q_{3S\max}} \rho_{3S} + \frac{Q_{2S}(t)}{Q_{2S\max}} \rho_{2S} \tag{3}$$

$$n_{ufa}(t) = \left(1 - dh_{fa}(t)\right) n_{fa0} \tag{4}$$

$$dh_{fa}(t) = \frac{Q_{FA}(t)}{Q_{FA\max}} \tag{5}$$

$$n_g + n_s + n_{w0} + n_{c0} + n_{fa0} + n_a = 1.0 \tag{6}$$

$$n_{hp}(t) = 1 - \left(n_g + n_s + n_{fw}(t) + n_{uc}(t) + n_{ufa}(t) + n_a\right) \quad (7)$$

where, Z(t) : conductivity of concrete at any time

n_g, n_s, n_a : volumetric ratio of gravel, sand and air

n_{w0}, n_{c0}, n_{fa0} : initial volumetric ratio of free water, cement and fly ash at the time of mixing (at t=0)

$n_{fw}(t)$, $n_{uc}(t)$, $n_{ufa}(t)$, $n_{hp}(t)$: volumetric ratio of free water, unhydrated cement, unhydrated fly ash and the hydrated product, respectively, at the time considered.

z_g, z_s, z_w, z_c, z_{fa}, z_{hp} : thermal conductivity of gravel, sand, cement, fly ash and the hydrated product, respectively.

$dh_c(t)$, $dh_{fa}(t)$: degree of hydration of cement and degree of reaction of fly ash at the time considered

V_c, V_{fa} : unit volume of cement and fly ash at the time of mixing (t=0)

Q_{3A}, Q_{AF}, Q_{3S}, Q_{2S}, Q_{FA} : heat generated by C_3A, C_4AF, C_3S , C_2S and fly ash, respectively.

Q_{3Amax}, Q_{AFmax}, Q_{3Smax}, Q_{2Smax}, Q_{FAmax} : maximum heat generated by C_3A, C_4AF, C_3S , C_2S and fly ash, respectively.

ρ_{3A}, ρ_{AF}, ρ_{3S}, ρ_{2S} : weight percentage of C_3A, C_4AF, C_3S and C_2S, respectively, in cement (%).

3.2 Specific Heat

Specific heat of concrete is expected to change with the moisture content as the hydration reaction proceeds. In the proposed model, specific heat of concrete at any time is calculated based on the weight fraction of the components and their individual specific heat values. As specific heat of a body is related to its mass, the weight fractions of the components are used in computing the specific heat of concrete. The proposed equations are as follows:

$$S(t) = w_g s_g + w_s s_s + w_{fw}(t)s_w + w_{uc}(t)s_c + w_{ufa}(t)s_{fa} + w_{hp}(t)s_{hp} \quad (8)$$

$$w_{uc}(t) = \left(1 - dh_c(t)\right)w_{c0} \quad (9)$$

$$w_{ufa}(t) = \left(1 - dh_{fa}(t)\right)w_{fa0} \quad (10)$$

$$w_g + w_s + w_{w0} + w_{c0} + w_{fa0} = 1.0 \quad (11)$$

$$w_{hp}(t) = 1.0 - \left(w_g + w_s + w_{fw}(t) + w_{uc}(t) + w_{ufa}(t)\right) \quad (12)$$

where, S(t) = specific heat per unit weight of concrete at the time considered.

w_g, w_s = weight ratio of gravel and sand per unit weight of concrete.

$w_{fw}(t)$, $w_{uc}(t)$, $w_{ufa}(t)$, $w_{hp}(t)$ = weight ratio of free water, unhydrated cement, unhydrated fly ash and the hydrated product, respectively, at the time considered.

s_g, s_s, s_w, s_c, s_{fa}, s_{hp} = specific heat of gravel, sand, water, cement, fly ash and the hydrated product, respectively.

w_{c0}, w_{fa0}, and w_{w0} = weight of cement, fly ash and water per unit weight of concrete at the time of mixing (at t=0).

4. Material parameters of fly ash

As fly ash can not continue the reaction independently without an activator, it is difficult to determine the heat of its reaction based on experiments. On the other hand, heat rate measured with the addition of a reagent affects the reactivity of admixtures. So reference heat rates for different types of fly ash are set comparing the analytical results with the experimental ones. The reference heat rate of a particular type of fly ash at a constant temperature is expressed as a function of the accumulated heat generated by the fly ash and the heat generation is again considered to be a function of the CaO content. It is assumed here that the total heat generation as well as heat generation rate is higher for a high calcium fly ash. The relationship proposed for a constant temperature of 20 ^{0}C is shown in Fig 1. The thermal activity of a fly ash is expressed as a function of its CaO content and a constant value is assumed for the whole hydration period. The proposed relationship is shown in Fig. 2

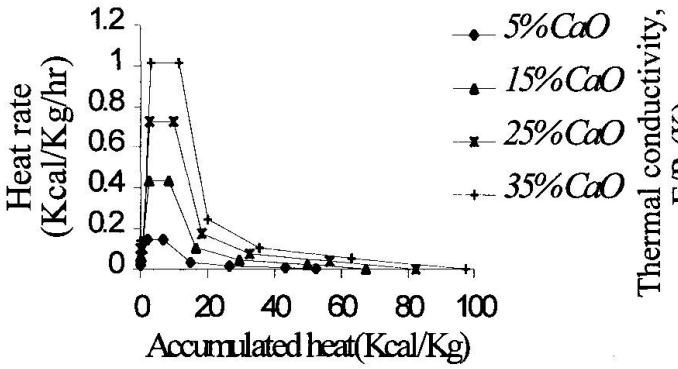

Fig. 1 Reference heat rate of fly ash

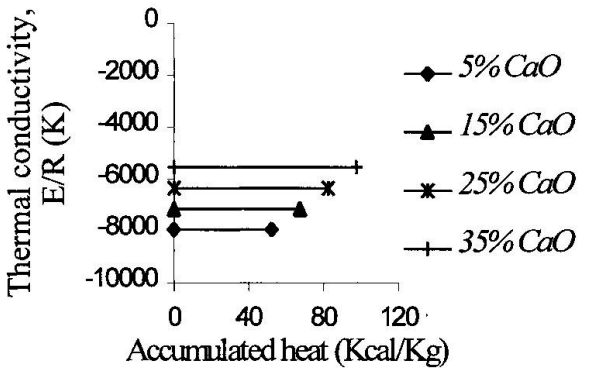

Fig. 2 Thermal activity of fly ash

5. Ca $(OH)_2$ consumption ratio for the reaction of fly ash

In the proposed models for material parameters of fly ashes, it is assumed that the supply of water and $Ca(OH)_2$ are enough for the reaction of the fly ash. The $Ca(OH)_2$ produced by the reaction of cement with water acts as an activator for the reaction of the fly ash to produce C-S-H. If there is an insufficient supply of $Ca(OH)_2$ in liquid state, the reaction of fly ash is retarded. This retardation of reaction is taken into consideration by introducing a term called consumption ratio of $Ca(OH)_2$. The consumption ratio of $Ca(OH)_2$ by fly ash is considered to depend on two factors, the ratio of CaO to SiO_2 (C/S) content of the fly ash and the percentage replacement of fly ash. It is assumed here that as the C/S ratio of the fly ash is increased, it consumes less amount of $Ca(OH)_2$ to produce the C-S-H. On the other hand, a higher cement replacement by fly ash causes a lower production and hence a lower consumption of $Ca(OH)_2$ at the later stages of hydration. So the average consumption ratio all over the reaction is decreased with the increase in percentage replacement of cement. Two different functions of the $Ca(OH)_2$ consumption ratio based on C/S ratio and percentage replacement of fly ash are proposed as shown in Fig.3 and Fig.4. Using these coefficients, the consumption ratio of $Ca(OH)_2$ for any type of fly ash and for any percentage replacement can be calculated by the following relationship:

$$R_{FACA} = R_{FACS} \times R_{FAPR} \quad (13)$$

where, R_{FACA} : Consumption ratio of $Ca(OH)_2$ by the fly ash used as cement replacement.
R_{FACS} : Consumption ratio based on the C/S ratio of the fly ash.
R_{FAPR} : Consumption ratio based on the percentage replacement of fly ash.

6. Comparison between test and computed results

The proposed models are incorporated into the multi-component hydration heat model of Kishi and Maekawa [2]. The multi-component heat model takes into account the heat produced by each oxide compound during the hydration including those generated in the process of ettringite formation, by proposing referential heat rate and thermal activity for each compound. Then, the total hydration heat can be summed from the heat generated by each component at any level of degree of hydration. For pozzolans, the referential heat rates and thermal activities of slag and fly ash were also proposed. The analytical results from the modified multi-component model are compared with experimental ones. In the experiment, cubic concrete specimens were cast in laboratory using cement only and cement with fly ash as binding material. Ordinary Portland cement Type 1 was used. Two samples of fly ash from Mae Moh generating plant were selected. Fine aggregate was river sand and coarse aggregate was crushed limestone. The chemical composition of cement and fly ashes used in the experiment are shown in Table 1. Table 2 shows the physical properties of the binders and aggregates. Mix proportions of the tested concrete were shown in Table 3. Figs 6 and Fig.7 show the temperature rise in specimens with 40%, 50%and 60% cement replacement by fly ash type A and B, respectively. The control concrete mixture for comparing with these fly ash concrete specimens is CC1. Fly ashes A and B contain CaO contents of 8.36% and 16.84%, respectively. It is shown in Fig.5 that for the cement mixtures, higher cement content results in higher temperature rise. Fig.6 and Fig.7 illustrate that replacing more cement with fly ash lowers the temperature rise in the concrete. By comparing Fig.6 and Fig.7, the fly ash with larger CaO content results in higher temperature rise of the fly ash concrete. Fig.8 shows the temperature history in a concrete footing with dimension

Table 1 Chemical composition of cement and fly ashes

Binder Type	Chemical composition (% by weight)								
	CaO	SiO_2	Al_2O_3	Fe_2O_3	MgO	SO_3	Na_2O	K_2O	Free lime
Cement	64.60	20.30	6.41	2.87	1.50	2.29	0.29	0.34	1.00
Fly ash FAA	8.36	46.02	26.79	10.09	2.47	1.20	0.74	2.68	0.11
Fly ash FAB	16.84	40.14	19.84	11.50	2.68	3.18	0.94	2.10	0.42
Fly ash FAC	13.30	41.00	20.90	13.20	2.70	4.00	0.91	2.35	0.20

Table 2 Physical properties of cement, fly ashes, fine aggregate and coarse aggregate

Physical properties	Cement	Fly ash FAA	Fly ash FAB	Fine aggregate	Coarse aggregate
Specific gravity (g/cm^3)	3.13	1.92	2.22	2.58	2.72
Blaine fineness (cm^2/g)	3350	1900	1990	-	-
Absorption (%)	-	-	-	0.89	0.31
Fineness Modulus	-	-	-	3.11	-
Maximum size (mm)	-	-	-	4	20

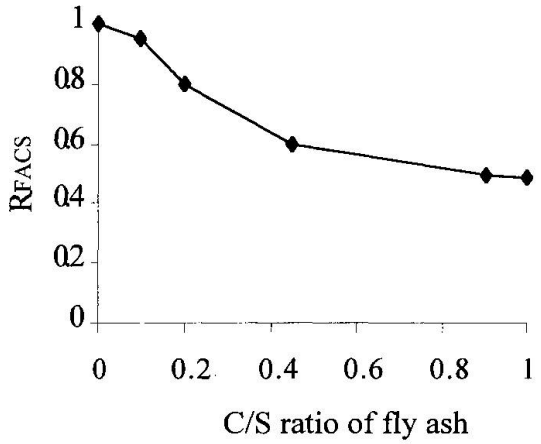

Fig.3 Relationship of R_{FACS} and C/S

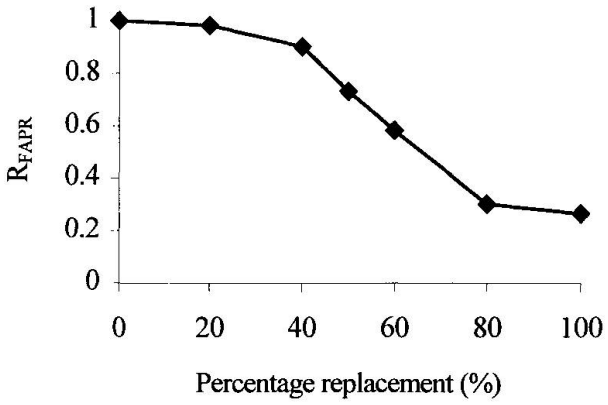

Fig.4 Relationship of R_{FAPR} and % replacement

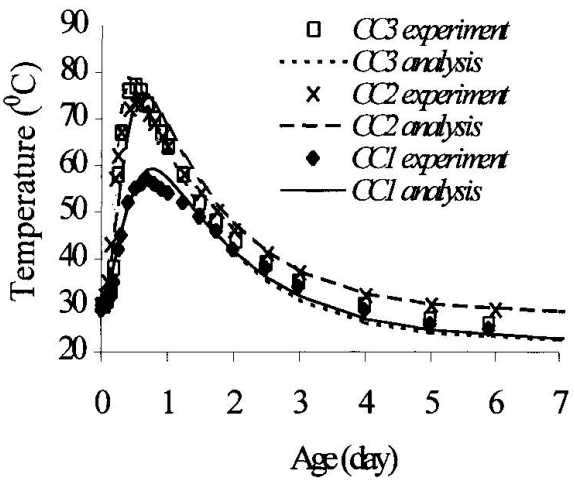

Fig.5 Temperature in plain concrete specimens

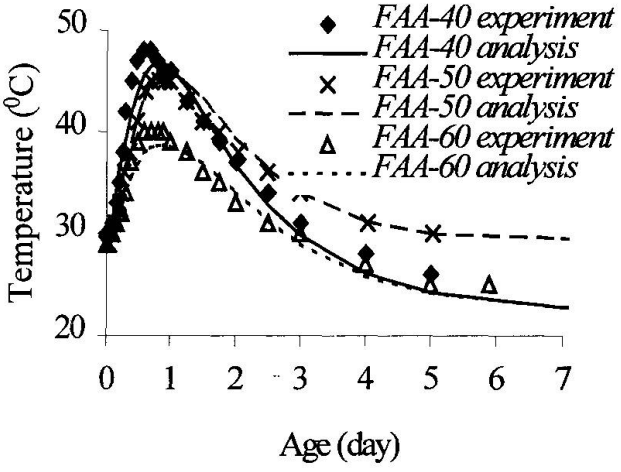

Fig.6 Temperature in concrete with fly ash FAA

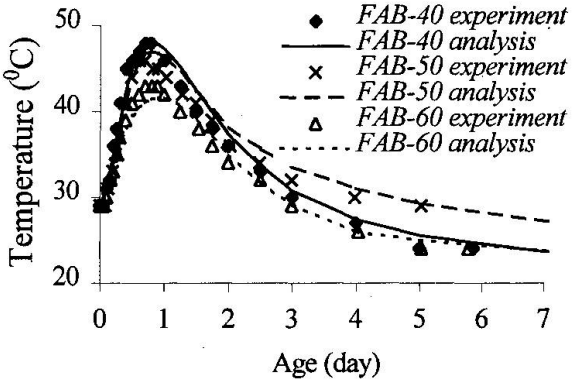

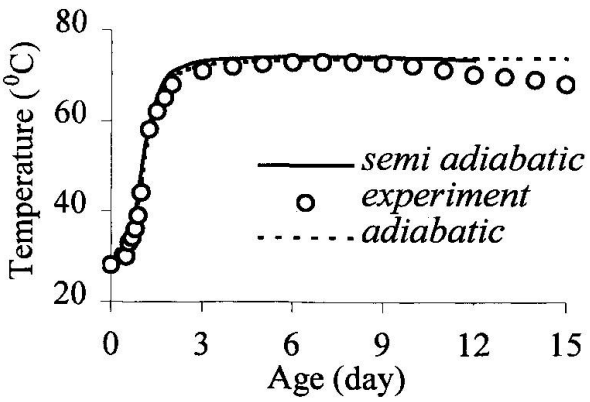

Fig.7 Temperature in concrete with fly ash FAB Fig.8 Temperature in a footing with fly ash FAC

Table 3 Mix proportion of the tested concrete

Mix	Component (kg/m^3)							Initial concrete temperature (°C)
	w/b (%)	f/b (%)	C	f	w	S	G	
CC1	50.0	0	350	0	175	818	1057	30.0
CC2	47.5	0	454	0	215	723	943	28.0
CC3	30.3	0	558	0	163	810	904	30.0
FAA-40	47.5	40	205	137	162	801	1035	30.0
FAA-50	47.5	50	174	174	165	781	1018	29.0
FAA-60	47.5	60	135	202	160	790	1021	29.0
FAB-40	50.0	40	210	140	175	786	1017	29.0
FAB-50	47.5	50	176	176	167	792	1032	29.0
FAB-60	47.5	60	141	211	167	793	1025	29.0
Footing*	40.0	47.5	210	190	160	810	1010	30.0

Remarks : w : water, b : total binder (c+f), f : fly ash, S : fine aggregate, G : coarse aggregate
* uses fly ash FAC.

of 38.4m×8.4m×4.75m using a fly ash replacement of 47.5%. Temperatures at the centers of all specimens were measured using thermocouples. Analytical results were obtained after incorporating the proposed models into the multi-component hydration heat model of Kishi and Maekawa [2]. Thermal coefficients of the concrete ingredients were assumed according to the recommendations of American Society of Heat and Refrigerating Engineers [4] and those for the hydrated products were obtained by data back analysis. Since the mat footing in Fig.8 was big enough to consider the condition of adiabatic at the center, the footing was analyzed in adiabatic condition.

7. Concluding remarks

Comparing the analytical results with the experimental ones for the test specimens and the practical structure as shown in Figs 5 to 8, it can be concluded that the models can be applied to concrete structures using a cement replacement by any type of fly ash and of any percentage. However, future studies still have to be carried out for a better prediction and also for other types of powder materials.

8. References

1. Tangtermsirikul, S. and Kitticharoenkiat, P. (1997). "Development of Low Heat Concrete using Fly Ash and Pumicite", *Research and Development Journal of the Engineering Institute of Thailand,* Vol.1, pp.88-98.

2. Kishi, T. and Maekawa, K. (1997). "Multi-Component Model for Hydration Heating of Blended Cement with Blast furnace Slag and Fly Ash", *Concrete Library of JSCE*, No.30, pp. 125-139.

3. Sarker, P. K. (1998), Hydration Heat Modeling of Concrete using Fly Ash, *A Master Thesis,* Asian Institute of Technology, pp. 81.

4. The American Society of Heat and Refrigerating Engineers Fundamentals Handbook (1997).

Hydration Heat Modeling for Cement with Limestone Powder

Toshiharu KISHI
Assistant Professor
Asian Inst. of Tech.
Bangkok, Thailand

Saruul, D., Researcher
Mongolian Governmental Implementing Agency for Construction and Architecture
Ulaanbaatar, Mongolia

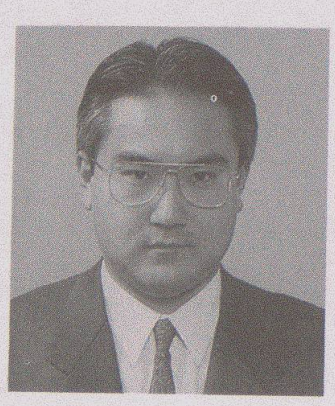

Kishi T., born 1967. received his B.Eng. in 1990, M.Eng. in 1992 and D.Eng. in 1996 from The University of Tokyo.

Saruul Dorjpalamyn, born 1972., received her B.Eng. from Mongolian Technical University in 1994 and M.Eng. from Asian Institute of Technology in 1998.

Summary

The filler effect of limestone powder on hydration heat of Portland cement was successfully implemented into the multi-component hydration heat model. The ratio between total surface areas of limestone powder and Portland cement is adopted as an indicator to express the filler effect since the surface of limestone powder particles is thought to play roll as precipitation site for cement hydrates. The applicability of the proposed model was verified with temperature measurements carried out at center points on concrete blocks covered by quasi-insulator.

1. Introduction

Self-compacting high performance concrete requires high powder content and low water-powder ratio to maintain high segregation resistance. However, in case of mass concrete structure the high content of binder brings shortcomings in viewpoint of prevention of thermal cracking since it yields large amount of heat of hydration. Thus, it is recommended to reduce unit cement content to mitigate temperature rise. Usually, the low water-binder ratio yields high strength. Then, it is possible to replace a part of binder by inert material like limestone powder with maintaining low water-powder ratio that is, physically, a crucial condition for self-compactability. Further, limestone powder has a preferable feature to improve flowability of self-compacting concrete with small dosage of superplasticizer. Therefore, the use of limestone powder has been recently increased as inert admixtures for self-compacting concrete.

On the other hand, the modeling of hydration process of cement including blending admixtures is required to predict temperature history of mass concrete for thermal crack analysis, and further to pursue property change of concrete with time in the scheme of life span simulation of concrete structures [1]. Here, the effect of limestone powder on hydration process of cement should be taken into account to achieve wider applicability of modeling, since it is well known that the existence of limestone powder promotes hydration process of cement. It can be said that the multi-component hydration heat model proposed to evaluate exothermic process of cement hydration at arbitrary temperature has proper frame to take into account the interdependence of reactions among powder materials, since the hydration process of cement is described by dissolving into minerals [2]. In this study, therefore it is attempted to implement the filler effect of limestone powder on hydration heat of Portland cement into that hydration heat model.

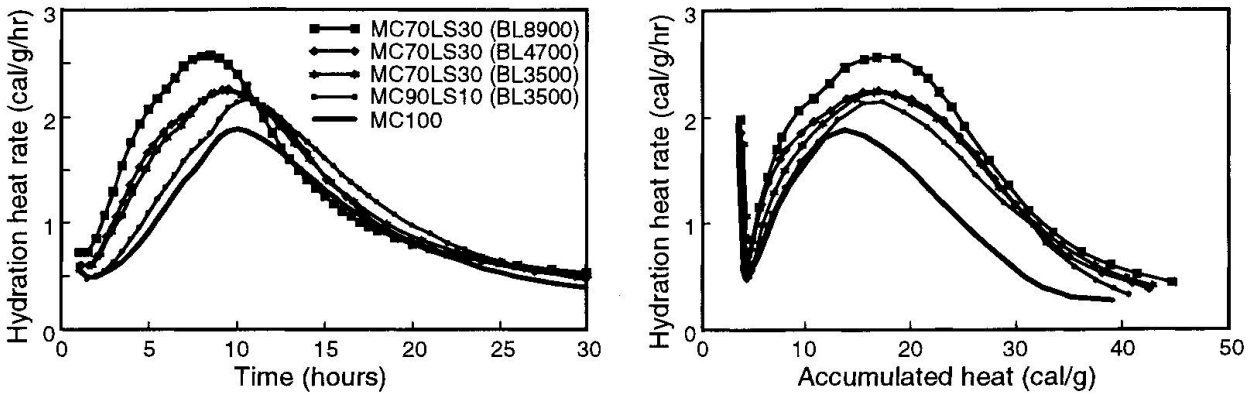

Fig.1 Accelerated hydration heat of cement in terms of time and accumulated heat [5]

2. Physical effect of inert powders on hydration heat process of cement

It is known that the strength of concrete and hydration process of cement is affected by addition of inert powder materials. Yamazaki quantitatively reported through well arranged series of experiments that mineral fines, which even does not have pozzolanic reactivity, physically promotes strength of concrete by increasing the degree of hydration of cement [3]. It was explained as promotion mechanism that inert powder materials could provide additional precipitation site for hydrates, which is an adjacent part of surface area being in contact with cement particle, by getting into flocculation of cement particles. Recently attention is paid towards the use of limestone powder and the related researches were conducted in terms of hydration heat process of cement with conduction calorimeter. Then, it was reported that cement hydration is accelerated according to amount and fineness of limestone powder especially at the second peak in the hydration heat process, which is mainly corresponding to active hydration of alite [4]. However, it is still hardly discussed how cement hydration is affected in viewpoint of controlling factors for reaction rate. Since the quantitative effects of inert powder to the rate controlling factors are not apparent, it was attempted to compare the hydration heat processes accelerated by limestone powder in terms of accumulated heat as shown in Fig.1 [5]. The legends in Fig.1 indicate weight fractions of moderate heat Portland cement and limestone powder with Blaine value of limestone powder shown in a parenthesis in the mixture of cement paste. Here, the relationship between the acceleration effect and division of hydration heat process could be discussed in viewpoint of same degree of hydration. Then it was found that the acceleration is remarkable at around and just after the second peak, where rate of hydration is thought mainly governed by diffusion mechanism at the hydrates formed around unreacted cement particles. Further, it was pointed out that the diffusion resistance at the layer of hydrates should be mitigated since the surface of limestone powder shares some part of them and consequently decreases loads for cement particles.

To adopt an appropriate indicator that can express the effect of inert powder on cement hydration it is necessary to know how the surface of inert powders contribute to precipitation of cement hydrates. Here, it is appreciated that Goto et. al. have directly observed by Scanning Electro Microscope (SEM) that hydrates were similarly formed on overall surfaces of both particles of alite and limestone powder in their mixture [6]. Based on this observation it is thought that the outer layer of hydrates could be precipitated from eluted ion phase at any locations even away from cement particles, and all surface areas of particles can contribute as precipitation site from the beginning of hydration. Further, they found in hydration heat of alite mixed with limestone powder that the linear relationship exists between the heat rate at the second peak and the total surface area of powder particles, those both are normalized by unit weight or volume of alite

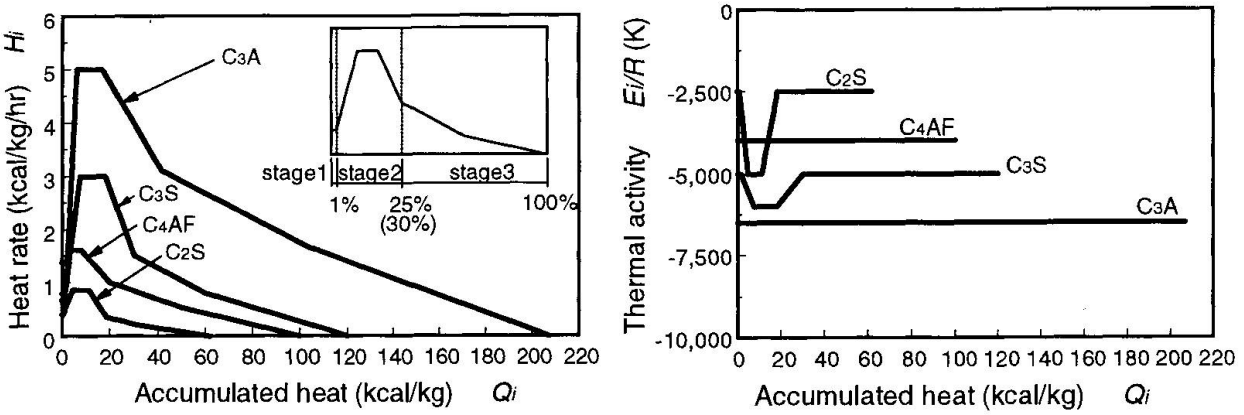

Fig.2 Reference heat rate and thermal activity of each mineral compound [7]

included [6]. These results indicate that the total surface area of powder particles normalized by some factors related to cement included, such as volume, weight or surface area, is suitable as an indicator to express the acceleration effect to hydration heat rate of unit weight of cement.

3. Implementation of the effect of limestone powder to hydration heat model

3.1 Multi-component hydration heat model [2]

In the model, hydration of cement is expressed by hydration of individual clinker minerals, which are regarded as fundamental units of reaction. The heat reactions for alite (C_3S), belite (C_2S), aluminate phase (C_3A) and ferrite phase (C_4AF) were individually described. The heat rate of cement is given as the sum of the heat rate of all reactions as follows,

$$H = \sum p_i H_i = p_{C_3A}(H_{C_3AET} + H_{C_3A}) + p_{C_4AF}(H_{C_4AFET} + H_{C_4AF}) + p_{C_3S}H_{C_3S} + p_{C_2S}H_{C_2S} \quad (1)$$

Where, i represents each mineral component. H and H_i are the heat rates per unit weight of cement as a whole and mineral i, respectively, p_i is the weight fraction of mineral i. H_{C_3AET} and H_{C_4AFET} are both heat rates as a result of the formation of ettringite.

The hydration heat rate of clinker minerals are described by two material functions shown in Fig.2, which are the reference heat generation rate at a constant temperature and the thermal activity indicating temperature dependence of the reaction [7]. The hydration heat rate of each component is generally expressed, with interdependence among the reactions, as follows,

$$H_i = \beta_i \cdot \mu \cdot s_i \cdot H_{i,T_0}(Q_i)\exp\left\{-\frac{E_i}{R}\left(\frac{1}{T}-\frac{1}{T_0}\right)\right\}, \qquad Q_i \equiv \int H_i dt \quad (2)$$

Where E_i is the activation energy of component i, R is gas constant, H_{i,T_0} is the reference heat rate of component i at constant temperature T_0 and also the function of accumulated heat Q_i, β_i is a coefficient to express reduction of heat rate due to shortage of free water (free space), μ is a coefficient to express change of heat rate related to difference of mineral composition of cement, s_i is a coefficient to express change of reference heat rate due to fineness of cement.

3.2 Implementation of physical effect of limestone powder

In Fig.1 it must be seen that the hydration heat rates around the second peaks, which are represented as Stage 2 in Fig.2, show approximately similar figures in terms of the accumulated

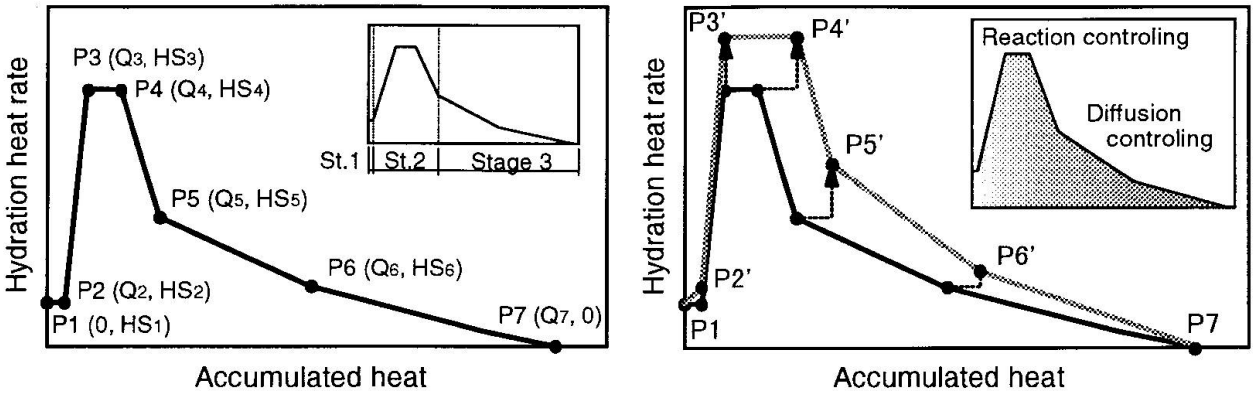

Fig.3 Schematic representation of physical effect model for limestone powder

heat, although they return to stagnated rate simultaneously in time domain. This indicates that not only the hydration heat rate at same degree of hydration but also the regions of respective stages, which are reaction and diffusion controlling ones, are affected due to the physical effect of limestone powder. In the exothermic process around second peak, the heat generation, which must accompany precipitation of hydrates, is thought to be attributable to two sources of ions eluted. One is a group of ions that were already eluted during the dormant period and stored at over-saturation, and the other is new elution of ions accompanied by simultaneous precipitation at that moment [2]. Hence, if the diffusion resistance at the layer of hydrates is mitigated, ions that can additionally elute during Stage 2 are thought to be increased, and consequently the region of the stage expands accordingly. In the model, therefore, the change of regions of stages due to physical effect of limestone powder should be expressed, besides acceleration of hydration heat rate that is supposed to be corresponding to precipitation rate of hydrates.

Fig.3 shows schematic representation of modeling for physical effect of limestone powder on cement hydration. As shown in Fig.2, the reference heat rate is graphically expressed as multi-linear function to represent complicated process. To express acceleration of the hydration heat process the coordinates of points in the function are shifted by the following relationships.

$$\begin{aligned}
&\text{For P2 and P3:} && Q'_{ij} = Q_{ij}, \quad HS'_{ij} = HS_{ij} \cdot (1 + k_{H1} r_s) \\
&\text{For P4 and P5:} && Q'_{ij} = Q_{i\max} - \left((Q_{i\max} - Q_{ij})/(1 + k_Q r_s)\right), \quad HS'_{ij} = HS_{ij} \cdot (1 + k_{H2} r_s) \\
&\text{For P6:} && Q'_{ij} = Q_{i\max} - \left((Q_{i\max} - Q_{ij})/(1 + k_Q r_s)\right), \quad HS'_{ij} = HS_{ij} \cdot (1 + k_{H3} r_s) \\
& && r_s = (P_{LS} \cdot B_{LS})/(P_{PC} \cdot B_{PC})
\end{aligned} \tag{3}$$

Where, j: point number in reference heat rate function, Q_{ij} and HS_{ij}: the accumulated heat and heat rate of point j of i component, Q_{imax}: the maximum heat generation of i component, P_{LS}, P_{PC} and B_{LS}, B_{PC}: weight fractions and unit weight surface areas of limestone powder and Portland cement. r_s is the ratio of surface areas between limestone powder and cement, which is adopted as the indicator to express the acceleration effect of limestone powder in this study. To represent the degree of contribution by limestone powder certain coefficients, those are k_{H1}, k_{H2}, k_{H3}, k_Q, are multiplied to r_s. Through the analyses shown later they are set as 0.3, 0.3, 0.1, 0.05, respectively. Tentatively, this model is equally applied to all four components of clinker minerals.

4. Verification for scheme of filler effect modeling

To verify the proposed scheme of model and set appropriate parameters, temperature measurements at center points were carried out on concrete blocks covered in styrene foam and

Table 1 Mineral composition of cement

	C_3A	C_4AF	C_3S	C_2S	CS2H	Blaine
Cement	11.0	10.4	53.9	18.8	5.83	3350

Note) CS2H: Gypsum dihydrate
Unit) Blaine value: cm^2/g

Table 2 Mix proportions of concrete

	W/P	W	C	LS	S	G	SP
OPC	30.3	171	565	-	820	915	1.0
LS15	31.3	173	480	74	820	915	0.8
LS30	32.7	177	396	146	820	915	0.7
LS40	32.6	172	311	218	820	916	0.7
LS55	32.6	168	226	291	820	916	0.7
LS70	32.0	165	155	362	820	915	0.7

Note) W/P: Water powder ratio in weight, C: Ordinary Portland cement, LS: Limestone powder (Blaine: 5650), SP: Superplasticizer
Unit) W/P: %, W, C, S, G: kg/m^3, SP: C%

Table 3 Initial and ambient temperatures

	OPC	LS15	LS30	LS40	LS55	LS70
Initial T.	30	30	28	28	28	28
Ambient T.	23	23	23	23	23	28

Unit) Temperature: °C

plywood formwork having depths of 30 and 15 mm, respectively. The specimen is outlined in Fig.4. Five different replacement ratios by limestone powder were tested. The mineral composition of cement and mix proportions of concrete are shown in Table 1 and Table 2, respectively. The initial and ambient temperatures are shown in Table 3. Thermal conductivity and heat transfer coefficient are assumed to be 41 kcal/m/day/°K and 35 kcal/m^2/day/°K, respectively.

Fig.5 shows comparison between the results of experiment and analysis. The analytical results by original model, in which no acceleration effect was considered, are also shown. It is seen that the proposed model can appropriately represent the acceleration effect of limestone powder on hydration heat of cement at arbitrary replacement ratio.

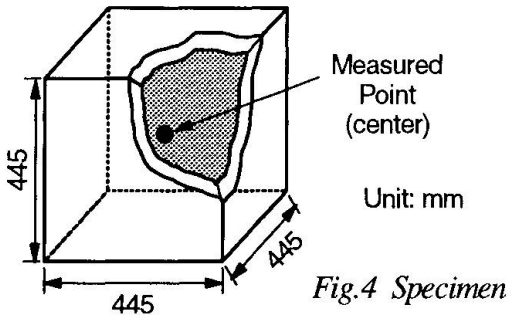

Fig.4 Specimen

Fig.5 Comparison between analysis and experiment

5. Conclusion

The model for physical effect of limestone powder on hydration heat of cement is successfully implemented into the multi-component hydration heat model. The ratio between total surface areas of cement and limestone powder, which are represented by weight fraction multiplied by Blaine value of them, is adopted as the indicator to express the contribution of limestone powder as precipitation site for cement hydrates. Based on review of previous researches, it was found that the change of regions having different rate controlling factors should be taken into account besides the acceleration of hydration heat rate at same degree of hydration. At and around second peak in the hydration heat process of cement, it is thought that the additional elution of ions can increase since diffusion resistance at the layer of hydrates is mitigated due to sharing by limestone powder. Then, both the acceleration of hydration heat rate and the change of ranges so called reaction control and diffusion control stages are expressed in the model. The applicability of the proposed model was verified with temperature histories at the center of small concrete blocks. A wide scope with sufficient accuracy was found in the engineering point of view.

The acceleration effect of limestone powder is thought as a physical effect on hydration of cement. Although the physical effect of limestone powder, that is inert material, is modeled in this study the similar effect would appear even when another inert or low reactivity powders are mixed. In case of blending cement mixed with pozzolanic admixtures, this effect would become apparent at higher replacement since pozzolanic reactions tend to stagnate due to their reaction dependence on cement one. In the multi-component hydration heat model for blending cement, this physical effect of blending powders is not taken into account at all so far [7]. Thus, it is required to rationalize modeling for hydration heat of blending cement by extending and incorporating the physical effect model of powder admixtures proposed in this study.

References

1. Maekawa, K., Chaube, R.P., Kishi, T.: Coupled Mass Transport, Hydration and Structure Formation Theory for Durability Design of Concrete Structures, Integrated Design and Environmental Issues in Concrete Technology edited by Sakai, K., pp.83-97, International Workshop on Rational Design of Concrete Structures, Hakodate, Aug. 1995
2. Kishi, T. and Maekawa, K.: Multi-component Model for Hydration Heat of Portland Cement, Proc. of Japan Society of Civil Engineers (JSCE), No.526/V-29, 1995. (in Japanese), translated in Concrete Library International of JSCE No.28, pp.97-115, 1996.
3. Yamazaki, K.: Fundamental studies of the effects of mineral fines on the strength of concrete, Transactions of JSCE, No.85, pp.15-46, 1962. (in Japanese)
4. Asaga, K. and Kuga H.: The effect of calcium carbon oxide on hydration rate of Portland cement, Proceedings of the 22nd meeting of cement concrete research group, pp.79-84, 1995. (in Japanese)
5. Uematsu, K. and Kishi, T.: Effect of limestone powder on hydration heat process of cement, Proc. of the 52nd annual conference of JSCE, Vol.5, pp.180-181, 1997. (in Japanese)
6. Goto, K., Ozawa, S, Hoshino, S. and Hirose, T.: Effect of limestone powder on cement hydration, Symposium on properties of limestone powder and its utilization for concrete, Japan Concrete Institute (JCI), pp.147-150, 1998. (in Japanese)
7. Kishi, T. and Maekawa, K: Multi-component Model for Hydration Heat of Blended Cement with Blast Slag and Fly Ash, Proc. of JSCE, No.550/V-33, pp.131-143, 1996. (in Japanese), translated in Concrete Library International of JSCE No.30, pp.125-139, 1997.

Effects on Re-expansion of Restrained Expansive Concrete

Liwen LIU
Research Associate
Asian Inst. of Tech.
Bangkok, Thailand

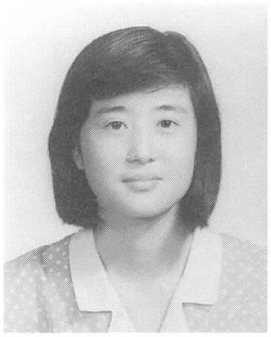

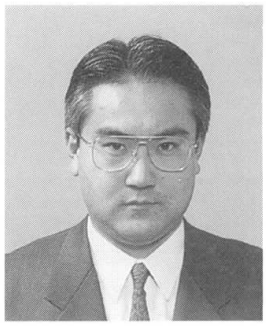

Liwen Liu, born 1964. received her B.Eng. from Tongji University in 1987 and M.Eng. from Asian Institute of Technology in 1998.

Toshiharu KISHI
Assistant Professor
Asian Inst. of Tech.
Bangkok, Thailand

Toshiharu Kishi, born 1967. received his B.Eng. in 1990, M.Eng. in 1992 and D.Eng. in 1996 from The University of Tokyo.

Summary

The re-expansion is defined as a property of expansive restrained concrete, which appears due to introducing cracks under wet condition after the initial expansion seems to become stable. In this study, it is deeply investigated through a series of experiments with different mix proportions, curing conditions and restraining steel ratios. It was indicated that the deformation of expansive concrete including re-expansion can be grasped in connection with the reaction of expansive agent that shows complicated behavior according to curing temperature and water-binder ratio.

1. Introduction

Expansive concrete being accompanied by expansion is often used for precast products and chemical prestressed concrete to compensate drying shrinkage and improve mechanical properties of members. Although the prestressing chemically introduced in expansive concrete is usually quite smaller than that of mechanical prestressed concrete, crack resistance and related durability performance of member are remarkably improved. However, this interesting and important feature of expansive concrete is not clearly recognized and not positively expected so far, since it is difficult to quantitatively estimate it. Consequently, the scope of application of expansive agent is limited to the aforementioned purposes and expansive agent is regarded as one of special admixtures for concrete. One of the reasons why the property of expansive concrete was rarely treated numerically is it shows very complicated behavior according to conditions such as mix proportion, curing and so on. Thus, it is necessary to rationally grasp volume change behavior of expansive concrete according to arbitrary conditions applied.

Usually concrete structures are exposed to ambient conditions and suffer mechanical loading. Thus, mechanical damages represented by cracks are often introduced, and then structure is seriously deteriorated. However, if the expansive agent is used for usual structures, it can be expected that the resistance for crack initiation is enhanced and introduced crack opening is mitigated. Further, it was found that the additional expansion could be introduced again in case of low water-binder ratio if cracks are introduced under wet condition [1]. If the additional expansion could take place after cracks are introduced it might be able to reduce mechanical damages and resist degrading of structure. In this study, therefore, expansion before and after introducing cracks under wet condition and influencing factors are investigated through series of experiments where mix proportion, curing and restraining conditions are changed.

2. Experimental details

Ordinary Portland cement and calcium sulfoaluminate type expansive agent were used as binders. The mix proportions of mortar are shown in Table 1. To investigate the effects of factors on re-expandability water-binder (powder) ratio, replacement ratio of expansive agent, restraining steel ratio and curing condition were appropriately arranged.

Fig.1 shows the outline of specimen in which a deformed bar was arranged to penetrate at center of the specimen in longitudinal direction. The dimension of specimens was 100x100x700mm and several sizes of bar in diameter were used to change restraining ratio. The formwork was removed after 24 hours from casting and all specimens were cured for around one week with wet cover till the initial volumetric change became stable. Then, specimens were treated and cured in different manners, respectively. Some specimens were subjected to introducing cracks just after initial deformation became stable, and then put into water to be cured. To introduce cracks, the axial tension force was applied to specimen by pulling restraining bar within elastic range and then force was released. Other specimens were exposed to ambient condition for around 3 weeks after initial curing finished. Then cracks were introduced to specimens in the same manner, and they were put in water again. Both the casting and ambient temperature of specimens were around 29°C. Through whole experimental period the strain of restraining steel was recorded. Notches were properly provided to avoid cracking at gauge position.

3. Expansions before and after introducing cracks

The expansions of specimens after casting are shown in Fig.2, where wet cover curing was provided. After expansive mortar was cast it tended to expand with hardening and chemical prestressing was introduced as a counteraction by restraining steel. The expansion that has been continuing with reaction of expansive agent seems to be stagnant after around one week from casting. It was clearly explained by previous research that expansion of specimen no longer increases due to the balance with creep and elastic deformation caused by compressive stress in this situation [2]. In Fig.2 we can see a tendency that specimens, which have relatively higher water-binder ratio, show larger expansion than lower ones irrelevant of both replacement ratio and amount of expansive agent. Further, it is seen in each case that the rate of expansion is very fast within 1 or 2 days from casting and then that becomes suddenly stagnant. It is known that reaction of expansive agent has high temperature dependence and the rate of initial expansion is severely dependent on curing temperature [3]. Therefore, it can be supposed that reaction of expansive agent could quickly proceed at higher temperature provided in this study, and then the

Table 1 Mix Proportion of Specimens

Specimen	W/(C+E) (%)	E/(C+E) (%)	W (kg/m^3)	C (kg/m^3)	E (kg/m^3)	S (kg/m^3)	SP (%(C+E))
EP28(-07)	28.0	10.0	140	450	50	1750	3.0
EP30(-07, 30)	30.0	5.0	207	655.5	34.5	1485	1.0
P30(-07,30)	30.0	0.0	207	690	0	1485	1.0
EP40(-07)	40.0	10.0	200	450	50	1600	1.0
EP60(-07)	60.0	5.0	300	475	25	1560	0.5
P60(-07)	60.0	0.0	300	500	0	1560	0.5

Note: 07 and 30 following specimen numbers in parentheses represent the age of specimens in days when cracks were introduced. W, C, E, S and SP: water, cement, expansive agent, sand and superplasticizer, respectively.

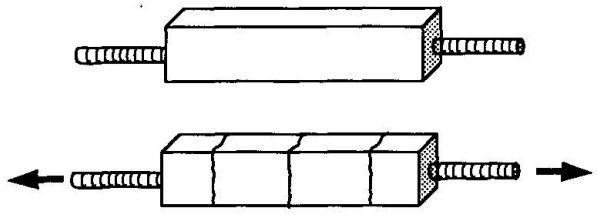

Fig.1 Appearance of specimen

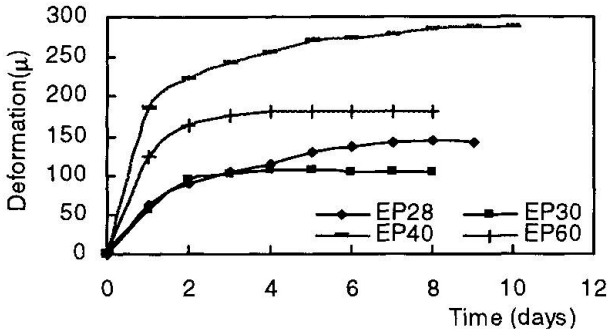

Fig.2 Expansion before cracking

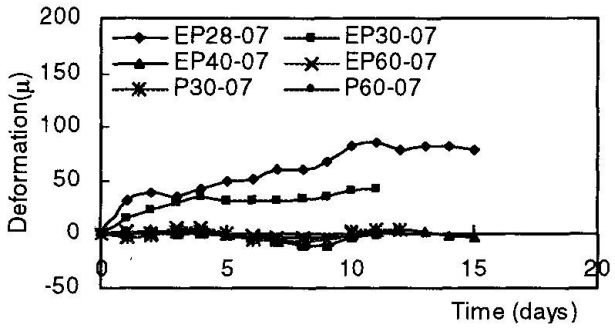

Fig.3 Expansion after cracking

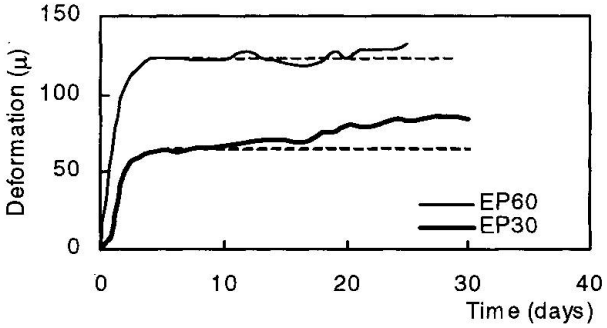

Fig.4 Long-term expansion in wet condition

initial expansion became stable at around one week from casting.

Fig.3 shows the deformation of specimens after cracks were introduced and they were put in water. The additional expansions can be observed only in lower water-binder ratio cases in which lower initial expansions were observed before introducing cracks, and no expansions are seen in higher ones even though expansive agent were included. In this study the expansion additionally introduced by introducing cracks is called as re-expansion. It was reported that the chemical prestressing could be sometimes introduced again under wet condition if initial one is released [2]. However, it must be noted that the initial stress could not be released by introducing cracks, then this phenomenon is not completely same as that appears due to the release of stress although both of them are thought to be truly dependent on the reaction of expansive agent. Here, it is thought in lower water-binder ratio that the reaction of expansive agent becomes stagnant before introducing cracks due to shortage of free water irrespective of higher ambient temperature. Then, it is supposed that introduced cracks play roll as the path of water supply from outside to remaining expansive agent, which could not react due to shortage of internal water, and consequently the re-expansion could appear only in cases of lower water-binder ratio.

The long-term deformations of specimens without cracks were also measured as shown in Fig.4. Although in case of higher water-binder ratio only negligible fluctuations are seen after initial expansion becomes stable, in case of lower one the expansion continues to take place with minute rate in long-term range. Here, it is thought that unreacted expansive agent, which remains due to low water-binder ratio can react with water being supplied from outside through dense pore structure, and specimen can continue to expand although high restraint stress applies. Strictly speaking, the reaction of expansive agent is not perfectly stopped in this situation though it seems stagnant. Thus, the effect of cracks is thought to affect the reaction rate of remaining expansive agent by changing permeability of hardened structure. In case of underground structure around which groundwater always exists the feature of re-expansion might decrease with the elapsed time since water could be continuously supplied even at minute rate.

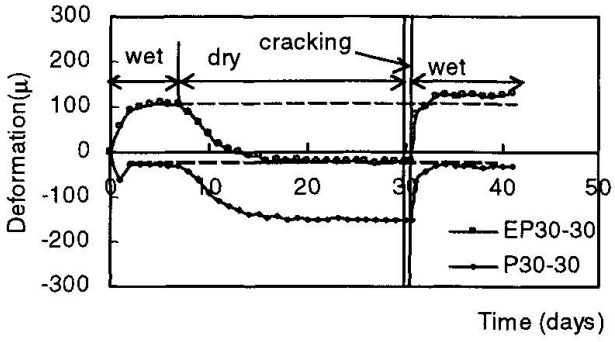

Fig.5 Deformation of specimens under drying and wetting

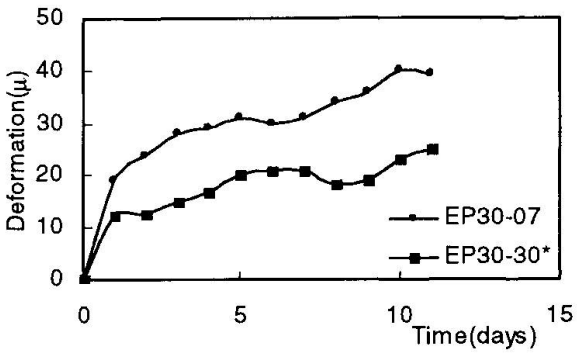

Fig.6 Re-expansions at different ages

4. Effect of curing condition on re-expandability

It was reported that if drying happens in expansive concrete before the initial expansion has been terminated, some expansion would still take place when cured in water later [2]. Thus, it is apparent that the reaction of expansive agent is stagnated due to drying. On the other hand, it was suggested in this study that the reaction of expansive agent might also be stagnated due to low water-binder ratio even though the external drying does not take place. Then, it was investigated whether the expandability maintained due to low water-binder ratio could remain for long time range. It was reported that expansive mortar, which had lower water-binder ratio and has been exposed to ambient condition for 8 months after the initial expansion had been stagnated, showed gradual expansion later under wetting condition after introducing cracks [1]. Here, although it is suggested that the re-expandability may remain for long time under drying condition, the deformation after cracking must include the release of drying shrinkage by wetting, which was introduced during exposed period. Therefore, the compensation of drying shrinkage should be distinguished to discuss the existence of re-expandability due to low water-binder ratio in aged and dried specimen.

Fig.5 shows deformations of both expansive and normal specimens having same low water-binder ratio under wetting and drying. It is seen that drying shrinkage is being introduced while specimen was exposed to surroundings. At the age of 30 days, cracks were introduced and specimens were transferred into water. The deformation after cracks are introduced is also shown to follow the previous deformation just before cracking is introduced. Here, it is difficult to distinguish the re-expansion and shrinkage recovery in terms of time since they must take place simultaneously. However, it is seen that the deformation of expansive specimen after introducing cracks overcomes that of before drying. In case of normal concrete, the drying shrinkage is only recovered up to almost same or slightly lower level of previous deformation. Hence, it is suggested that some re-expansion occurred in expansive specimen. Although both expansive and normal specimens have same water-binder ratio, the introduced drying shrinkage is approximately 5% higher in expansive mortar than normal one. Then, to roughly estimate the re-expansion of expansive specimen in terms of time it is attempted to exclude the deformation corresponding to the release of drying shrinkage from the total one. The release of drying shrinkage is estimated by proportionally increasing that of normal specimen according to ratio between introduced drying shrinkage to them. Fig.6 shows the estimated re-expansion of the dried specimen based on the above assumption with that of young specimen to which no drying was applied. Although the degree of the re-expansion is not remarkable due to small amount of

expansive agent it can be said that a certain amount of re-expandability due to low water-binder ratio remains even in aged specimen if drying is made to occur.

However if specimens are cured in water for long time, the re-expandability of expansive concrete might be lost with time. As shown in Fig.4 the expansion energy would be gradually exhausted with external supplies of water even though water-binder ratio is low. In that situation it is understood that the additional chemical prestressing would be gradually introduced instead of the loss of re-expandability. On the other hand, in case of superstructure that is exposed to the ambient air the re-expandability would remain for long time due to hindrance to reaction of expansive agent caused by drying. Then, it might be expected that remaining expansion energy be consumed suitably due to rain, so that drying shrinkage could be mitigated.

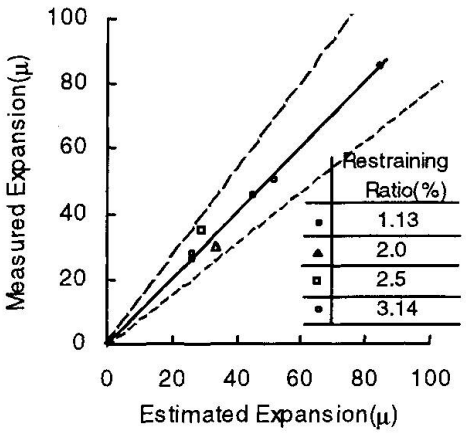

Fig.7 Relationship between the estimated and the measured re-expansion

5. Re-expansion at different restraining steel ratio

The concept of work quantity is thought as a sole evaluation method for expansion of restraining expansive concrete member with sufficient accuracy so far. It was known in practice that the quantity of work performed by expansive concrete on restraining steel is constant if mix proportion and curing methods are identical [4]. Here, the quantity of work U performed by a unit volume of concrete is expressed as,

$$U = \frac{1}{2} pE\varepsilon^2 \tag{1}$$

where, p: restraining steel ratio, ε: expansive strain of steel and E: elastic modulus of steel. Thus, the expansion of restraining specimen changes according to restraining steel ratio under the same work quantity identified by provided conditions. Here, the expansive strain of steel at any restraining steel ratio can be expressed based on a result of standard specimen (p_0, ε_0) as,

$$\varepsilon = \sqrt{\frac{p_0}{p}} \cdot \varepsilon_0 \tag{2}$$

If the re-expansion follows this concept of work quantity, it can be said that the remaining expansion energy after the initial expansion becomes stable must also be constant according to mix proportion and curing methods as initial one. Then, the re-expansions with several restraining steel ratios were measured with two different mix proportions. Fig.7 shows comparisons between measured and estimated re-expansion where that of 1.13% restraining steel ratio is adopted as standard in the above formula. The dot lines beside the diagonal one show the error of 17%. It is seen that the re-expansions at various restraining steel ratios can be appropriately estimated. Thus, it can be said that the constant work quantity concept is applicable to not only initial expansion but also the re-expansion of restraining expansive specimen.

Through this discussion it is proved that the remaining expansion energy is constant irrespective of restraining steel ratio and is dependent only on mix proportion and curing methods, which are thought to definitely affect the reaction process of expansive agent. The degree of restraint represented by restraining steel ratio is not thought to affect the reaction process of expansive agent at all. Based on the amount of exhausted expansion energy under applied conditions only the introduced strain varies according to the restraining steel ratio as a result.

6. Conclusion

The re-expansion of expansive restrained concrete, which appears under wet condition if the cracks are introduced even after the initial expansion seems to become stable, is investigated with different mix proportions and curing conditions. The followings are concluded through experiments and discussions.

1. The re-expansion due to introducing cracks under wet condition is seen not in higher water-binder ratio but in lower one. In case of low water-binder ratio the reaction of expansive agent is thought stagnated due to shortage of internal water. The re-expansion is thought as a phenomenon caused by the accelerated reaction of remaining expansive agent, which is enabled under the supply of water from outside through introduced cracks. The re-expansion is not completely similar to the additional expansion due to the release of chemical prestressing, which had been found with arbitrary water-binder ratio [2].
2. Based on comparison with data of previous researches at 20°C temperature it is supposed that the reaction of expansive agent is greatly accelerated and almost terminates shortly at higher temperature, then the initial expansion becomes stable even for around ten days.
3. Provided that water curing is supplied for low water-binder ratio specimen even after the initial expansion seems stagnant, the expansion gradually continues at minute rate. It is supposed that expansive agent, which still maintains unreacted parts due to shortage of water, can continue to react with water supplied from outside through dense structure in this situation.
4. By distinguishing the re-expansion from the release of drying shrinkage, it is clearly indicated that the re-expandability of expansive concrete can be maintained for long time under drying condition. However, in wet condition it would be gradually exhausted with time even in low water-binder ratio, since the gradual expansion could continue.
5. The concept of work quantity, whose applicability had been widely verified for initial expansion of restraining expansive concrete, is also applicable for the re-expansion. It is proved that the expansion energy is definitely constant if mix proportion and curing conditions are identical even after the initial expansion seems to become stagnant.

To estimate the expansion of concrete in an actual member is indispensable for utilizing expansive concrete more widely. Through discussions in this study where the re-expandability is focused, it is indicated that overall behavior of expansion is governed by the reaction process of expansive agent that must be significantly affected by curing temperature and water-binder ratio. To establish universal evaluation scheme for deformation of expansive concrete the development of reaction model for expansive agent, which is applicable to follow arbitrary conditions in terms of time, is required.

References

1. Nanbu, R.: Deformation and Crack-control of Reinforced Concrete with Expansive Admixtures, Master thesis submitted to University of Tokyo, 1995 (in Japanese).
2. Okamura, H., Tsuji, Y. and Maruyama, K.: Application of expansive Concrete in Structural Elements, Journal of the Faculty of Engineering, The Univ. of Tokyo (B), Vol.34, No.3, 1978.
3. Miyake, N.: Study on application of ettringite for cement concrete, Doctoral dissertation submitted to Tokyo Institute of Technology, 1987 (in Japanese).
4. Tsuji, Y.: Method of Estimating Expansive Strains Produced in Reinforced Concrete Members Using Expansive Cement Concrete, American Concrete Institute, SP-64, pp.311-319, 1980.

Properties of Volcanic Ash and Pumice Concrete

Khandaker M. A. **HOSSAIN**
Lecturer in Civil Engineering
The PNG University of Technology
Lae, Papua New Guinea

Khandaker M. A. Hossain, born in 1963, received BSc and MSc in civil engineering from Bangladesh University of Engineering & Technology, Dhaka and PhD from Strathclyde University, Glasgow, UK. Previously, he worked as a Research Fellow, in the Department of Engineering, University of Aberdeen, UK and also as an assistant professor of Civil Engineering in Bangladesh. He received 1998 Ken-Francis award for his research on blended cement.

Summary

The properties of concrete using different percentages of volcanic ash (VA) and pumice (VP) as cement and aggregate replacements respectively are evaluated by conducting comprehensive series of tests. Tests were conducted by using up to 50% of VA and up to 100% of volcanic pumice aggregate (VPA) in the concrete mix. The concrete properties in both fresh and hardened states are evaluated. Results showed good potential for the manufacture of concrete using VA and VP. It is intended to develop design charts that can be used as guidelines for mix design of volcanic ash and pumice concrete.

1. Introduction

The search for cement replacement materials and new aggregates for concrete had been continuing for the last decades. This paper is focused on the use of volcanic ash and pumice in concrete production with particular preference to Papua New Guinea. The 1994 volcanic eruption that occurred in the East New Britain province devastated the province and created an environmental disaster. This research is put forward to explore the possible utilisation of this volcanic debris in concrete production that can not only provide low cost cement and concrete but also can help to decrease environmental hazard. Volcanic ash and pumice powder [1, 2,3] are pozzolanic materials and can form cementitious compounds because of their reaction with lime, liberated during the hydration of cement. These materials can also improve the durability of concrete and the rate of gain in strength and reduce the rate of liberation of heat that is beneficial for mass concrete.

Recent research [3] suggested that the production of Portland volcanic ash cement (PVAC) or Portland volcanic pumice cement (PVPC), similar as Portland fly ash cement (PVFAC), is possible by using up to 20% VA or VP with cement. On the other hand, the potential use of comparatively weaker and porous volcanic pumice as lightweight aggregate in concrete can be very useful. Nevile [4] described that satisfactory concrete which is 2 to 3 times lighter than normal concrete having good insulating characteristics with high absorption and shrinkage can be manufactured using volcanic pumice. Currently research is ongoing [5] on the use of light

weight volcanic pumice concrete (VPC) in thin walled filled sections intended to be used as beams and columns for houses in volcanic areas. The light weight and enhanced ductility make this form of construction suitable and economic for earthquake prone areas especially in the context of Papua New Guinea. The optimum use of VA can improve workability [6,7] of concrete and can provide low cost volcanic ash concrete (VAC) of satisfactory strength. This paper describes the properties of VAC and VPC in connection with percentage of VA (as cement replacement) and VPA (as stone aggregate replacement) used in the concrete mix.

2. Experimental study

2.1 General Remarks

The volcanic ash (VA) and pumice (VP) used in this study were collected from the Rabaul area in the East New Britain province of Papua New Guinea and the source is a volcano called Mount Tavurvur (see Fig 1).

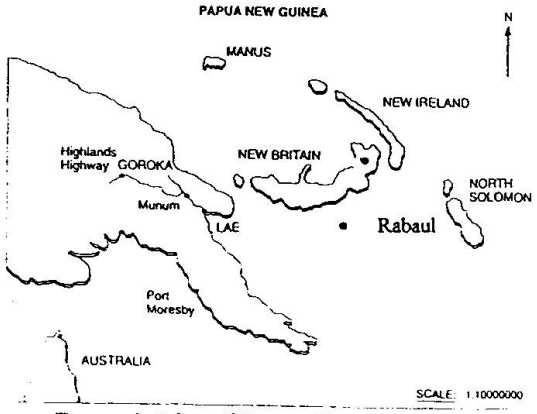

Figure 1: Map of Papua New Guinea

Chemical analysis (Table 1) indicated that the VA and VP have similar composition, composed principally of silica (about 60%) along with cementitious compounds like calcium oxide, alumina and iron oxide (total about 31%). 20 and 10mm maximum size aggregates with river sand are used for VAC while 20mm maximum size VPA with river sand are used for VPC. The cement used was locally manufactured Portland cement called 'Paradise'.

Table 1: Study of Chemical properties

Chemical Composition (%)			
	VP	VA	Cement
Calcium oxide (CaO)	4.44	6.10	60-67
Silica (SiO_2)	60.82	59.32	17-25
Alumina(Al_2O_3)	16.71	17.54	3-8
Iron oxide (Fe_2O_3)	7.04	7.06	0.5-6.0
Sulphur trioxide (SO_3)	0.14	0.71	1-3
Magnesia (MgO)	1.94	2.55	0.1-4.0
Sodium oxide (Na_2O)	5.42	3.80	0.5-1.3
Potassium oxide (K_2O)	2.25	2.03	0.5-1.3
Loss on ignition	1.52	1.03	1.22

2.2 Tests on VAC and VPC

Mix details

The particle size distribution of aggregates performed according to AS (Australian Standard) 1289.C6.1-1977 are presented in Fig 2. VPA (bulk density of 763 kg/m^3) is found to be 3.24 times lighter than normal stone aggregate (bulk density of 2470 kg/m^3). High degree of porosity in VPA leads to almost 13 times higher water absorption (37%) than normal stone aggregate (2.86%).

Volcanic ash concrete (VAC)

A series of tests was carried out to investigate the possible manufacture of concrete using volcanic ash and also to determine the variation of compressive strength with varying percentage of volcanic ash added as cement replacement. The mixes have constant water cement ratio and manufactured from same aggregates producing mixes of variable workability.

The concrete mixes are classified into six mixes according to the percentage of cement replaced by volcanic ash. All concrete mixes had the same over all ratio of 1:2:4 (cement including VA : sand: aggregate) on the volume basis. After calculation of the volume required for the cement including volcanic ash, it was transformed into weight on the basis of cement. Then from the equivalent weight of cement, the amount of volcanic ash was calculated based on % cement replacement by weight. The coarse aggregate consisted of 70% of 20 mm with 30% of 10 mm maximum size crushed gravel. River sand was used as fine aggregate. The mix parameters and some characteristics of the fresh concrete are presented in Table 1. The first numeric in the mix designations represents % of volcanic ash and the second numeric represents aggregate cement (cement including VA) ratio by weight.

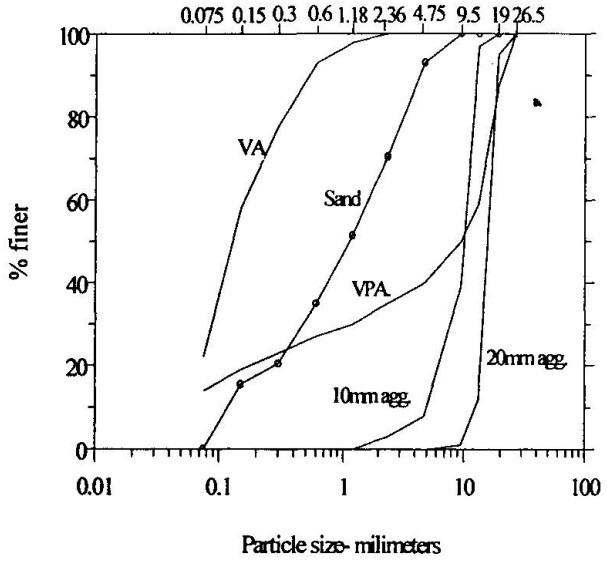

Figure 2: Particle size distribution

Table 2: VAC and VPC mix details

VAC mixes				VPC mixes			
Mix	Cement kg/m³	VA kg/m³	W/ (C+VA) ratio	Mix designation	VPA kg/m³	10mm agg. kg/m³	NW/C * by weight
Aggregate - (C+VA) ratio =4.95				VPC Mix-1: 1:2:3 , Cement =814 kg/m³			
0-4.95	438	0	0.354	100-36.9-2.38	358	0	0.465
5-5.21	416	22	0.368	90-25.6-2.55	322	119	0.44
15-5.83	372	66	0.368	75-19.4-2.80	268	297	0.39
25-6.61	328	110	0.381	50-11.3-3.22	179	594	0.376
35-7.61	285	153	0.409	0-0-4.07	0	1188	0.36
50-9.90	219	219	0.461				

W=water ; C=cement ; * Net water excluding water absorbed by VPA

Volcanic pumice concrete (VPC)

A series of tests was performed using different percentages of volcanic pumice as replacement of coarse aggregate in concrete. The concrete mixes had the over all ratio of 1:2:3 (mix 1) and 1.2:4 (mix 2) on volume basis. Each of the two mixes were classified into five sub-mixes according to the % of VPA as a replacement of normal coarse aggregate (by volume). The coarse aggregate consisted of 10 mm maximum crushed gravel and VPA with river sand as fine aggregate. The mix parameters and some characteristics of the fresh concrete for mix 1 are presented in Table 2. The first numeric in the mix designations represents % of VPA of total coarse aggregate by volume, second numeric represents % of VPA of total aggregate by weight and the third numeric represents total aggregate cement ratio by weight.

Test specimens and testing procedure

The test specimens were cast using the optimum water-cement ratio for each mix. The specimens were 100 x100x100 mm cubes and 100 x200 mm cylinders for compressive strength. Total 4 cubes were cast from each sub-mix. The samples were compacted on a vibrating table. The specimens were demoulded after 24 hours and cured under water at a temperature of 23 ±2°C until tested.

3. Results and Discussion

3.1 Properties of fresh VAC and VPC

The investigation on fresh VAC suggested that the workability of the mix increases (slump value increased from 80mm to 140mm) as the % of VA is increased from 0 to 15% and increase of VA beyond 15% (up to 75%) reduces the workability (slump value decreased from 140mm to 40mm). This confirms the possibility of using VA as water reducing admixtures and research is now ongoing on this aspect. More water is needed to get a workable mix as the % of VPA is increased from 0 to 100%. The total water requirement is much higher due to high water absorption capacity (about 37%) of VPA as well as the presence of higher quantity of fines in the VPA compared to replaced 10 mm aggregate. The high absorption of water by VPA in the initial stages of mixing, can cause balling-up of cement and a loss of slump. To avoid this, the aggregate was first mixed with at least one half of the mixing water before cement was added into the mixer. For 100% VPC, a slump of 50 to 60 mm represents satisfactory workability compared to 80-82 mm slump for 0% VPC. However, to make VPC with 50 to 100% VPA having satisfactory workability, the range of slump values should be 50 to 75 mm.

3.2 Properties of hardened VAC and VPC

The variation in compressive strength (cylinder) of VAC with different percentages of VA is shown in Fig 3. As expected, strength decreased as the VA content increased. It is possible to obtain a concrete having 28 days strength of 25 MPa with VA content of 35%. It is found that the strength of the VAC reduced sharply when the VA content is increased beyond 35%. The specimens were found to disintegrate when 50% VA was used. Higher alkali presence in the VA may have caused the disintegration of concrete due to reaction with some aggregate and also may have affected the rate of gain in strength of cement.

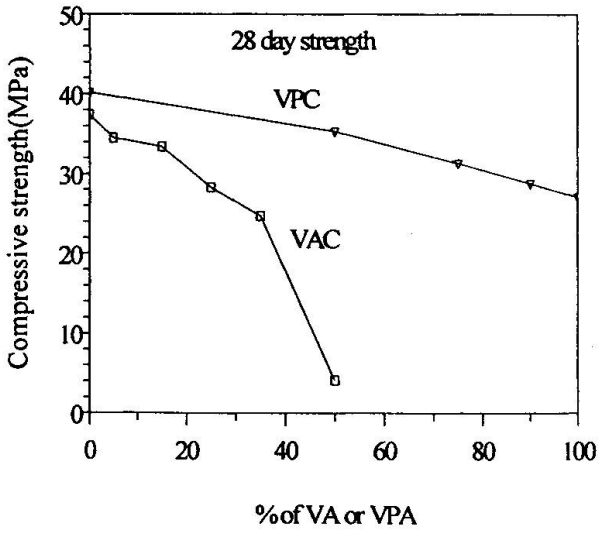

Figure 3: Compressive strength of VAC or VPC

The variation in the 28-day compressive strength (cylinder) of VPC (1:2:3) with different percentages of VPA is also shown in Fig 3. As expected, strength decreased with the increase of VPA due to the replacement of normal stone aggregate by relatively weak pumice aggregate. Results showed that by using 100% VPA, it is possible to obtain a VPC of 27 MPa (1:2:3) and 22 MPa (1:2:4). The variation of density of VAC at 28 day with percentage of VA is presented in Fig 4. The variation of density of VAC at 28 day with percentage of VA is presented in Fig 4. The density of VAC decreased with the increase of VA . This is due to the replacement of comparatively heavier cement by lighter VA. The fresh density is found to be higher than those at 7 and 28 days due to subsequent removal of water from the fresh specimen with age. The density is found to be decreased with ages. For 50% replacement of cement by volcanic ash, it is possible to produce a VAC only 5% lighter than the normal concrete. Use of 100% replacement of coarse aggregate by VPA (designated as 100% VPC) can produce a VPC 25% lighter than the normal concrete (see Fig 4).

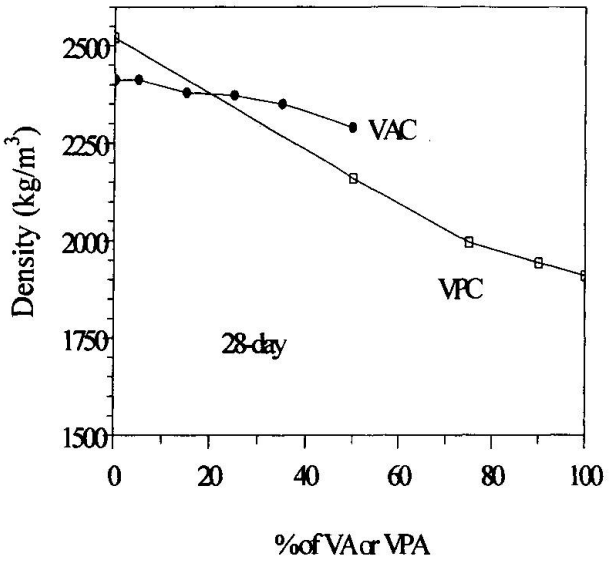

Figure 4: Variation of Density of VAC

4. Design charts

It is aimed to produce design charts for VAC and VPC relating mix design parameters. A preliminary chart showing the prediction of cylinder strength for a particular VAC mix is shown in Fig 5.

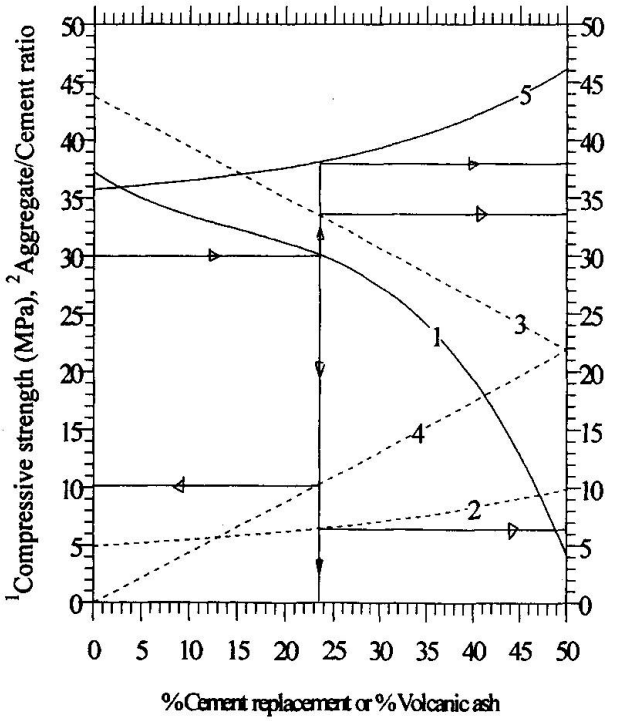

Figure 5: Typical mix design chart for VAC

The numeric superscripts in the y-axis label identify the designated curve number shown in the body of the graph. The chart illustrates through arrow diagrams, the determination of mix design parameters for a 30 MPa VAC. For 30 MPa concrete, mix design parameters are: amount of cement (curve 3) =336kg/m^3, amount of volcanic ash (curve 4)=102 kg/m^3, % of volcanic ash=23.6, aggregate cement ratio(curve 2)=6.3 and W /(C+VA) ratio (curve 5) =0.38 (38%). The design mix will also satisfy the workability requirement. This chart is valid only for similar conditions of VA and aggregate described in the paper. The reliability [6] of the charts is to be checked based on repeatability of the test results and comprehensive series of tests on mix-design procedures for various mixes is now under progress towards that objective.

5. Conclusions and future research

Results showed that by using up to 35% VA, it is possible to obtain a VAC of 25 MPa (28 day). Use of 50% VA can produce a VAC only 5% lighter than the normal concrete. It possible to obtain a VPC of strength 27 MPa and 25% lighter than the normal concrete. Design charts are developed which can be used as guidelines for mix design of VAC and VPC. It is confirmed that the volcanic ash and pumice can be used as a resource in concrete production and can be used in low cost construction especially in the post-disaster rehabilitation project in the volcanic areas of Papua New Guinea. More work is needed and currently research is in progress to investigate short and long term behaviour of VAC and VPC including shrinkage, durability, permeability, corrosion and fire resistance.

6. Acknowledgements

The author is grateful to the Papua New Guinea University of Technology for providing financial assistance in this project. The author is also grateful to the Technical staffs of the materials laboratory of the Department of Civil Engineering and National Analysis laboratory.
Sincere thanks to Mr. Jabin Basitau and Mr. Sariman of the department of Civil Engineering for their assistance.

7. References

1. Swamy, R.N.,"Cement Replacement Materials", Concrete Technology and Design, Vol.3, Surrey University Press, Great Britain,1986.

2. Swamy, R.N., "New Concrete Materials", Concrete Technology and Design, Vol.2, Surrey University Press, Great Britain, 1983.

3. Hossain, K.M.A, "Volcanic ash and pumice based blended cement", Proce. of 23rd Conference on Our world in Concrete & Structures incorporating 3rd International Seminar on blended cements, Singapore, 24 August, 1998, pp. 297-302.

4. Nevile, A.M., "Properties of Concrete", 3rd Edition, Pitman Publishing Limited, London, 1981.

5. Hossain, K.M.A., " Behaviour of thin walled composite sections as structural elements",Proce. of the Australasian Structural Engineering Conference, Auckland, 30 Sept.-2 Octo., 1998, vol. 1, pp. 175-180.

6. Hossain, KMA, "Effect of volcanic ash as cement replacement material in cement and concrete", Under preparation for possible publication in the Journal of ACI.

7. Hossain, K.M.A. " Volcanic ash as cement replacement material ", Proce. of the IEPNG International Conference, September 25-27, 1998, Rabaual, PNG, pp. 26-31.

Effect of Fly Ash Size and Curing on Concrete Strength

Montri NITHIKUL
Postgraduate student
Kasetsart University
Bangkok, Thailand

Suvimol SUJJAVANICH
Associate Professor
Kasetsart University
Bangkok, Thailand

Prasert SUWANVITAYA
Associate Professor
Kasetsart University
Bangkok, Thailand

Summary

Particle size and curing temperature are important factors influencing mechanical properties of fly ash concrete. This paper reports the strength development of fly-ash concrete using three plant-classified particle sizes from Mae Moh power plant. The effect of two curing temperatures, 40 °C and 60 °C were studied, compared with that of room temperature. Of the three cement replacement percentages used ie 20%, 30% and 40%, the test results indicated that concrete with 20% replacement yielded highest strength gain for all particle sizes and curing temperatures. Within the range studied, size effects appeared to be much higher than temperature effect, particularly for the finest one. The effect of increasing temperature from 40 °C to 60 °C is minimal. However, the effect of curing at 40 °C compared to the room temperature is significant.

1. Introduction

In Thailand, the largest source of fly ash is the electricity generating facility in Mae Moh, Lampang province, in the North of Thailand. The fly ash, some 8,000 tons produced daily, has until recently been regarded as waste and has been treated accordingly. The past several years have seen better results in the attempts at utilization of the fly ash from this source as a pozzolanic material. Although studies have shown good results in terms of contribution to strength development (1,2), several other parameters remain uninvestigated. This study proposed to determine the influence of fly ash particle size and curing temperature on the compressive strength of fly ash concrete.

Two factors that are of current interest with regards to Mae Moh fly ash are the fly ash particle size and the curing temperature of the fly ash concrete. The interest in the particle size arises early in the installation of particle classifier in the plant. Particles are classified into three groups of varying mean particle sizes. The effects of such classified fly ash on concrete properties should be of substantial benefit. The other factor, the curing temperature, is thought to be significant in this region, since large numbers of on site concrete members are cured under temperature in the range of 30-40 C. The effect on the strength development, particularly when fly ash is involved, should lead to better understanding on the use of this material

2. Influence of particle size

Because the pozzolanic reactions that fly ash undergoes are surface reactions, the finer particles (hence, the greater specific surface) has been found to show higher rate of contribution to strength development (3,4). There are several other aspects associated with particle sizes and fly ash specific surface that may influence the pozzolanic activity of the ash. Chemical compositions of fly ash vary with particle sizes. Larger particles tend to have higher carbon content but less alkali, sulphate and chloride than finer ones, even though all particles have been collected from the same source, at the same time. It can be seen that after the particles have been separated into several sizes, the differences among the colllectors are not limited to size only, the chemical compositions are normally different as well. Even with these variances associated with particle sizes, using the fly ash samples collected from the classifier from the same plant at the same time was considered the best alternative in the investigation of the size effect.

3. Influence of curing temperature

Generally, higher temperature increases the rate of strength development of portland cement concrete and portland-fly ash concrete, particularly at early age. At temperature higher than 80 °C, however, portland cement concrete experiences strength reduction while the fly ash concrete still show large increase in strength (5).

4. Test program

Fly ash samples were obtained from Mae Moh electricity generating facility. Four samples were used, all collected from the same generating plant. Fly ash T was collected from unclassified collector. Fly ash A and C were collected after classification with fly ash A being the coarsest and fly ash C being the finest. The samples were tested for chemical composition and particle size distributions. The results are shown in Table 1 and 2.
The fly ash was mixed with Type I Portland cement at the proportion of 0%, 20%, 30% and 40% cement replacement by weight. Each binder was used to manufacture concrete specimens with binder content of 480 kg. per cubic meter of concrete for all mixes. The specimens were 75 mm. cubes. The water to binder ratios were 0.40, 0.45 and 0.50. The specimens were tested for slump and then divided into three sets for curing at room temperature (28 °C) and at 40 °C and 60 °C respectively. They were then tested for compressive strength at 7 and 28 days.

5. Test results

The results of slump tests are shown in Table 3. It can be seen that inclusion of fly ash in the mix sharply increased the slump. For water/binder ratio of 0.45, the increase was from 8.3 cm. for the control mix to an average of 15.0 cm. for mixes with 20% replacement with fly ash. The slump increases were larger with higher replacement percentage. The average slump values of 18.4 cm. and 21.0 cm. were found for 30% and 40% fly ash replacement respectively. The same trends can be seen for water/binder ratio of 0.40 and 0.50. The results were as expected. The spherical shape of the ash is known to help reduce interparticle friction and hence increase the flow of the composite mixtures. However, the finer particle sizes produce an increase in overall specific suface of the binder phase and, in some cases, result in an overall increase in water demand. For

the fly ash used in this study, the latter trend was probably smaller than the lubricating effect of the ash.

The results of effect of curing temperature on the compressive strength of fly ash concrete, for water/binder ratio of 0.45, are shown in figures 1, 2 and 3, for fly ash T, A and C respectively. It can be seen that, as expected, the higher the curing temperature, the more rapid the strength development. This trend is very clear at 7 days age, even for mixes with 40% cement replacement. However, it can be seen that curing at 60 °C resulted in a relative drop in the rate of strength gain at 28 days. This behaviour has been observed in portland cement concrete, and probably results from the same mechanisms. Again, the same trend was observed for water/binder ratio of 0.40 and 0.50.

The effects of particle sizes and their distribution are shown in figures 4, 5 and 6 for replacement percentages of 20, 30 and 40 percent, respectively. It can be seen that fly ash C, the finest sample of the three, contributed most to the strength development of the fly ash concrete. The influence is clear and consistent for all replacement percentages studied. The same influence can be seen for water/binder of 0.40 and 0.50. These trends are as expected, since the smaller size yields larger specific surface, the site for chemical reactions. The larger the site, the faster the reaction rate.

6. Conclusion

1. For the fly ash used in this study, the inclusion of fly ash in the binder phase helps increase slump to a very high degree.
2. Higher temperature increases the rate of strength development. However, at 28 days, relative drop in the rate of strength gain was observed for specimens cured at 60 °C.
3. Small, plant classified, fly ash particle size contributes positively to the rate of strength development, probably because of the larger specific surface.

Reference

1. Kokkamhaeng, S. 1998. Utilization of Mae Moh lignite fly ash in roller compacted concrete dam in Pak Mun. Proceedings, 6th CANMET /ACI International Conference on Fly Ash, Silica Fume, Slag and Natural Pozzolans in Concrete, Bangkok, 1998. Supplementary Paper, pp. 17-31.
2. Akram, M. and Nimityongskul, P. 1998. A Model for Predicting Strength Development of Fly Ash Concrete. Proceedings, 6th CANMET /ACI International Conference on Fly Ash, Silica Fume, Slag and Natural Pozzolans in Concrete, Bangkok, 1998. Supplementary Paper, pp. 33-48.
3. Ravina, D. 1980. Optimized Determination of PFA (fly ash) fineness with reference to pozzolanic activity. Cement and Concrete Research, 10: 573-580.
4. Cabrera, J.G., and Gray, M.N. 1973. Specific Surface, pozzolanic activity and composition of pulverized fuel ash. Fuel, 52: 213-219
5. Owens, P.L., and Butler, F.G. 1980. The reaction of fly ash and portland cement with relation to the strength of concrete as a function of time and temperature. Proceedings, 7th International Congress on the Chemistry of Cement, Paris, France, v. 3. Pp. 60-65.

Table 1 Chemical composition of fly ash

Type of fly ash	Chemical composition (wt.)								
	SiO_2	Al_2O_3	Fe_2O_3	CaO	K_2O	MgO	SO_3	Na_2O	MnO
T	41.86	25.17	12.84	9.59	3.11	2.03	1.28	1.10	0.06
A	46.46	27.87	11.87	5.98	3.32	1.79	0.95	0.98	0.05
C	36.57	21.68	13.24	14.16	2.97	2.18	3.75	1.32	0.12

Table 2 Physical properties of fly ash

Physical properties	Type of fly ash		
	T	A	C
Specific gravity	1.92	1.63	2.58
Blaine specific surface area (cm^2/g)	3233	3122	7290
Volume weight mean diameter (μm)	67.68	108.1	4.87
% Retained on a 45 μm sieve	39.5	53.3	1.0

Table 3 The result of slump and compressive strength tests

W/B (ages)-Temp	75 mm. Cubes. Compressive strength (ksc)									
	control	fly ash T			fly ash A			fly ash C		
	0%	20%	30%	40%	20%	30%	40%	20%	30%	40%
0.40 (7) - R	470	443	368	323	429	371	322	521	430	388
0.40 (7) - 40	487	485	418	390	472	399	382	544	459	438
0.40 (7) - 60	508	508	454	442	509	432	425	608	516	475
0.40 (28) - R	589	606	533	479	558	512	464	711	679	612
0.40 (28) - 40	607	621	573	517	593	561	517	754	717	666
0.40 (28) - 60	554	534	471	458	532	454	439	619	559	494
slumps (cm.)	3.0	4.5	8.5	12.5	4.3	6.8	11.5	6.0	10.5	14.0
0.45 (7) - R	405	380	328	293	389	339	298	460	381	347
0.45 (7) - 40	446	444	377	337	435	366	351	501	428	404
0.45 (7) - 60	447	471	404	391	482	382	387	519	452	416
0.45 (28) - R	507	533	444	411	519	451	413	632	607	554
0.45 (28) - 40	509	538	489	426	556	487	470	675	655	590
0.45 (28) - 60	480	487	435	408	497	403	395	535	516	440
slumps (cm.)	8.3	15.3	18.3	20.3	15.0	17.8	20.8	14.8	19.0	22.0
0.50 (7) - R	357	350	285	251	335	274	245	377	314	300
0.50 (7) - 40	390	374	308	288	369	300	281	423	389	357
0.50 (7) - 60	414	397	348	324	406	322	309	440	400	372
0.50 (28) - R	462	468	371	342	460	362	337	528	492	454
0.50 (28) - 40	478	494	410	385	472	400	375	559	524	482
0.50 (28) - 60	420	431	362	334	415	338	320	457	419	380
slumps (cm.)	18.5	21.0	23.5	>25	20.8	22.5	25.0	22.0	25.0	>25

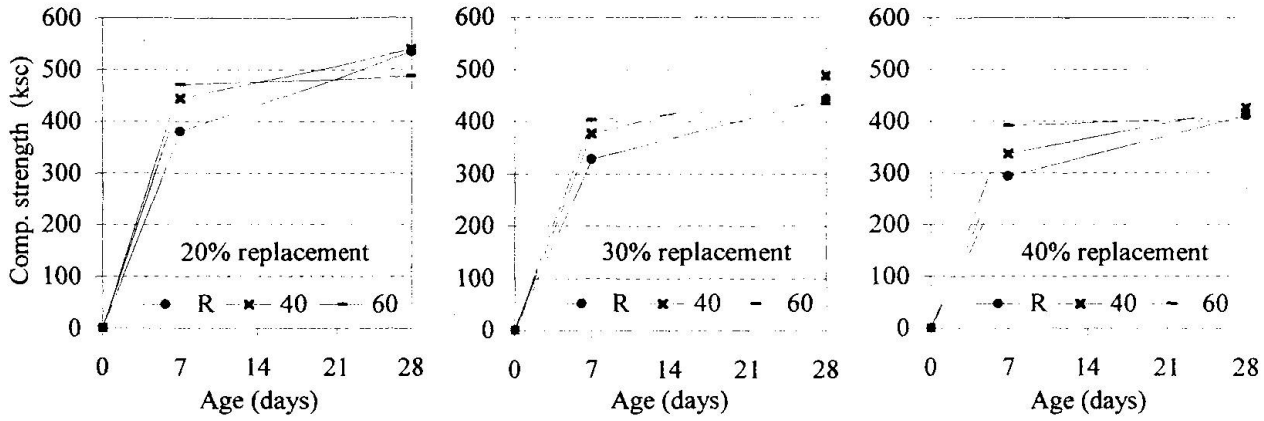

Fig. 1 Effect of temperatures on compressive strength for fly ash T concrete (W/B = 0.45)

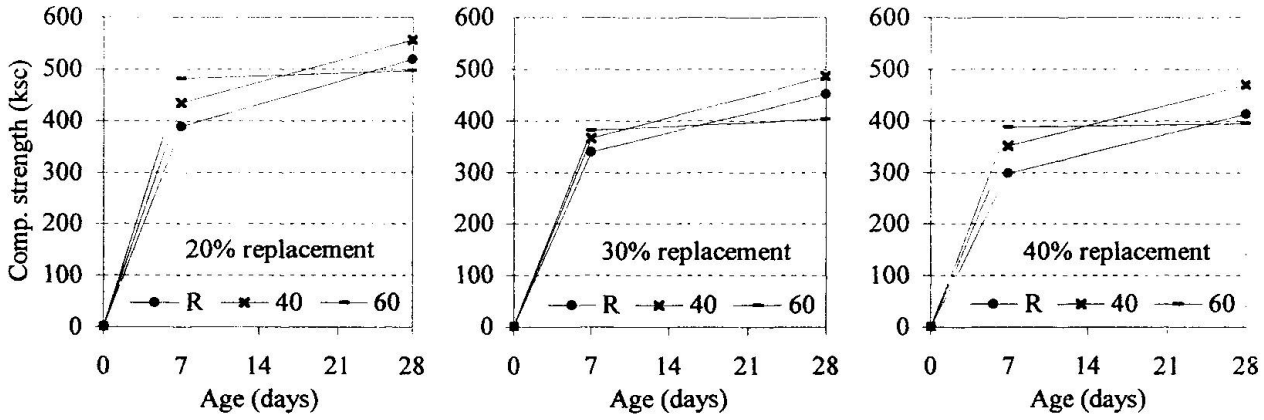

Fig. 2 Effect of temperatures on compressive strength for fly ash A concrete (W/B = 0.45)

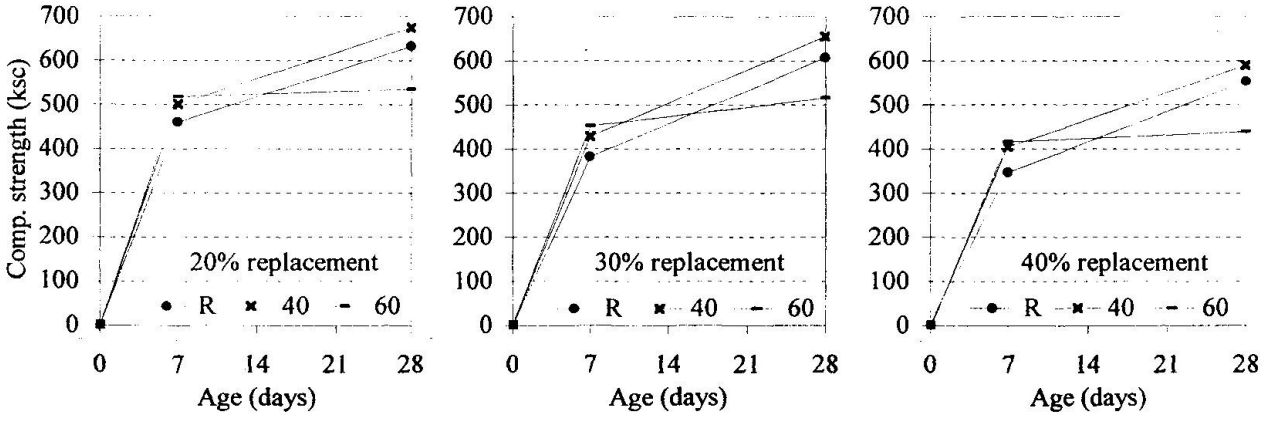

Fig. 3 Effect of temperatures on compressive strength for fly ash C concrete (W/B = 0.45)

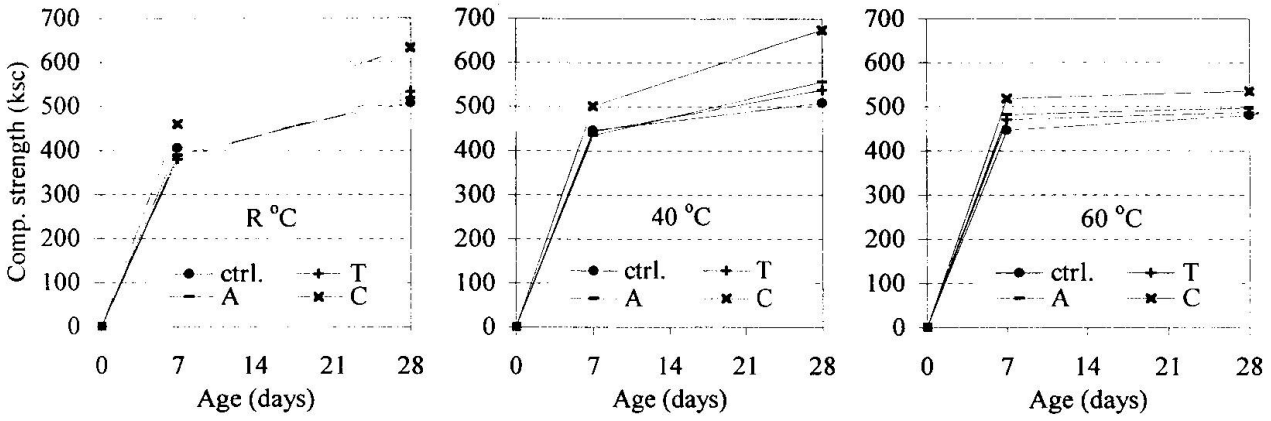

Fig. 4 Type of fly ash on compressive strength at 20% replacement (W/B = 0.45)

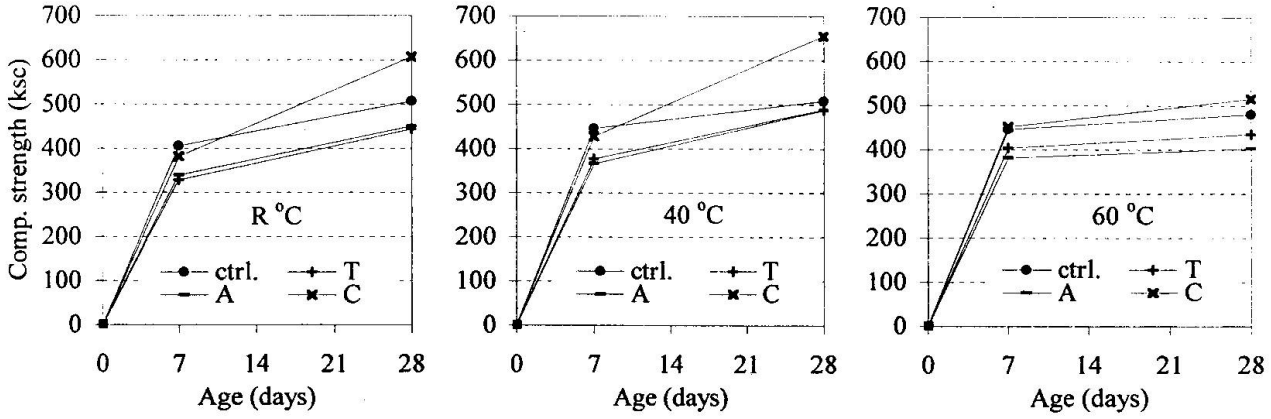

Fig. 5 Type of fly ash on compressive strength at 30% replacement (W/B = 0.45)

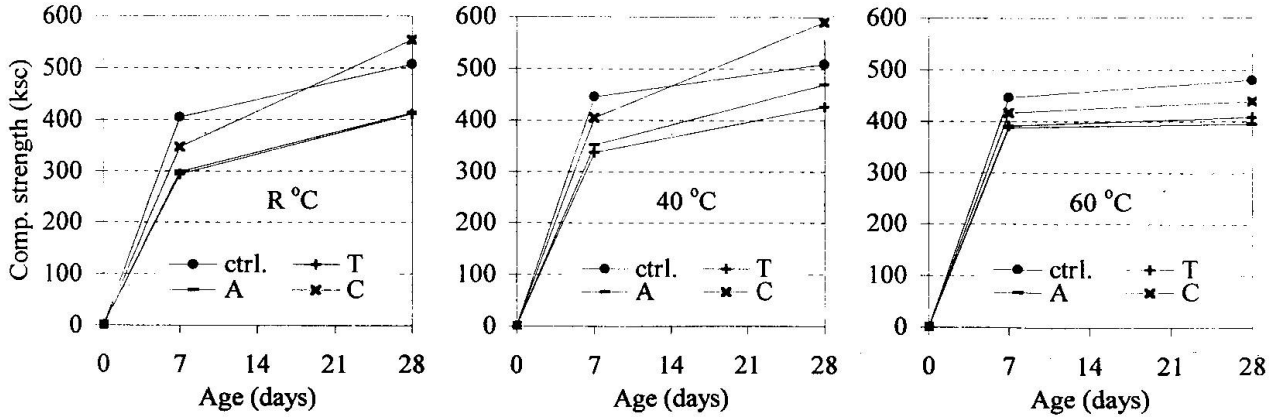

Fig. 6 Type of fly ash on compressive strength at 40% replacement (W/B = 0.45)

A Quality Control Method of Concrete of Tall Composite Pier Construction

Toshiaki KATO
Registered Civil Engineer
Manager of Design Dept.
Obayashi Co.
Tokyo, Japan

Masaru KOBAYASHI
Manager of structural Engineering Division
Japan Highway Public Co.
Sendai, Japan

Summary

The steel pipe-concrete composite pier exhibits not only high seismic performance in effect of ductile steel pipes and spiral high strength strands, but also a rapid construction method. In concrete works such as high pier construction, the quality control for the mass concrete is necessary. Especially in the steel pipe-concrete composite pier, it is important to control thermal cracks caused by section characteristics, and the curing is also important after placing concrete, because curing period is very short for rapid construction. As for materials of concrete, usage of low heat cement is effective to reduce the thermal stress due to the temperature rise. In this paper the concept of construction method (Hybrid-Slipform Method), the quality control method and requirements for mass concrete are described.

1. Introduction

The recent lessons of structural damages occurred to the number of bridge substructures during 1995 Earthquake in Kobe make a new bridge construction more expensive and time consuming because of the high standard of earthquake resistant design. The construction of Yamagata Expressway in the northern part of Japan includes Ouami River Bridge (544m) and Koami River Bridge (627m), where the Ouami has two tall piers of 60.5m and 47.5m high, and the Koami has five piers of 37m, 75m, 70.5m, 48.5m, and 36m high. (see Fig. 1, Fig. 2)

Those two bridge piers are required to be built within a reduced schedule in the heavy snow country. Snow closes the site 5 months, and it usually starts in the beginning of December and melt in the end of April. In order to speed up the expressway service earlier, the jobs on the critical path, which means the bridge construction, are needed to reduce the construction period. Additionally, the other issues promote a drastic improvement of pier construction in the both of design and site operation, such as :

- Structural reinforcement to improve the shear strength and ductility against

earthquake shaking

- Safety protection of the site operation at high position
- Reduce the number of skilled labor

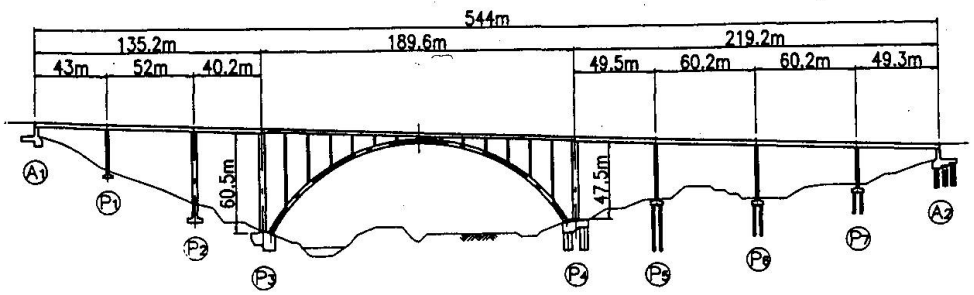

Fig.1 General Plan of Ouami River Bridge

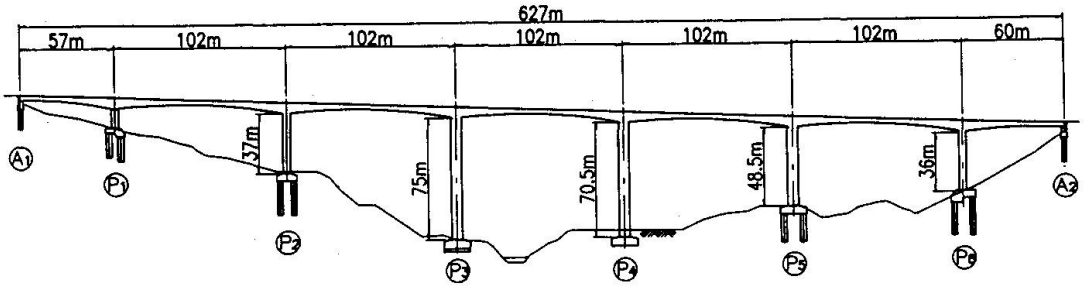

Fig.2 General Plan of Koami River Bridge

2. Concept of Hybrid-Slipform Method

The design of a conventional reinforced concrete pier may be an appropriate solution in terms of material efficiency and cost, while the overall construction cost as well as the construction period may not be optimum. The left hand side of Fig. 3 shows a typical configuration of the conventional hollow type structure, which has one- or two-boxes. The right hand side of Fig. 3 illustrates a typical cross section of the Hybrid- Slipform design, which is a composite structure of the steel pipe and the minimum amount of reinforcement.

A long term social trend in labor market is the shortage of skilled labor and the decrease of annual working hours. This trend enhances the engineering development for a drastic improvement of construction time and labor force required for the bridge construction. The constructor's goal of Hybrid-Slipform method is one half in construction time and one third in labor input compared to the conventional design and jump-form construction. Fig 4 illustrates the equipment and structural arrangements of the new method.

The construction sequence of the method is described in Fig. 5. The first step of construction is the erection of prefabricated segment of steel pipes, which length is about 10m long each. Those erected steel pipes have the structural stability against the wind load until the concrete

is placed. At every 10m of the pipe segment erection, the group of steel pipes is strengthened by bracing, connecting each pipe together. When the erection reached to the pier top, a reaction frame is installed and fastened at the pipe head. The reaction frame supports the vertical slipforming load transmitted through the vertical tension wires made of the standard strands.

The second step follows the assembly of slipform, working decks, scaffold and jacking system(6 center hole jacks). The slipform system has four working decks. The top deck has a loop of rail track where the automated pc strand feeder runs on the track. The main deck is used for the jobs of formwork, re-bar installation, concerning and jack operation. The lower decks are for the removal of Sheet-in-Form and the work of concrete curing. In stead of a sophisticated computer control for jacking system, the manual operation is used to lift the scaffold up 2.7m every day.

Once completed the slipform installation, the highlight of Hybrid-Slipform Method begins with the pier construction by the daily repetition of jobs sequence. The cycle consists of the jack up of the slipform system, the placement of Sheet-in Form, the concrete work, and the re-bar installation. The height of concrete placed by each daily cycle is planned to be 2.7m for this project.(see Fig.6)

The old Sheet-in-Form persists its position and is remained at the old position of concrete placed on the previous day. As soon as the scaffold is settled to the new position, the new Sheet-in-Form is placed for the next concrete pouring. The advantages of utilization of the sheet-in-form are significant : a smooth surface finish of concrete as same as the fixed form, a drastic change of the slipforming procedure from continuous from lifting to at once lifting at any time, a better curing protection to the concrete surface, and more easier positioning of the slipform. (see Fig.7)

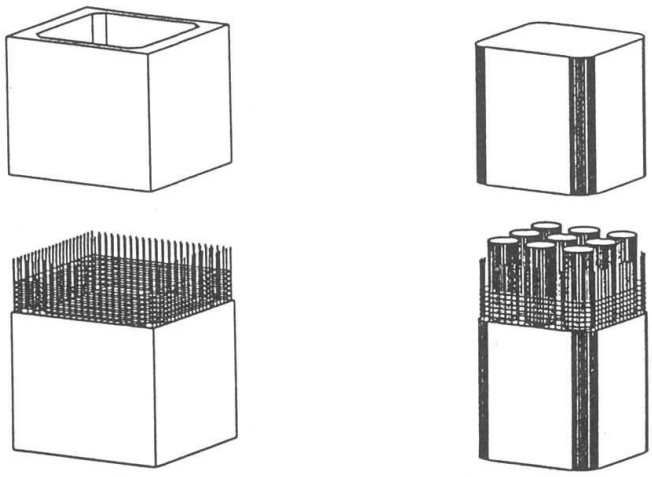

A. Conventional B. Hybrid-Slipform Alternative

Fig.3 Structural Concept of Conventional and Hybrid-Slipform Alternative

The horizontal reinforcement of pc strand is spiraled along the vertical reinforcement by using the automated strand feeder. The placement takes one and a half hour by a few workers, which is needed for fastening the strands to the vertical re-bars. When the slipform has reached to the final elevation of pier structure, the working decks and scaffolds are easily lifted down together to the ground by the reversal use of jacking system. During the down ward process, any necessary finishing job for the concrete surface of pier can be done by using the working decks. (see Fig.8)

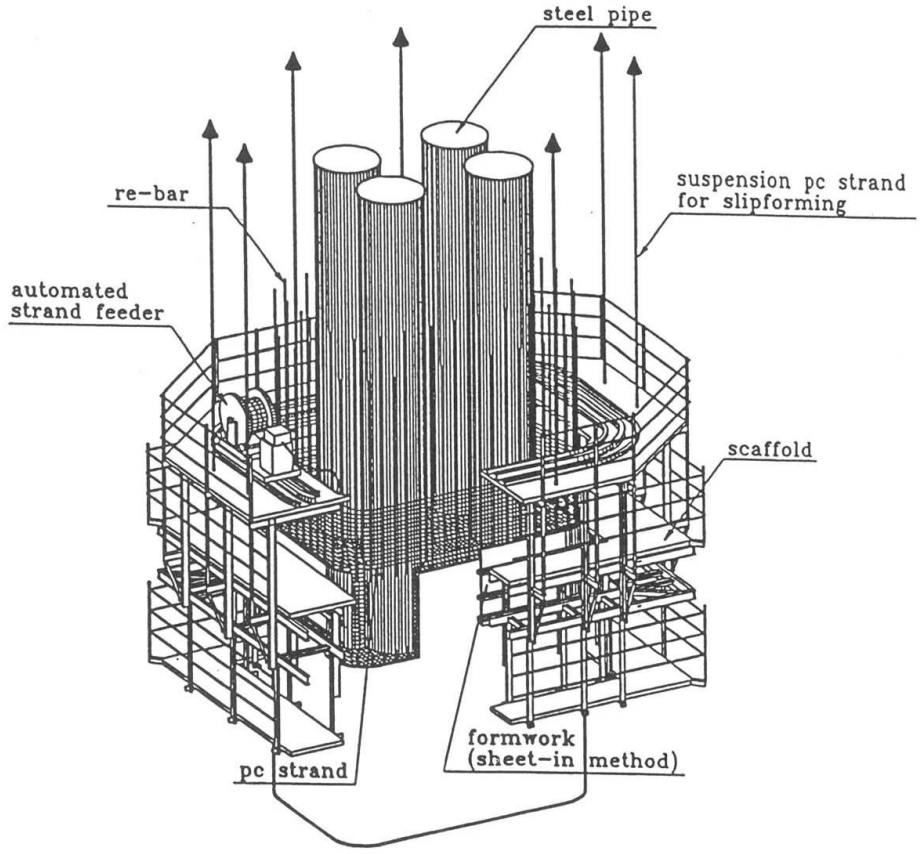

Fig.4 Illustration of Structural System and Equipment of Hybrid-Slipform Method

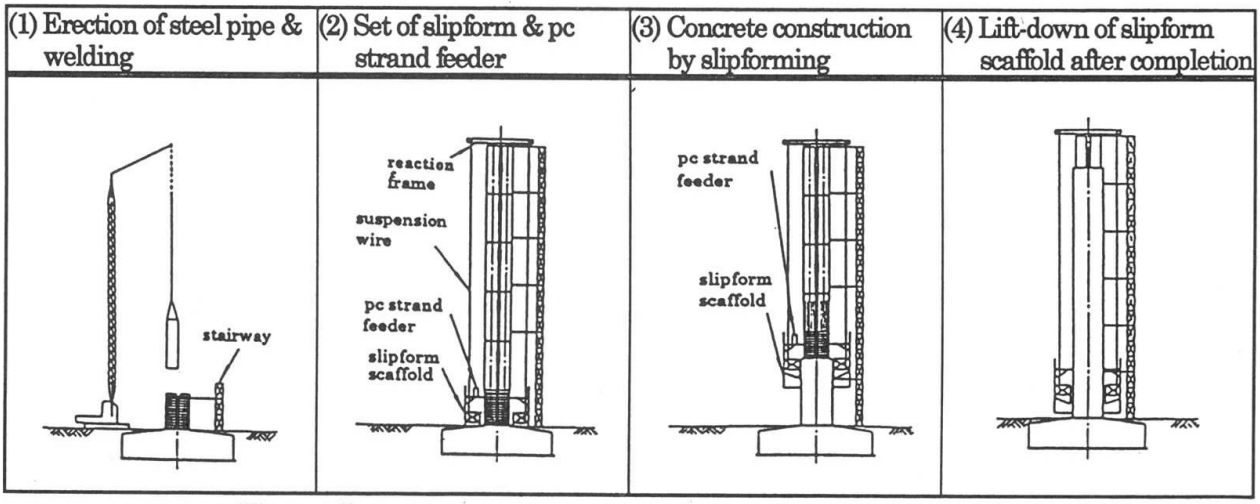

Fig.5 Construction Procedure of Hybrid-Slipform Method

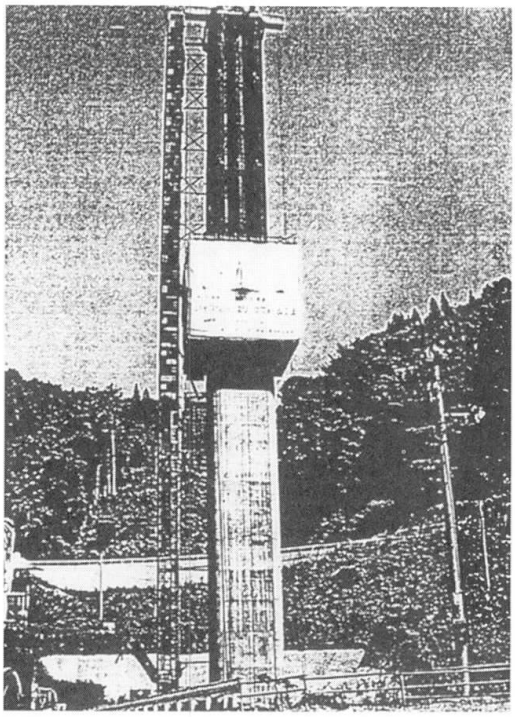

Fig.6 Hybird-Slipform method construction

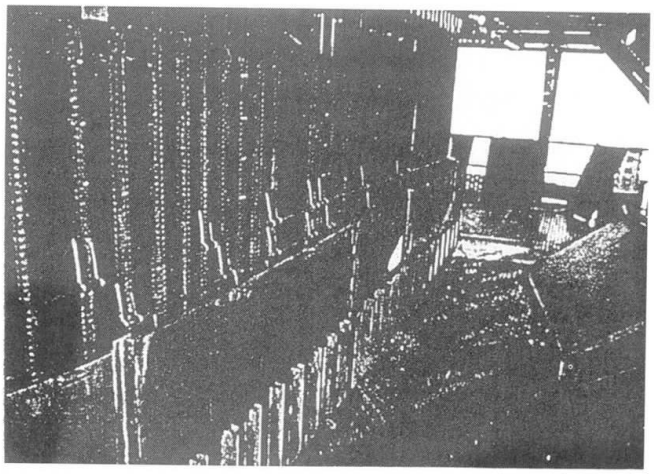

Fig.7 Installation of Sheet-in-form

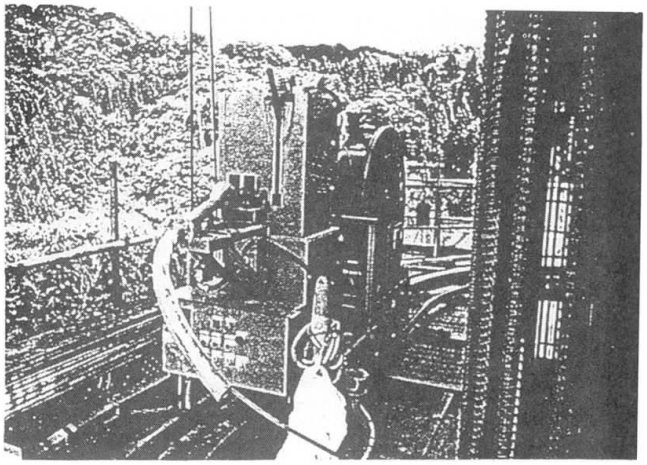

Fig.8 Automated PC strand Feeder

3. Control of cracks by low heat cement

In concrete works such as high pier construction, the quality control for the mass concrete is necessary. Especially in the steel pipe-concrete composite pier, it is important to control thermal cracks caused by structural characteristics i.e. unbalanced section (see Fig.9), temerature difference between surface and core. A possible crack width has been estimated by FEM analysis. The analysis result shows that in the case of using normal portland cement the crack width is possible to exceed allowable width (see Table 1) and usage of low heat cement is effective to reduce the thermal stress due to the temperature rise.

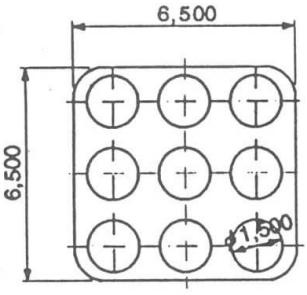

Fig.9 section of composite pier

Table 1 Permisible crack width ωa (mm)

Type of reinforcement	Environmental conditions for corrosion of reinforcement		
	Normal environment	Corrosive environment	Severely corrosive environment
Deformed bars and plain bars	0.005C	0.004C	0.0035C
Prestressing steel	0.004C	–	–

C : concrete cover (in this case = 70mm)

4. Evaluation of concrete strength based on temperature measurement

In Hybrid-Slipform method it is necessary to check the real time concrete strength in an early age for rapid construction. For this purpose the estimation method which is calculated by integrated temperature (maturity) has been used. A temperature of concrete is measured by thermos-sensor. The checked strength of concrete are as follows:

- Concrete strength at the lift up time of slipform
- Concrete strength at the end of curing
- Concrete strength at 91 days (design strength)

Table-2 shows the tolerance of concrete strength for each step.

Table 2 Quality control of concrete

Items	Minimum compressive strength (N/mm^2)	Evaluation method
lift up of slipform	$\sigma \geqq \alpha\ \omega\ h$ α : safety factor (=2.0) ω : unit weight of concrete h : hight for each lift	measurement by thermos-sensor
Removal of forms (end of curing)	ordinary weather 3.5	measurement by thermos-sensor
	cold weather 5.0	
Design strength	30 (in this design)	test on specimens

5. Conclusions

The Hybrid-Slipform method provides an appropriate solution not only for rapid construction, but also for the ductile structural performance suitable for the tall bridge pier particularly in a highly seismic region. In this new construction method it is important to control and check the concrete strength at early ages. The strength evaluation method by temperature measurement using thermos-sensor is available for this purpose. And also low heat cement is quite effective in controling thermal cracks of mass concrete.

References

1) Standard Specification for Design and Construction of concrete Structures, 1996, JSCE

Precast Concrete Integrated Deck System for Highway and Railway Bridges

Adel R. ZAKI
Adjunct Professor
McGill University
Montreal, QC, Canada

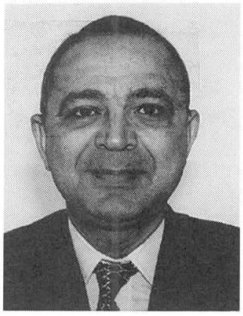

Prof. Adel Zaki is Senior Consultant Engineer. He received his Civil Engineering Degree in 1972 from Cairo Univ., Egypt. He spent 20 years in the field of design and assessment of highway and railway bridges and developed an expertise for the use of integrated deck system in Canada and South East Asian.

Mohamed LACHEMI
Assistant Professor
Ryerson Polytechnic University
Toronto, ON,Canada

Dr. Mohamed Lachemi received his M.A.Sc. and Ph.D. in Structural Eng. from Sherbrooke Univ., Canada. His areas of interests include finite element analysis of reinforced concrete structures, instrumentation and field monitoring of structures, and use of high-performance concrete in bridges.

Summary

The aim of this paper is to share information and design experiences gathered by the authors relating to the use of integrated deck system for highway, railway and pedestrian bridge superstructures. Instead of a comparison between different codes, a number of selected projects dealing with either the North American Model or the Asian Model and involving the use of high-performance concrete are presented. Each case study discusses the rationale for selecting the structural system over other alternatives. After model restrictions have been taken into account, the final selection of a particular structural type usually hinges on economic factors.

1. Introduction

The first precast prestressed concrete Railway Bridge was constructed in 1954 for the Chicago Burlington and Quincy Railroad, Missouri. Since then, many short and medium span bridges constructed by using prestressed precast concrete girders have been successfully built in North America [1,2]. Many prefabricated elements and systems have been standardised for integrated deck bridge construction. These prefabricated elements and systems can be used with less disruption at the job site, can reduce much of the environmental impact in the surrounding areas during construction, can reduce design effort, and can speed up field construction, saving time and cost. Details regarding the different standard elements can be found elsewhere [3,4].

In recent years, the accelerated deterioration of bridges and the cost of their repair and rehabilitation have been become a major concern. Many steel bridges in South East Asia were constructed in the last decades under European standard specifications. Regional social culture and other environmental parameters have created geographical "corrosive areas" within which these specifications have proven sub-optimal when considering the life-cycle cost of the bridge. On Java Island, Indonesia, the primary concern for the railway bridge superstructures is the deep corrosion in many steel bridge decks that result from exposure to human waste and from insufficient routine maintenance.

Through his recent experience with the government-owned Indonesian Railway System, the first author suggests an optimised methodology for bridge superstructure replacement and the construction of new short and medium span bridges in corrosive areas. This involves the construction of prestressed precast high performance concrete girders. The durability of the material and the reduced erection time provide economical benefits.

This state-of-the-art design is based on an integrated deck system for highway, railway and pedestrian bridge superstructures. This calls for the use of prestressed precast high performance concrete solid slab, channel sections, hollow box girders or Bulb-Tee girders, for spans ranging from 7 to 35 meter long. The compressive strength of high performance concrete ranges from 50 to 70 MPa. Details concerning these alternatives and the use of precast concrete slabs with ballasted deck on steel railway bridges are given in this paper.

2. Case Studies

Some projects involving the use of precast high performance concrete integrated deck systems, which are familiar to the authors, are selected. These projects are used to illustrate different factors, which have influenced the use of the structural system for economic reasons. In each case, a general description that touches, among other things, the suitability of using high-performance concrete for that particular application is given. The selected case studies, which are considered under either the North American Model or the Asian Model, are described hereafter.

2.1 The North American Model

2.1.1 Example 1 – Roadway Bridge

In 1992, an existing short-span bridge located in St-Eustache, Qc, Canada, was evaluated. The original bridge consisted of a steel beam girder with a cast-in-place concrete deck slab. The steel beams showed signs of significant corrosion and the deck slab had suffered deterioration. An evaluation and bridge rating procedure was carried out and it was found that the deterioration was such that the bridge would either have to be posted, rehabilitated or replaced. Because of the repair costs together with the short future life of the original bridge, it was determined that it was more economical to replace the bridge superstructure.

Two alternatives, a composite steel girder superstructure and a precast pre-tensioned girder superstructure, were studied. The precast pre-tensioned girder solution utilised high-performance concrete in the girder and was the more economical solution. One of the key features in the economical study was the extended life of the high-performance concrete used to construct the girders [5].

Fig. 1 shows the cross section of the final solution. The bridge spans 17 m centre-to-centre of bearings. The girders are supported on neoprene bearing pads. The channel-shaped girders each contained 24 – 15-mm pre-tensioned strands that had straight tendon profiles. Diaphragms were placed over the supports only. Each channel-shaped girder is 950 mm deep and 1200 mm wide. The surface created by placing the girders side-by-side eliminated the need for formwork for the cast-in-place deck slab. The concrete for the precast pre-tensioned bridge girders had a specified 28-day compressive strength of 70 MPa. It is important to note that the structural design of this bridge did not require a high-performance concrete. The stresses in this short-span bridge were

well within acceptable limits, even with normal strength concrete. The reason for using the high-performance concrete was to improve the durability and therefore extend the expected useful life of the bridge.

The deck slab had a 28-day specified compressive strength of 30 MPa. The deck slab was made composite with channels by roughening the top surface of the channels during casting and by providing small shear keys in the corners of the precast channel members. A waterproof membrane was applied to the top surface of the deck slab before asphalt was added to the surface.

2.1.2 Example 2 – Pedestrian Bridge

In 1992, an existing pedestrian bridge, crossing a six lane highway (3 lanes in each direction plus a central median and 2 shoulders), was examined in Laval, Qc, Canada. The original concrete pedestrian showed signs of significant concrete deterioration and reinforcement corrosion. A decision was taken to replace the bridge and precast elements solution offered the most economical solution.

Fig. 2 shows the cross section of the new pedestrian bridge made with high-performance concrete. The bridge spans 35 m centre-to-centre of the neoprene bearings. The cross section consists of two Z-shaped precast girders with the shape providing a bottom ledge for supporting the precast panels for the deck slab. Each of the Z-shaped girders was pre-tensioned with 40 – 15-mm diameter strands. The depth of the precast pre-tensioned girders is 1370 mm and the widths are 250 mm. One of the key features of the design was the need for rapid erection to cause the least amount of disturbance to the traffic flow under the pedestrian bridge. The girders were erected in one evening to limit the disruption of traffic. The Z-shaped girders are structurally interconnected at both supports and at midspan by casting concrete in 300-mm thick reinforced concrete closure strips. These closure strips produce a U-shaped cross section at these locations and serve as structural diaphragms. The diaphragms served to connect the girders to enable sharing of vertical loading and to interconnect the Z-shaped girders to aid in resisting torsion.

The precast concrete panels were pre-tensioned with 13-mm diameter strands and were supported by the lower ledge of the girders. A latex modified concrete was cast-in-place to form the wearing surface of the bridge deck. The specified 28-day compressive strength of the concrete for the girders and the panels was 70 MPa.

2.1.3 Example 3 – Railway Bridge

The bridge is located at mileage 40 of the Drummondville subdivision, Qc, Canada, over the main line of the Canadian National (CN) Railway [6]. During periodic inspection of the structure, it was found that the open-deck bridge steel span, built originally in 1914, had become badly corroded and that immediate replacement was needed. The substructure, which consists of stone masonry abutment and wing-walls, was found in a good condition.

To promote competition and to achieve the most-cost-effective solution, two structure types were designed and tendered. The first alternative was a steel deck plate girder (DPG) span with a ballasted precast prestressed concrete deck slab (Fig. 3). However, CN Rail awarded the job to the lower bidder, who submitted a quote on the second alternative, which consisted of precast

prestressed concrete box girders. Besides a substantial economy in the basic cost and long term maintenance costs, the choice of precast prestressed concrete boxes allowed a more shallow structure that if the steel girder were to be used, a choice which proved to be very helpful in improving a restricted vertical clearance.

The single-span simply supported bridge spans 23 m, and it is designed for Cooper E-85 Railroad Loading. It is the longest precast prestressed span ever used by CN Rail. It is composed of 4-precast box girders (Fig. 4). Each girder is 1.70-m deep and 0.90-m wide, with transverse diaphragms at the fifth points. The girders were tied together by using 26-mm diameter DYWIDAG thread bars having an ultimate strength of 1034 MPa at diaphragms location, to carry a load of 240 kN each after seating of anchorages. After the transverse tie assemblies were in place, the anchors were grouted with non-shrink grout.

Each box girder was provided with 50 pre-tensioned 15-mm diameter stress-relieved strands having an ultimate tensile strength of 1860 MPa. The centre of gravity of these strands was set to be 330 mm from the bottom. In order to prevent tensile cracks at top of girder, caused by camber at release, the effective prestressing force had to be reduced. This was achieved by debonding 18 stands for a determined development length l_d where:

$$l_d = \text{Transfer Length} + \text{Flexural Bond Length}$$

2.2 The Asian Model

Through a World Bank funded Railway Efficiency Project for the Indonesian State Railway (Perumka), a bid package has been prepared in 1998 for the construction of several bridges in the double track section between Giganea and Sukatani corridor at central Java. Prestressed precast concrete girders, integrated system, have been proposed at the designated "corrosive areas" zone. Three different ballasted deck girder types were designed, according to their span length.

- Type 1: Prestressed Precast Concrete Box-Type Girder for span lengths of 16 to 19 m (See Fig. 5).
- Type 2: Prestressed Precast Concrete Channel-Type Girder for span lengths of 10 to 15 m (See Fig. 6).
- Type 3: Prestressed Precast Concrete Bulb-Tee Girder for span length of 20 m (See Fig. 7).

For these cases, the Railway bridge Live Load is in accordance with the Indonesian Load Scheme 1921.

3. Concluding Remarks

Premature deterioration of bridges has become a major problem in the last 30 years. The use of standard prestressed precast concrete integrated deck as a replacement of older superstructures or for new constructions offers an attractive alternative to insure a long-term durability especially in corrosive environment. It allows also achieving substantial economy, by minimising the disruption of traffic during construction. Furthermore, the use of high-performance concrete will allow the design of smaller sections, and with its low permeability and higher strength should result in improved durability and hence extended service life for bridges.

4. References

1. Goldberg, D. "Thirty Years of Prestressed Concrete Railroad Bridges," *PCI Journal*, **28**(5), Sept-Oct. 1983.
2. Dunker, K.F., Rabbat, "Performance of Highway Bridges," *Concrete International*, August 1990.
3. Lin, T.Y., Burns, N.H. "*Design of Prestressed Concrete Structures*," John Wiley & Sons, Third Edition, 1981.
4. Transportation Research Board, "Prefabricated Bridge Elements and Systems," NCHRP No. 119, August 1985.
5. Mitchell, D., Pigeon, M., Zaki, A.R., Coulombe, L.G. "Experimental Use of High-Performance Concrete in Bridges," Proceedings of the CPCA/CSCE Conference, 1993.
6. Zaki, A.R., "Duchene River Railway Bridge," *PCI Journal*, **34**(5), Sept.-Oct. 1989.

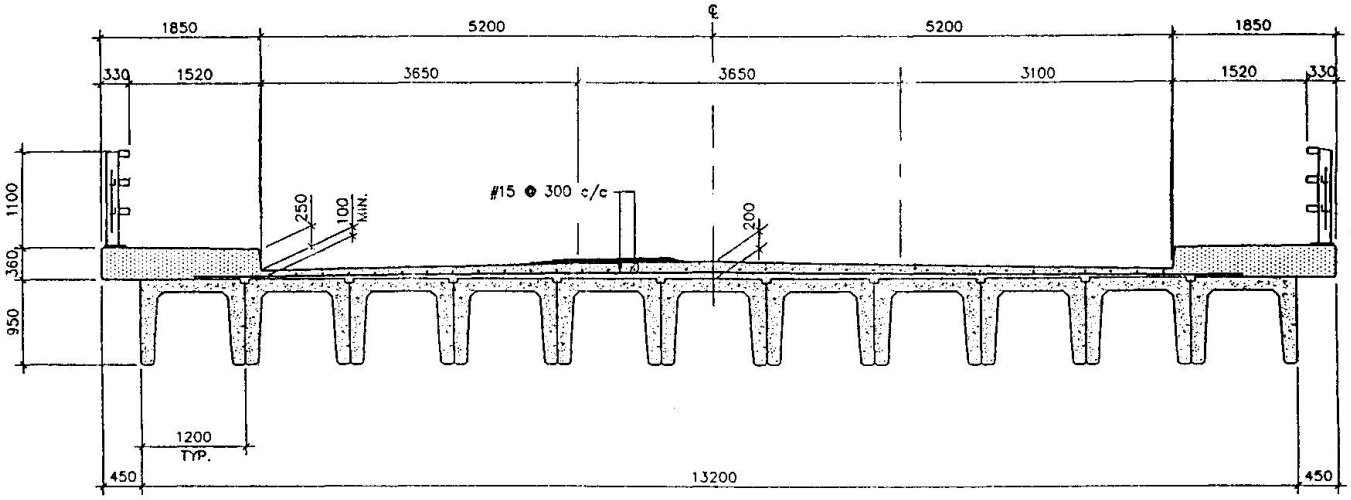

(a) Cross section of bridge

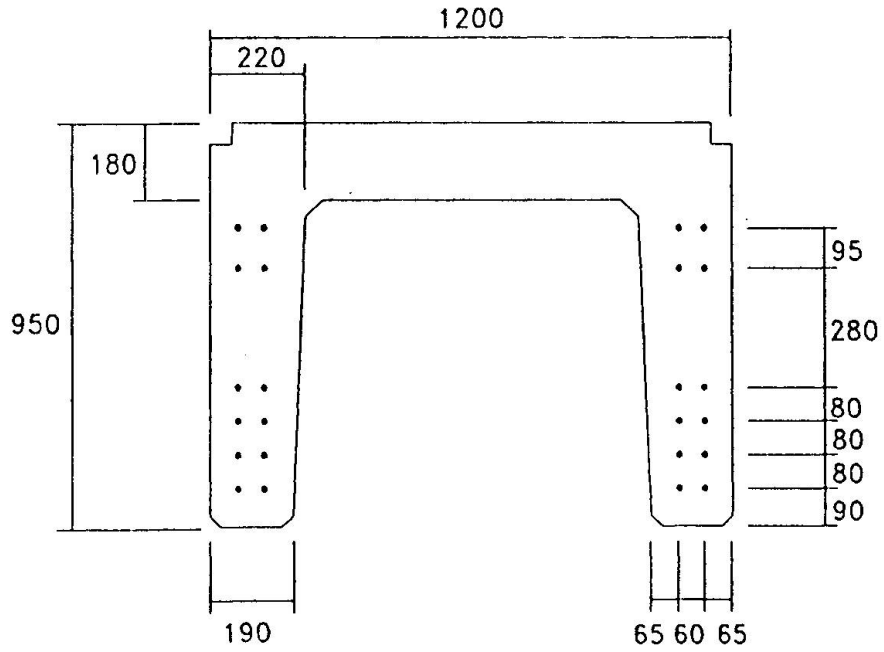

(b) Strand pattern (15 mm diameter strands)

Fig. 1 – Roadway Bridge

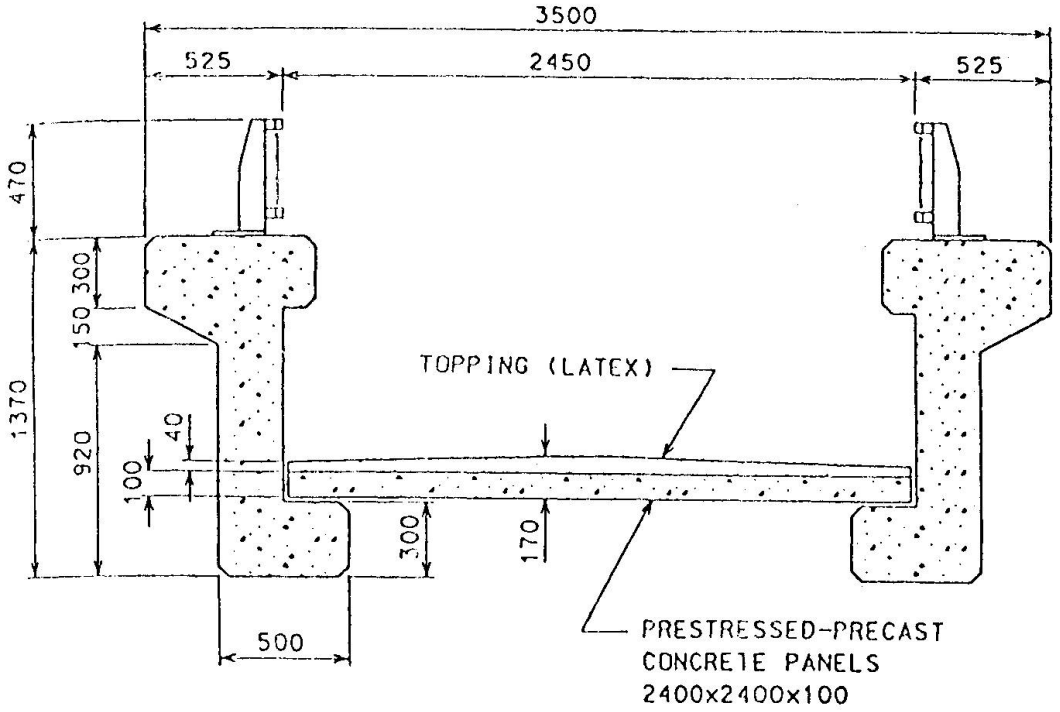

(a) Cross section of bridge

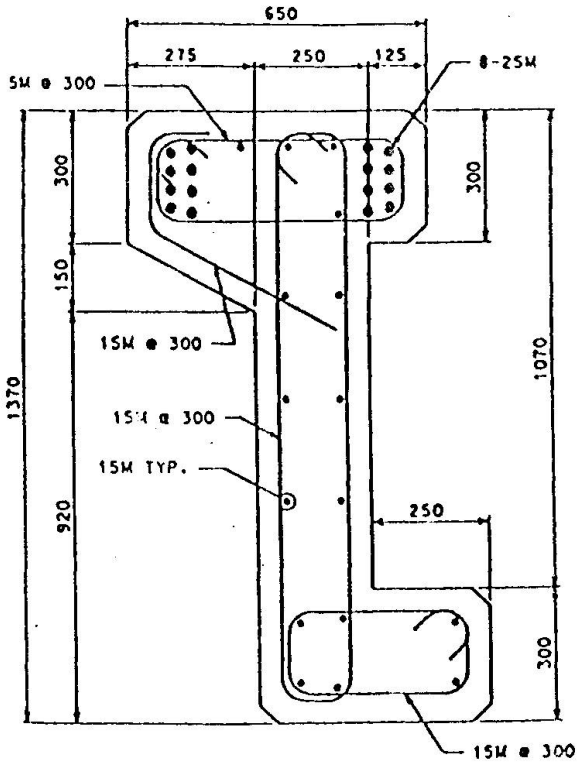

(b) Reinforcement

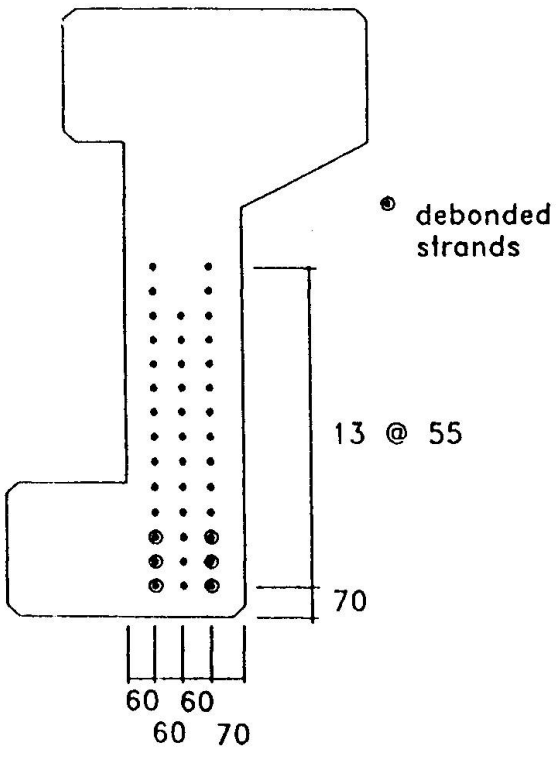

(c) Strand pattern (15 mm diameter strands)

Fig. 2 – Pedestrian Bridge

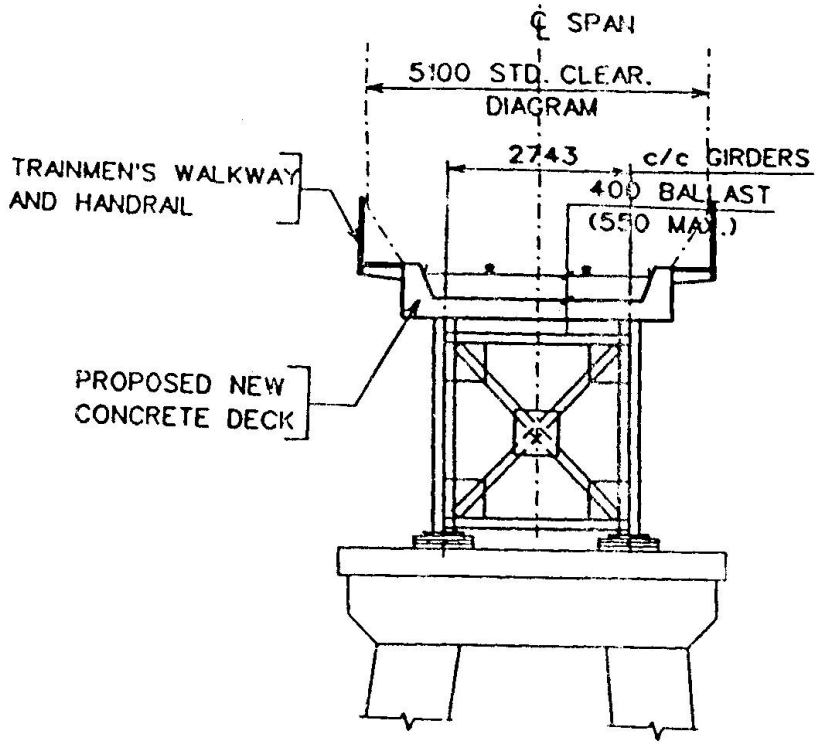

Fig. 3 – DPG Railway Bridge

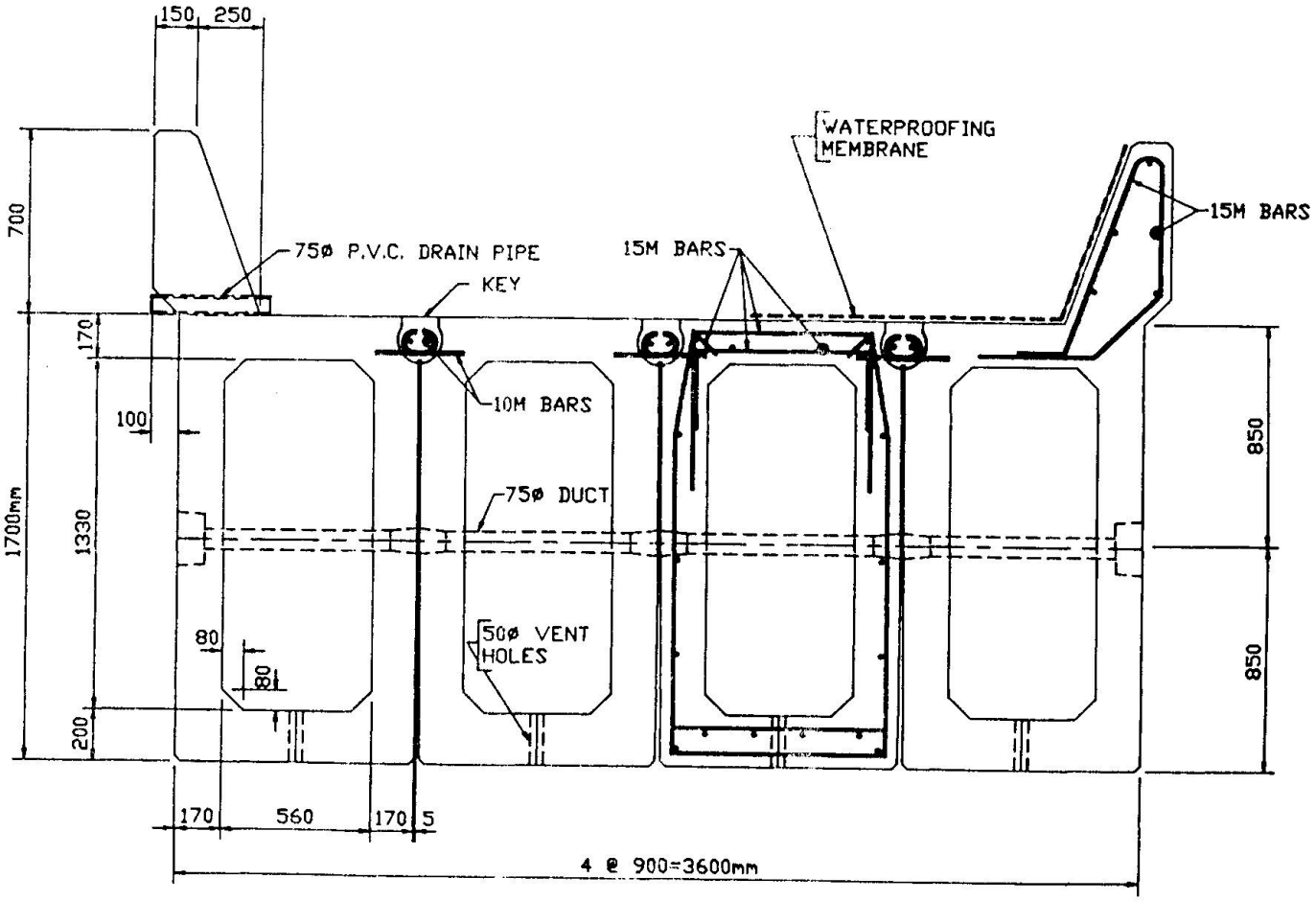

Fig. 4 – Box Girder Railway Bridge

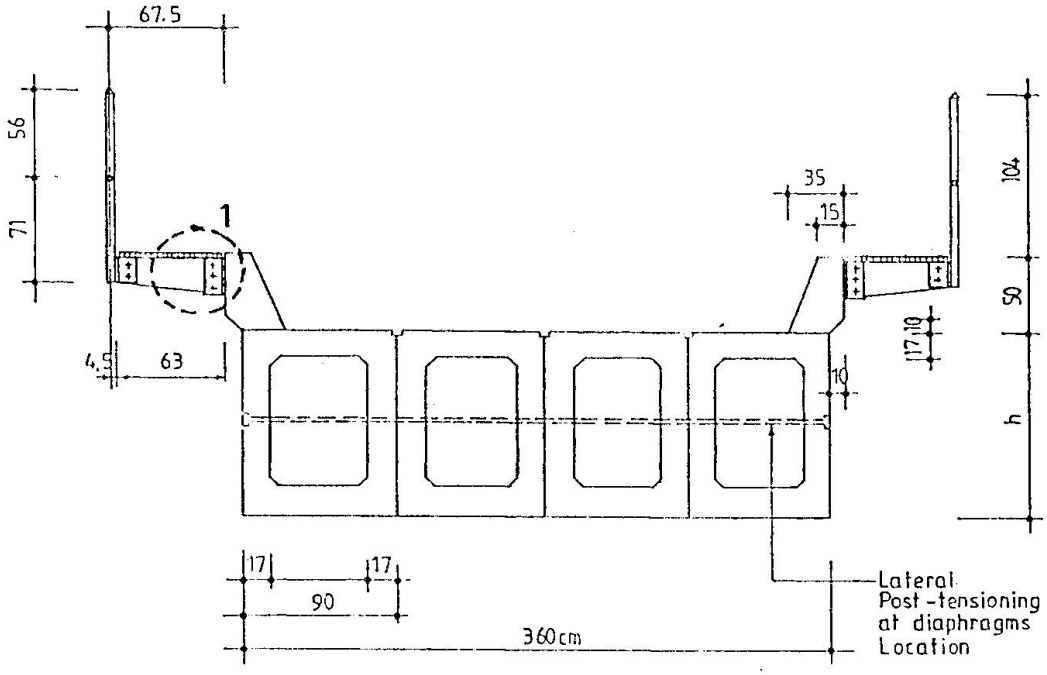

h = 123 cm For span = 18.60 meters
h = 110 cm For span = 16,70 meters

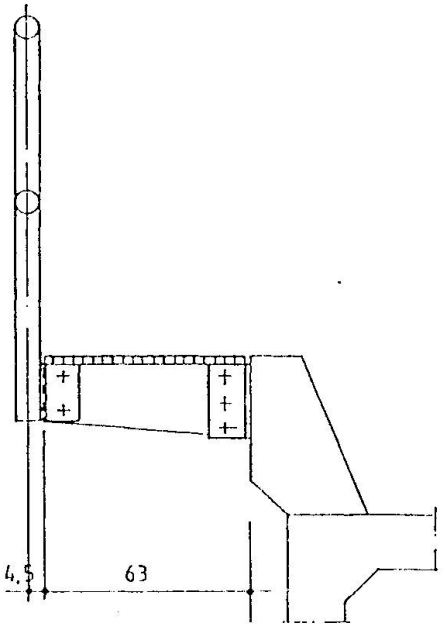

DETAIL 1

Fig. 5 - Box-Type Girder Bridge

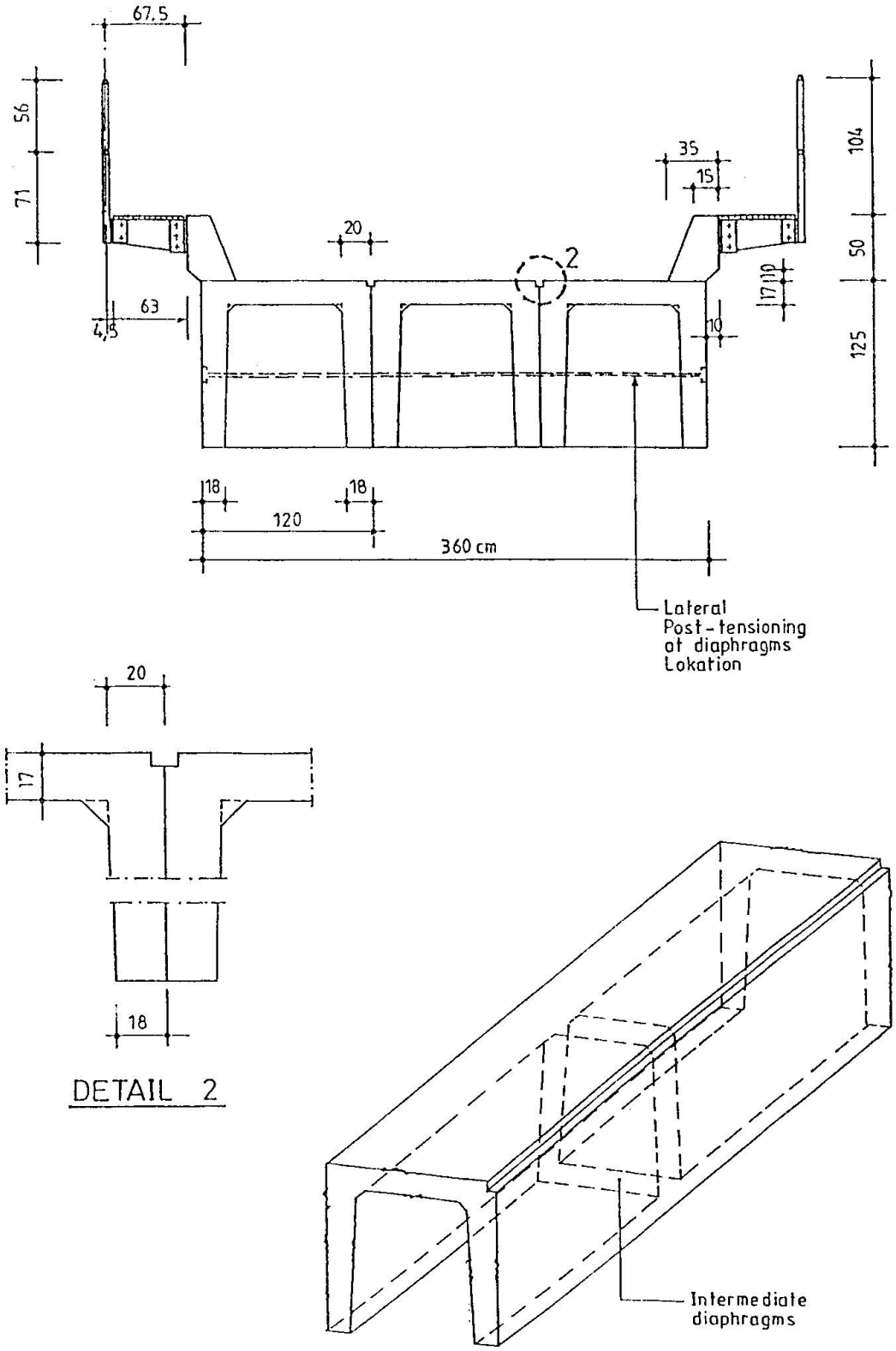

Fig. 6 – Channel-Type Girder Bridge

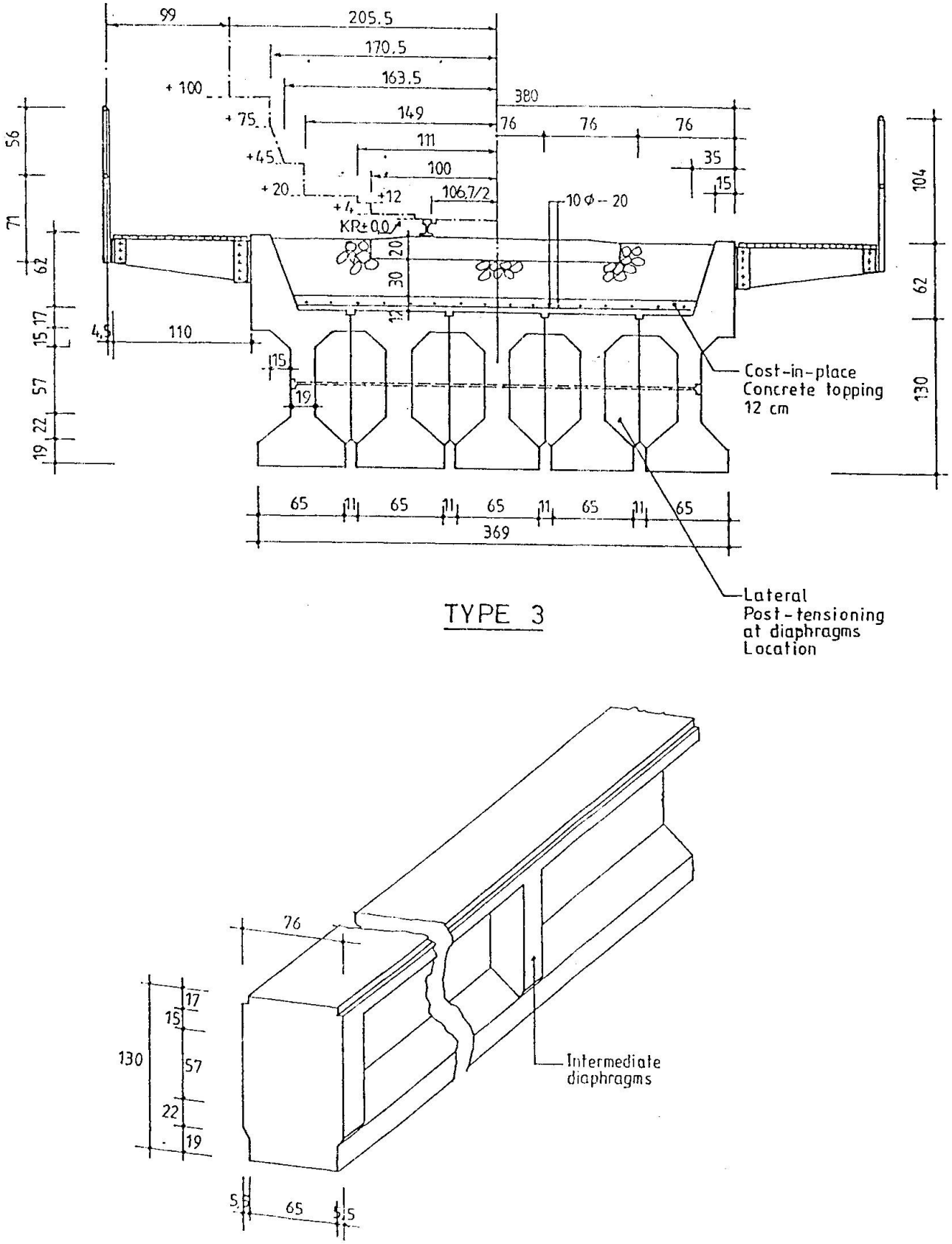

Fig. 7 – Bulb-Tee Girder Bridge

Reinforcing Method for R/C Suspended Slabs Connected to a Bottom Flange of H-shape Steel Beam

Koji YOSHIMURA
Professor
Oita University
Oita, JAPAN

Kenji KIKUCHI
Associate Professor
Oita University
Oita, JAPAN

Masayuki KUROKI
Research Associate
Oita University
Oita, JAPAN

Ikuo IIDA
President
Iida Design and Planning Office
Oita, JAPAN

Koji OKITA
President
Renace Institute
Oita, JAPAN

Takato MAEDA
Graduate Student
Oita University
Oita, JAPAN

Takafumi SASAKI
Graduate Student
Oita University
Oita, JAPAN

Summary

In order to propose a better reinforcing method for reinforced concrete (R/C) suspended slabs connected to the bottom flange of the steel H-shape beams in the steel building structure, nine full scale specimens with different slab-to-beam connection details were tested under monotonic vertical loading. Test results indicate that, in cases, where the bottom flange of the H-shape steel beam is located within the R/C floor slabs, special diagonal reinforcing bars are quite effective to prevent the occurrence of the brittle shear failure and to increase the ultimate strength of the inverted T-shape suspended slabs. Furthermore when the bottom flange of the H-shape steel beam is located at the bottom surface of the R/C slabs, suspended slabs can develop their flexural moment capacities and excellent deformation capacities as good as the ordinary T-shape floor slabs. In addition, supplemental top reinforcing bars are effective enough to provide the much higher strength of the inverted T-shape suspended slabs.

1. Introduction

A new type of building structure with double floor slab system as shown in Fig. 1 was first proposed by the authors more than ten years ago. Using this concept, the first R/C residential building with seven stories was built in 1994 in Oita City, Japan and the first steel reinforced concrete (SRC) residential building with eleven stories was built in 1996 in Fukuoka City, Japan. Top floor of this double-floor system is a lumber decking which is composed of plywoods and light-gauge steel sub-beams without any intermediate supports. On the contrary, bottom floor of this double-floor system is an R/C suspended slab which has an inverted T-shape or L-shape cross-section at the slab-to-beam connections. This double floor slab system can insulate the sound transmission from upper-story residents, and provides satisfactory storage spaces for household effects between top and bottom floor slabs.

Although this type of double-floor slab system is expected to be adopted to the multi-story residential, office and hospital building floor systems for steel structures as well as R/C and SRC building structures, systematic experimental studies on the effect of reinforcing details on its structural behavior have not been conducted sufficiently. In the past experimental studies conducted by the authors for developing a better reinforcing details for R/C suspended slab connected to R/C and SRC beams with inverted T-shape, some of the slabs with inadequate reinforcements showed much poorer structural behavior than ordinary T-shape slabs [1, 2, 3].

Main objective of the present study is to examine the structural behavior of inverted T-shape reinforced cast-in place concrete suspended slabs connected in fixed support condition to steel H-shape beam experimentally and to propose a better reinforcing method for strength and ductility of this type of suspended slabs. In the present experimental study, eight different full-scale specimens with inverted T-shape slabs were tested under monotonic vertical loading and test results were compared with those obtained from the ordinary T-shape specimen.

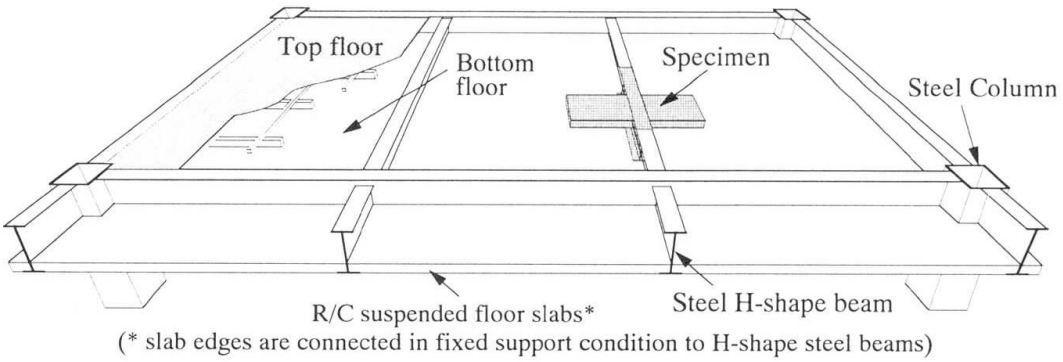

Fig. 1 Double-floor slab system

2. Test Specimens

A total of nine full-scale specimens with different slab-to-beam connection details were designed and constructed. Eight specimens have the suspended slabs with inverted T-shape cross-sections, and only one specimen has an ordinary T-shape cross-section. Each specimen is composed of one steel H-shape beam element and two R/C slab elements connected to each other along the top flange of the steel beam for the T-shape specimen and the bottom flange of the beam for the inverted T-shape specimens, respectively. Fig. 2 shows size and shape of the typical specimens, which correspond to the slab-beam assemblages as shown in Fig. 1. Reinforcing details for all specimens are listed in Table 1 together with the material properties of the concrete and reinforcing bars, and the slab-to-beam connection details of all specimens are shown in Fig. 3. Inverted T-shape specimens are classified into two groups according to the location of bottom flange of the steel H-shape beams. Bottom flange of the steel H-shape beams for S-ITM Group specimens is located within the R/C floor slabs. While in case of S-ITB Group specimens, bottom flange of the steel H-shape beams is located at the bottom surface of the R/C slabs.

Specimen S-OT is a model of ordinary T-shape beam-slab subassemblage (where floor slabs are designed considering an ordinary T-shape slab system), where required amount of reinforcement and connection details are designed in accordance with the current structural design standard in Japan [4].

Other eight specimens are inverted T-shape specimens with different slab reinforcements and slab-to-beam connection details. Specimen S-ITM has the same slab reinforcements with specimen S-OT except that the slabs are located at the bottom of the steel beam, where the top reinforcing bars pass through the holes in the web plate of the steel H-shape beam section, and are continuous

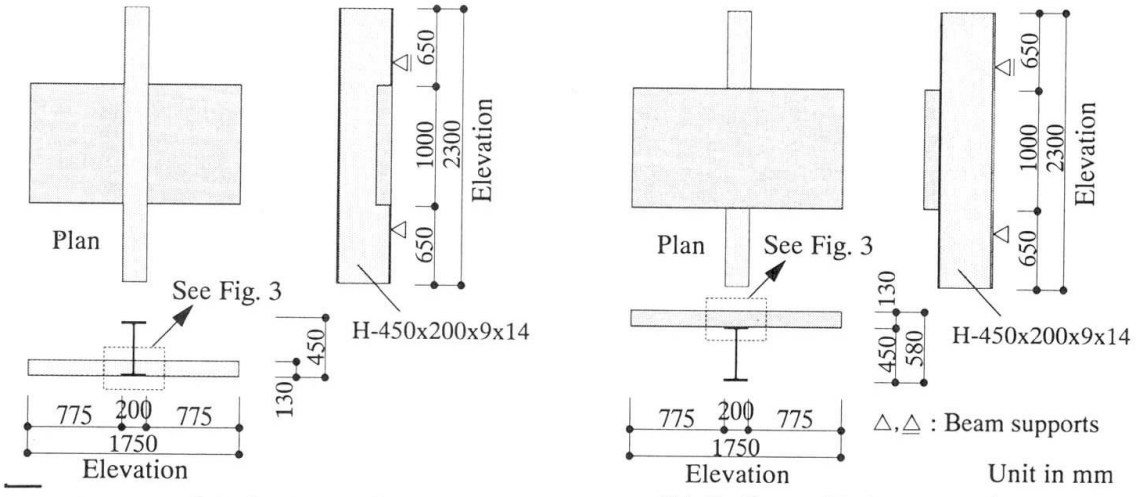

(a) Inverted T-shape specimen *(b) Ordinary T-shape specimen*

Fig. 2 Size and shape of test specimens

Table 1 Details of test specimens

Specimens	Reinforcements					Compressive strength of concrete [kgf/cm^2]	Yield strength of reinforcements	
	Slabs		Slab-to-beam connections				D13 (#4) [kgf/cm^2]	D10 (#3) [kgf/cm^2]
	Top bars	Bottom bars	Top Re-bars	Bottom Re-bars	Diagonal Re-bars			
S-OT	D13 (#4) D10 (#3) Alternate @200	D10 (#3) @400	None	None	None	269	3540	3460
S-ITM			None	None	None	164	3920	3830
S-ITM-D					D13 @250	246	3540	3460
S-ITM-DD					2-D13 @250	252		
S-ITM-DB				D13 @250	D13 @250	261		
S-ITB30			None	None	None	221	3920	3530
S-ITB42						156		3830
S-ITB30-T			D13 @250			235		3530
S-ITB42-T						220		

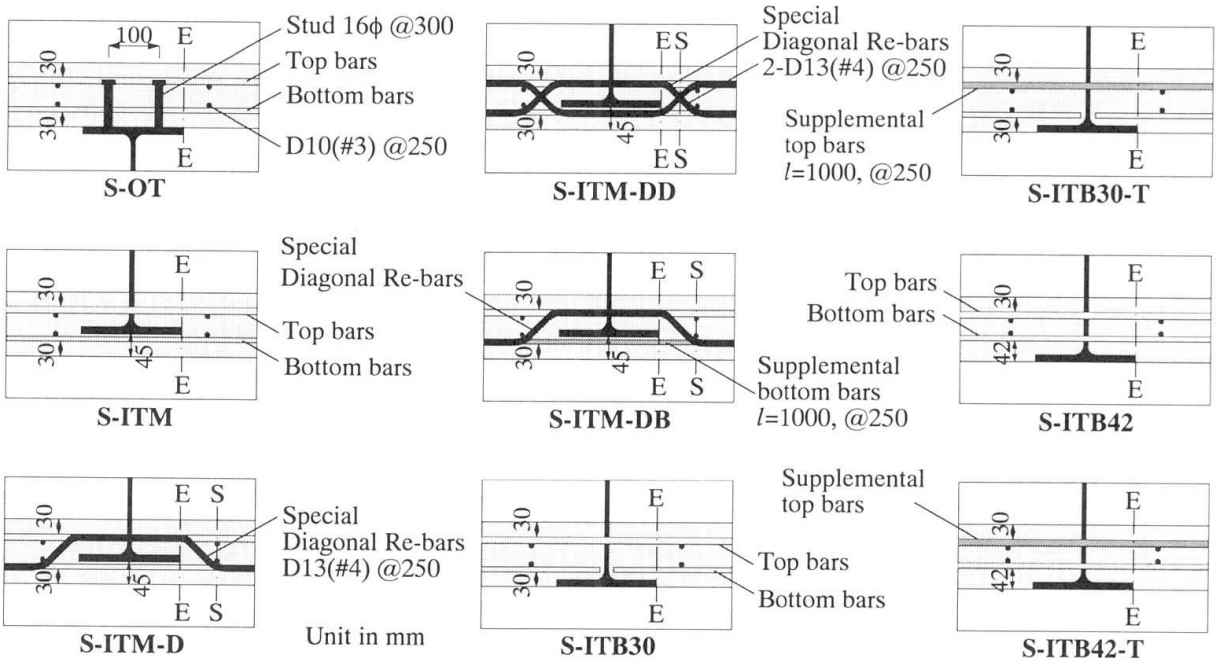

Fig. 3 Reinforcing details in slab-to-beam connections

throughout the left and right suspended slabs. In addition to this slab-to-beam connection detail, special diagonal and supplemental bottom reinforcing bars are provided in the specimens S-ITM-D, S-ITM-DD and S-ITM-DB as shown in Fig. 3 and Table 1.

Specimen S-ITB30 has the same slab reinforcements as specimen S-OT, however, bottom reinforcing bars of the slabs are not continuous across the web plate of the steel H-shape beam section, but extreme edges of these bars are placed close to the web plate surface as shown in Fig. 3. This is because it is not easy work to drill many holes around the web filet area of the ordinary rolled H-shape steel sections. While in specimen S-ITB42, bottom bars with a distance of 42mm from the bottom surface of the slab are provided continuously throughout the left and right suspended slabs as are the top reinforcing bars. In the specimens S-ITB30-T and S-ITB42-T, supplemental top bars are provided to the beam-to-slab connection details adopted respectively for the specimens S-ITB30 and S-ITB42.

3. Test Setups

Fig. 4 shows the test setup for inverted T-shape specimens. All the test specimens were simply supported at both ends of their steel H-shape beams. Vertical load to the slab-end, V, was applied as a concentrated line load, the loading point of which was 50 cm from the beam web.

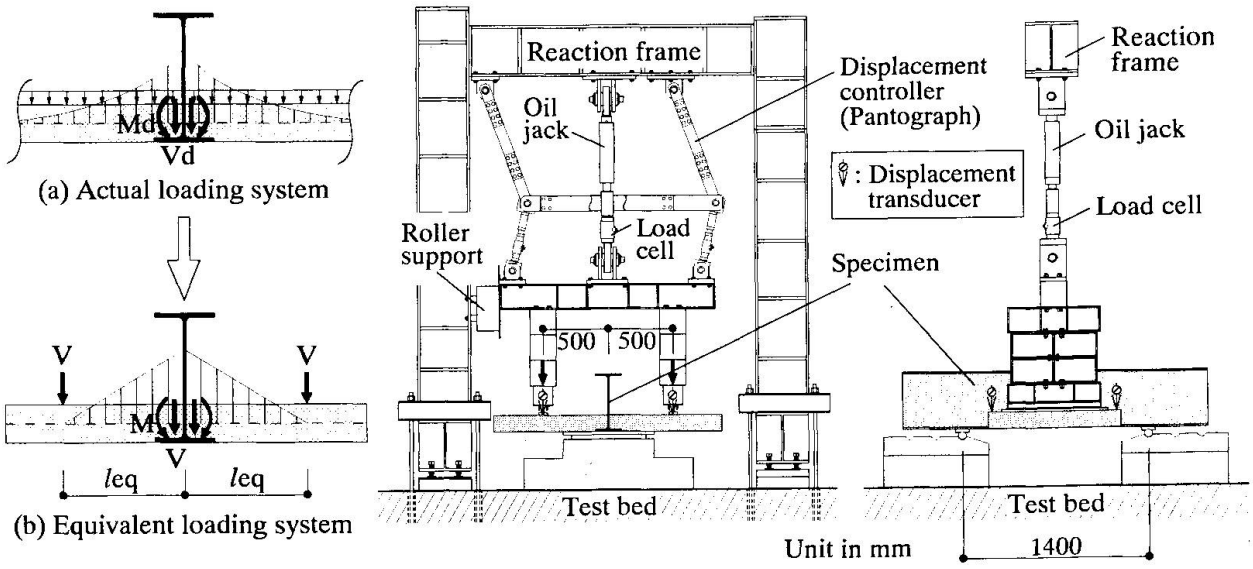

Fig. 4 Test setup for inverted T-shape specimens

Illustrations (a) and (b) in Fig. 4 show the way how to determine this loading system. The illustration (a) is the actual bending moment diagram when the slabs are subjected to uniform distributed design dead plus live loads specified in the Building Code and Standard of Japan [4, 5], Md and Vd are the design bending moment and shear force at the fixed end of the slabs. While M and V as shown in illustration (b) are the bending moment and shear force at the fixed end of the slabs when the slabs of the specimens are respectively subjected to a concentrated load of V. In the present tests, application point of vertical loading (*l*eq) was determined so that ratio of the M/V would equal to the Md/Vd.

One displacement Controller (or Pantograph) as shown in Fig. 4 was installed in order to keep both of the vertical displacement at the left and the right loading points equal during the experiment.

4. Test Results and Discussions

Applied vertical load (V) versus corresponding vertical displacement (δ) relations obtained from the S-ITM Group and S-ITB Group specimens are shown in Figs. 5(a) and 5(b), respectively. (V)-(δ) relation of the specimen S-OT is presented in both Figs. 5(a) and 5(b) for comparison. In these figures, the vertical load (V) is the average of two measurements, and the vertical displacement (δ) is the average of four measurements at the left and the right slabs. On each curve of the (V)-(δ) relations in Figs. 5(a) and 5(b), information obtained from the strain-gage measurements or visual observation is also marked using an open circle, an open square and a solid rectangle meaning respectively the initiations of tension-yielding in top and bottom bars for slab main reinforcement and crushing of the compression concrete at the fixed end of the floor slab. Also in each figure, the allowable strength for the ordinary T-shape specimen S-OT for long-term loading [4] and the ultimate strengths for all the specimens determined by a theory [4] are presented by dotted line and dashed lines, respectively. In addition, the design loads (Vd) based on the current Japanese Standards are also given in each figure. The theoretical strengths for all the specimens and ultimate strengths obtained from the experiment are presented in Table 2. Theoretical strengths for the specimens S-ITM-D, S-ITM-DD and S-ITM-DB presented in Fig. 5(a) and Table 2 are determined by the ultimate flexural strength taking into account the increase in flexural strength due to the contribution of special diagonal reinforcements.

The findings from the test results can be summarized as;
(1). The observed ultimate strengths (Vutest) of the test specimens except for S-ITM specimen are more than 6.7 to 11.7 times as large as the design load (Vd), and more than 1.6 to 2.5 times as large as the allowable strength for the long-term loading (Va).
(2). The ordinary T-shape specimen S-OT could develop its ultimate flexural moment capacity (Mu) and had excellent deformability without any concrete crushing.

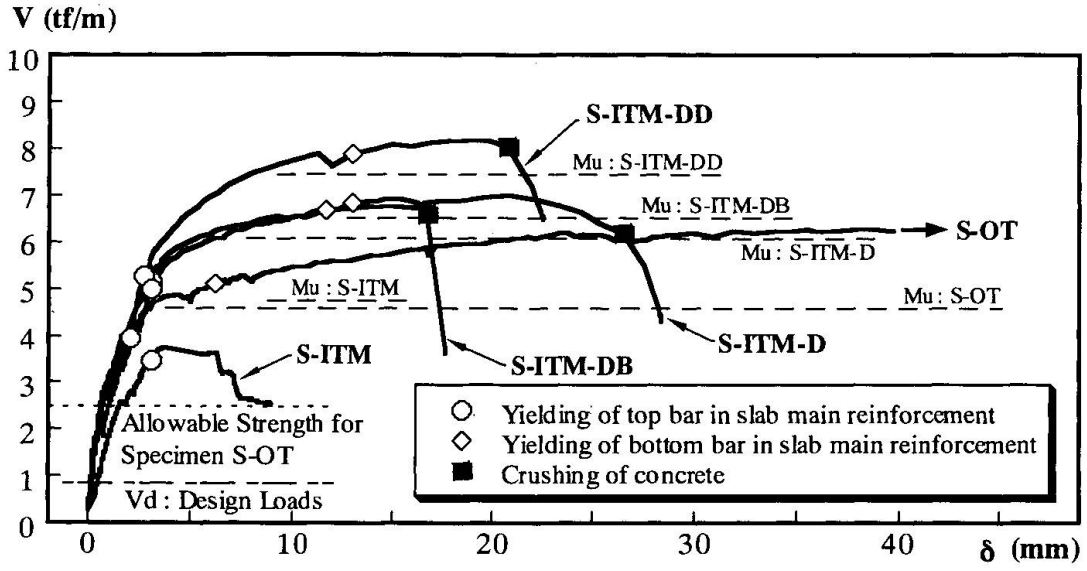

(a) S-ITM Group and S-OT specimens

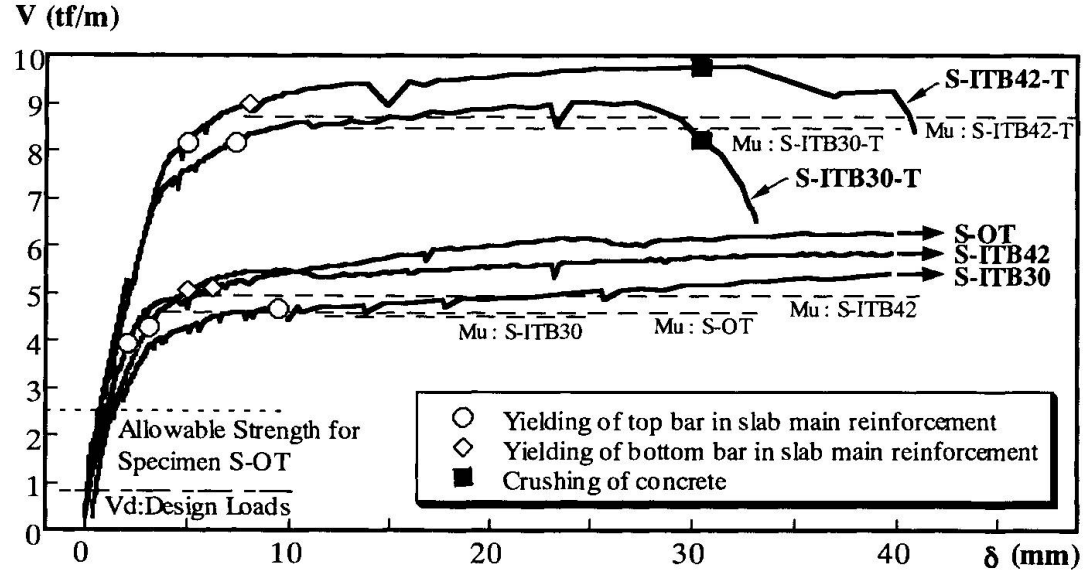

(b) S-ITB Group and S-OT specimens

Fig. 5 Vertical load(V) versus displacement(δ) relations

(3). For specimen S-ITM, which is an inverted T-shape specimen having the same slab reinforcing details as the ordinary T-shape Specimen S-OT, brittle shear failure occurred in a relatively small deformation area at the fixed ends of the R/C slabs as schematically shown in Fig. 6(a), and the ultimate flexural moment capacity could not be reached. This type of failure, which was also observed in the corresponding experimental specimens using R/C and SRC beams [1, 2, 3], could not be predicted by the existing design methods for ordinary T-shape R/C slabs as recommended by the current structural design standard in Japan [4].
(4). The special diagonal reinforcements, as provided in slab-to-beam connections of specimens S-ITM-D, S-ITM-DD and S-ITM-DB, could prevent the brittle shear failure as schematically shown in Fig. 6(b) and contributed to the increase in the ultimate flexural strength of the floor slabs.
(5). In the specimen S-ITM-DB, which is supplemented with the bottom reinforcements to slab-to-beam connection details adopted for specimen S-ITM-D, the crushing of compression concrete occurred in a smaller deformation area than that for the specimen S-ITM-D.
(6). Specimens S-ITB30 and S-ITB42 could develop their ultimate flexural moment capacities (Mu) and had excellent deformabilities without any concrete crushing.
(7). The supplemental top bars, as provided in specimens S-ITB30-T and S-ITB42-T, increased the ultimate strength of the floor slabs considerably.

Table 2 Allowable strengths and ultimate strengths

Specimens	Theoretical Predictions				Test Results
	Allowable Strengths for Long-term Loading		Ultimate Strengths		Ultimate Strengths
	Flexure : Ma* [tfm/m]	Shear : Va [tf/m]	Flexure : Mu* [tfm/m]	Shear : Vu [tf/m]	Shear : Vutest [tf/m]
S-OT	1.00	2.51	1.83	4.58	6.28
S-ITM	1.11	2.78	1.90	4.75	3.74
S-ITM-D	1.70	4.24	2.81 (2.07 **)	7.03 (6.08)	6.98
S-ITM-DD			2.98 (2.94 **)	7.45 (7.96)	8.17
S-ITM-DB			3.05 (2.22 **)	7.63 (6.52)	6.92
S-ITB30	1.09	2.73	1.80	4.51	5.57
S-ITB42	1.11	2.78	1.98	4.95	5.86
S-ITB30-T	2.18	5.45	3.38	8.46	9.02
S-ITB42-T			3.49	8.73	9.77

* Bending moment at extreme-edge of bottom flange (E-E Section in Fig. 3)
** Values in parenthesis are bending moments at S-S Sections in Fig. 3.

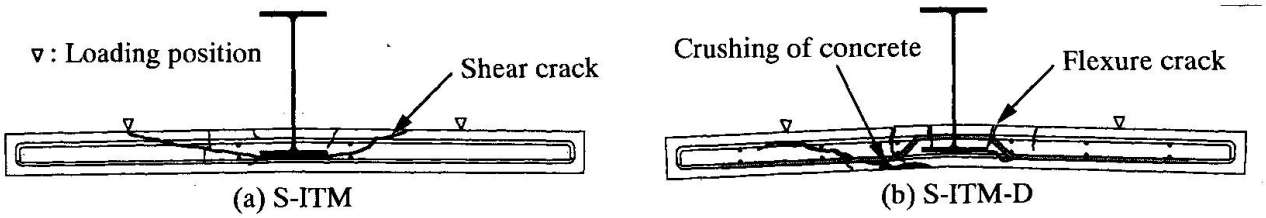

(a) S-ITM (b) S-ITM-D

Fig. 6 Typical crack patterns after test

5. Concluding Remarks

In order to propose a better reinforcing method for R/C suspended slabs connected to the bottom flanges of steel H-shape beams, experimental study was conducted. Based on the obtained test results, it may be concluded that, in cases, where the bottom flange of the H-shape steel beam is located within the R/C suspended floor slabs, strength and deformation capacity of the inverted T-shape suspended slabs are very poor. However, it is possible to increase their ultimate strength and deformation capacity considerably by providing special diagonal reinforcing bars to the slab-to-beam connections. Also, when the bottom flange is located at the bottom surface of the R/C slabs, suspended slabs can develop their flexural moment capacities and excellent deformation capacities as good as the ordinary T-shape slabs. In addition, if supplemental top reinforcing bars are provided in the slab-to-beam connection, R/C suspended slabs can develop much higher strength.

6. References

[1] Yoshimura, K., Kikuchi, K., Kuroki, M., Yoshida, K., Iida, I. and Okita, K. Experimental Study on Strength and Ductility of R/C Suspended Slabs. Proc. of 15th Conference on Our World in Concrete & Structures, August 1990, Singapore, pp.381-388.
[2] Yoshimura, K., Kikuchi, K., Iida, I. and Okita, K. A New Building Structure with Double-floor Slab System. Proc. of the Fifth East Asia-Pacific Conference on Structural Engineering and Construction, July 1995, Gold Coast, Australia, pp. 1845-1850.
[3] Yoshimura, K., Kikuchi, K., Iida, I. and Okita, K. A New Steel-Concrete Composite Building with Double-floor System. IABSE International Conference Report of Composite Construction - Conventional and Innovative-, September 1997, Innsbruck, Austria, pp. 457-462.
[4] Architectural Institute of Japan. Standard for Structural Calculation of Reinforced Concrete Structures, 1988.
[5] Building Standard Law of Japan. 1994 edition.

Development of Steel Plate-Concrete Composite Deck (SC Deck)

Satoshi FUKUOKA
Senior engineer
Kawada Industries, Inc.
Tokyo, Japan

Satoshi Fukuoka, born in 1966.
Received his civil engineering degree
From Tokyo Denki Univ. in 1989

Summary

A steel plate-concrete composite deck (SC-Deck) has been improved based on the steel-concrete composite deck girder which was developed in 1986. SC-Deck consists of bottom steel form, concrete and upper reinforcing bars, and needs no staging and scaffolding. Trial fabricating test of bottom steel form, concrete casting test and wheel trucking test of SC-Deck are conducted using real-size models. Results of those tests show that SC-Deck has no structural problems, and has required strength and durability.

1. Introduction

Commonly in Japan, cast-in-situ reinforced concrete slab (hereinafter RC slab) has been adopted as the decks of highway bridges with steel plate girders, considering its advantages on low cost and easy construction procedure. However, recently, serious damages and deterioration on RC slab have been observed due to repetitions of heavy traffic load, which were unforeseen at the time of design. And hot discussions are being made as to durability of RC slab and the method of remedial work. In addition to above, RC slab used for viaducts and overpasses in urban area has another problem that the use of enough space under the bridges for the staging and scaffolding during concrete casting, is usually not allowed. On the other hand, prestressed concrete slab, which has definitely the higher stiffness than RC slab, requires the special skill at site as to prestressing, thus results in costly deck. Comparing with above slabs, the composite deck which consists of steel plate and concrete slab has the following advantages;

- No staging and scaffolding is required during concrete casting
- High load capacity and durability is expected
- Reduction of thickness of slab is can be achieved

We have developed, as one of alternative from steel-concrete composite deck named as Robinson deck, SC Deck for the purpose of further simplification and shortening of site work. SC Deck has been used in the Kariyasuga Viaduct in Tokai-Hokuriku Motorway of Japan Highway Public Corporation. In the process of development of SC Deck, we have executed the wheel trucking test using real size models, in addition to trial fabrications of the bottom steel form and concrete casting test for the checking of deflection of bottom steel form.

2. Structural Details of SC Deck

One of the authors had modified the steel plate-concrete composite deck named as Robinson deck by welding of longitudinal and transverse ribs to the steel plate, as shown in Fig.1. This modified type deck girder was adopted to several steel bridges in Japan, refer to references [1] and [2]. The remarkable points of this type of deck girder are;

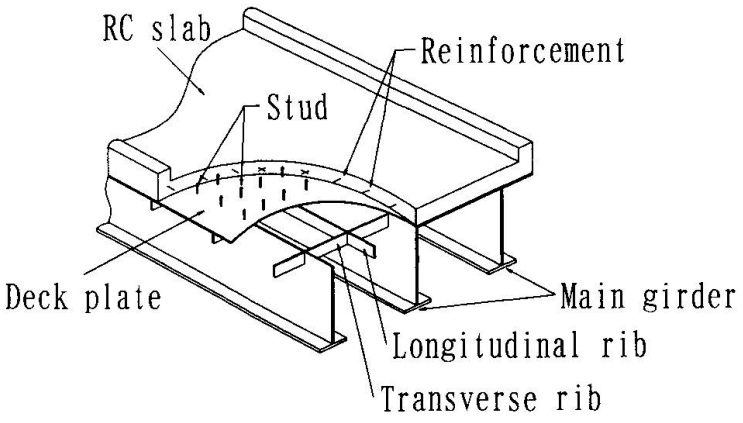

Fig.1 General view of modified composite deck girder

- Steel deck plate is designed not only as an upper flange of plate girder but also as a steel form of deck.
- The longitudinal and transverse ribs are welded to the bottom surface of steel plate.

On the contrary, SC Deck is designed such that bottom steel form is pre-fabricated separately from upper flange of girder and has only transverse ribs. Since the bottom steel form divides into small panels per span of slab, SC Deck shall be applicable to the following areas of bridges and rehabilitation works of slab;

- Repairing of slab and replacing of slab
- Viaducts and Overpasses
- Open box steel Girders

Fig.2 shows general view of SC Deck. SC Deck consists of bottom steel form, concrete slab and upper reinforcing bars. Bottom steel form is designed in 2 steps, one is as steel form during concrete casting, and the other is as lower reinforcement after hardening of concrete. Thus SC Deck requires no staging and scaffolding, and no additional lower reinforcing bars are necessary. Upper reinforcing bars are just straight bars and set on the transverse ribs. Pre-fabricated bottom steel form panel consists of steel plates, transverse ribs and studs. Each panel, which size depends on the limitation of transportation, shall be connected with High Strength Bolts after installation at site. Bottom steel form is just set on main steel girder and any bolt connection or welding is not made. For the adjustment of alignment, rubber strip is inserted between bottom steel form and main steel girder. Transverse ribs are designed to minimize deflections of bottom steel form during concrete casting, so that the safety of work and uniform concrete thickness of slab shall be ensured. Bottom steel form and concrete are to be composite by

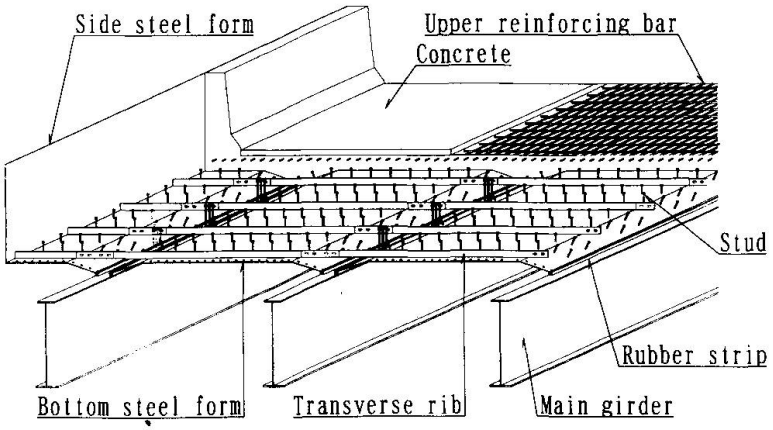

Fig.2 General view of SC Deck

studs. Bottom steel form shall be hot-dip galvanized or painted, and if the condition of atmosphere is not severe, atmospheric corrosion resisting steel shall be used. If side steel form is to be welded or to be bolt jointed to bottom steel form, no additional work for installation of form is required for concrete barrier and curb.

3. Design of SC Deck

SC Deck is to be designed in accordance with references [3] and [4]. A concept of design is that bottom steel form itself resists to dead load of weights of bottom steel form, fresh concrete and reinforcing bars, while composite section of bottom steel form and concrete slab resists to dead load of pavement, concrete barrier and curb, etc. and live load. Calculation of stress shall be made as follows ;

- For pre-composite load : To superimpose the membrane stress of bottom steel form onto the stress of T-section beam consisting of bottom plate and transverse rib.
- For post-composite load : To calculate the stress as a composite section of bottom plate and concrete.

Table 1 shows basic design criteria of SC Deck. Table 2 shows outline of real-size model utilized for wheel trucking test, and Fig.3 shows its section.

Design strength of concrete	$\sigma ck = 30$ N/mm² (Approx.)
Raito of Young's modulus	$n = 10$ or 15 *
Thickness of concrete slab	Minimum thicknes of RC slab by reference [3]
Thickness of bottom steel form	$ts = 9$ mm (Approx.)
Height of transverse rib	Approx. half of thickness of concrete slab
Span of slab	$L = 2.0 \sim 6.0$ m

* : under severe load condition

Table 1 Basic designe criteria

Design strength of concrete	$\sigma ck = 30$ N/mm²
Raito of Young's modulus	$n = 15$
Span of slab	$L = 3.0$ m
Thickness of concrete slab	$tc = 20$ cm
Upper reinforcing bar	Main upper bar : D19(SD345) Distributing bar : D16(SD345)
Thickness of bottom steel plate	$ts = 9$ mm
Interval of transverse rib	$dr = 750$ mm
Height of transverse rib	$hr = 100$mm
Thickness of transverse rib	$tr = 16$mm
Diameter of stud	$\phi 16$
Interval of stud	$ds = 250$mm or less
Height of stud	$hs = 120$mm

Table 2 Outline of real-size model

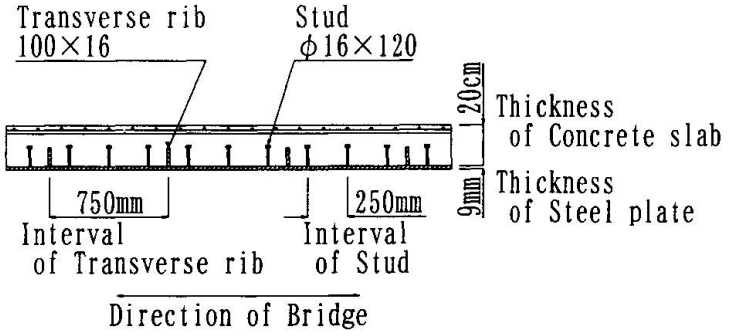

Fig.3 Section of real-size model

4. Tests of SC Deck using real-size model

4.1 Trial fabrications of bottom steel form

We have made trial fabrications in order to obtain the following data;

- Amount of deformation of bottom steel form due to hot-dip galvanizing

· Checking of details at joints of bottom steel form

In order to obtain the amount of deformation of bottom steel form due to hot-dip galvanizing, we have fabricated 2 types of panel for test, one is that the transverse ribs are continuously welded to bottom plate and the other one is intermittently welded. Thickness of bottom steel plate in both panels was 9 mm. Amounts of deformation for each panel were only about 10 mm, and we have confirmed that such amounts would cause no problem for installation of bottom steel form panel to steel girders at site. Since deformation by intermittent weld were slightly smaller than that of continuous weld, we have decided that transverse rib are to be intermittently welded to bottom steel form. And also we have confirmed that there would be no problem as regard to joint details of bottom steel form pannel for the installation at site.

4.2 Concrete casting tests using real-size model

We have made concrete casting tests to confirm the following points;

· Leakage of water under concrete casting
· Deflection of bottom steel form under concrete casting
· Propagation of cracks due to shrinkage

In order to ensure safety of concrete-casting work and ensure the designed thickness of slab, max. 5 mm was to be considered as an allowable deflection of bottom steel form during concrete casting. And also we have confirmed that there would be no problem as regard to leakage of water and propagation of cracks.

4.3 Wheel trucking test

Wheel trucking test of SC Deck has been executed using real-size model at Osaka Institute of Technology. Fig.4 shows phtograph of wheel trucking test. The purpose of this test is as follows;

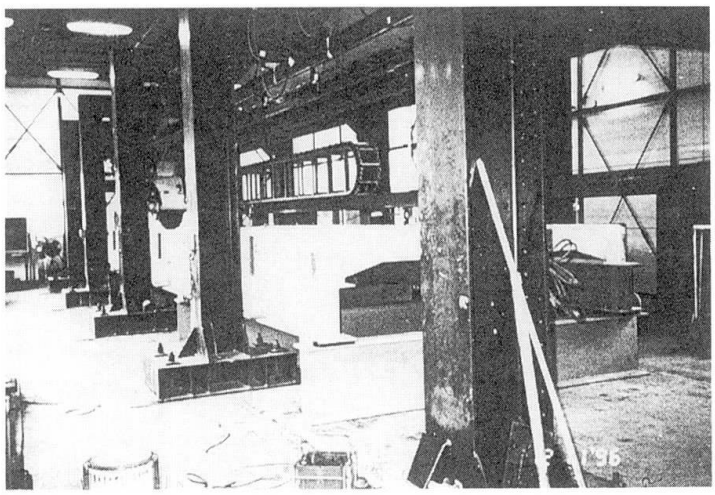

Fig.4 Photograph of wheel trucking test

· Evaluation of load capacity and durability of SC Deck in compared with ordinary RC slab
· Determination of most suitable type of transverse rib
· Checking for the behavior of joints of bottom steel form pannel

Since the transverse ribs are to be embedded into concrete, it was anticipated that cracks would be propagated from top of rib plate to upper surface of concrete, thus resulting in serious damages to composite slab. So we have made comparison for details of transverse rib, using 3 different types of specimens A, C, and D as shown in Table 3. In addition ,we have also made comparison for propagation of cracks between ordinary concrete and expansive concrete (specimens A and B).

It was observed for all types of specimen that the behavior as to deflection and strain remained within the range of elasticity and the propagation of cracks did not occur. Test results for joint details of bottom steel form were also satisfactory, and we have decided to select specimen A from the economical point of view. Water proofing agent shall be applied to the surface of concrete. Another wheel trucking test using real-size model with slab span of 2.5 m for various types of slab including SC Deck has been executed at Public Works Research Institute, Ministry of Construction. In this test, wheel loading, initially starting from 156.8 kN, was increased by 19.6 kN every 40 thousands of cycle wheel loading up to 392 kN. The result of this test showed that deformation of SC Deck remained within the range of elasticity up to 392 kN (520 thousands cycles), while the ordinary RC slab was destroyed at the load stage of 254.8 kN (220 thousands cycles).

Type	Note	Concrete	Sketch
A	Steel plate only	Ordinary Concrete	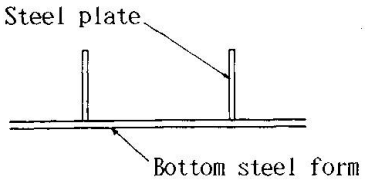
B	Steel plate only	Expansive Concrete	
C	Combination of Steel plate and Welded Wire Net	Ordinary Concrete	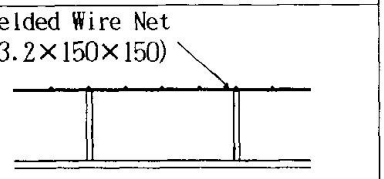
D	Combination of Steel plate and Deformend bar	Ordinary Concrete	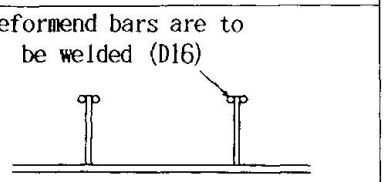

Table 3 Types of specimen

5. Construction of SC Deck

Results of several tests mentioned above had verified that SC Deck had enough load capacity and durability, and also had good workability at site. Thus, finally, SC Deck had been adopted to the Kariyasuga Viaduct in Tokai-Hokuriku Motorway of Japan Highway Public Corporation, with structural outline as follows;

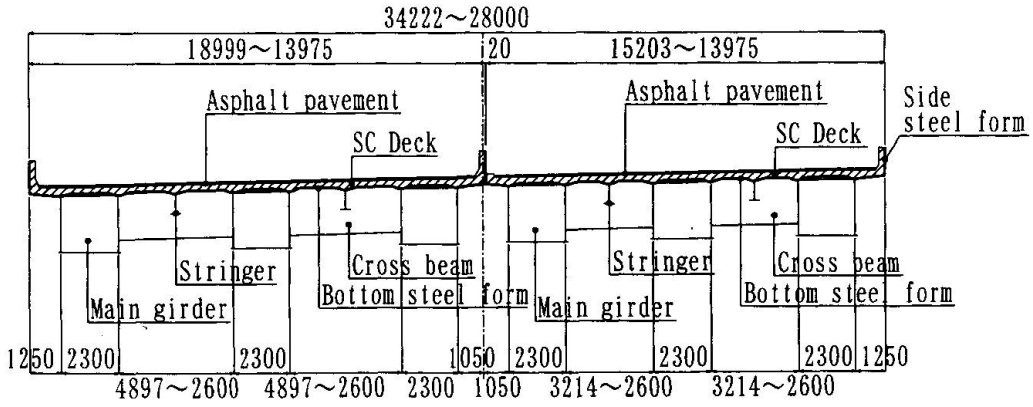

Fig.5 Typical cross section of the Kariyasuga Viaduct

· Type of Bridge : 2 Nos. of 3-spans·continuous steel box girder
· Length of Bridge : 140m + 160m
· Total width of Bridge : 43.352m to 34.222m and 34.222m to 28.000m (variable)

Typical cross section is shown on Fig.5 and photographs of construction scene are shown in Fig.6 to Fig.7

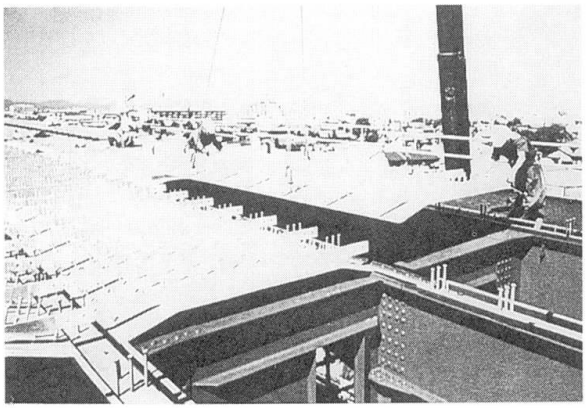

Fig.6 Erection of Bottom form

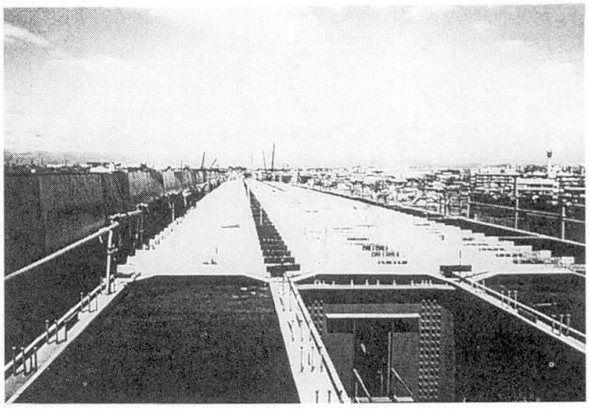

Fig.7 Setting of Bottom form on girders

6. Conclusions

We are still investigating further improvement on SC Deck as below;
· Reduction of Nos. of stud by clarifying distribution of horizontal shear force
· Simplification of joint detail for bottom steel form

If SC Deck is to be planned to adopt in case that there would be the limitation for usage of underbridge space during slab work, or in case that the span of slab in excess of 3.0 m would be required, we believe that SC Deck could demonstrate its cost advantages to RC slab and PC slab .Therefore, we expect that SC Deck would be used for many of steel bridges.

Finally, we take this opportunity to express our thanks to the staffs of Japan Highway Public Corporation concerned, Prof. and Dr. S.Matsui of Osaka Univ. and Prof. and Dr. T.Horikawa of Osaka Institute of Technology for giving us kinds advices as for the development of SC Deck.

References

[1] S.Matsui , T.Akiyama , H.Watanabe , Y.takeda : Steel-concrete composite deck girder The design and construction of The Tanaka Bridge, Bridge Engineering, pp.31～39, No.11,1986. (in Japanese)
[2] S.Matsui , H.Sasaki , Y.Fukumoto , H.Watanabe : Fatigue character of composite slab under repetitions of traffic load, The 42th Annual Conference of JSCE, I-164, pp.362～363, Sep.1987. (in Japanese)
[3] Japan Road Association : Specifications for Highway Bridges、Part Ⅰ : Common Specifications、Part Ⅱ : Steel Bridges, 1996-12. (in Japanese)
[4] JSCE : Design Code for Steel Structures PART B : Composite Structures, 1997 (in Japanese)

A Study on Shear Resistance of Stud Connectors Used with Profiled Steel Sheeting

Xiamin HU
Assoc. Prof.
Nanjing Arch. & Civil Eng. Institute
Nanjing, P.R. China

Xiamin HU, born in 1958, associate Professor at Nanjing Architectural and Civil Engineering Institute, His research interests include composite structures and concrete structures.

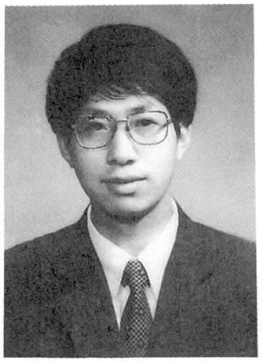

Helmut BODE
Prof. Dr-Eng.
University of Kaiserslautern
Kaiserslautern, Germany

Helmut BODE, director of Steel Construction Institute, University of Kaiserslautern. His research interests include composite structures and steel structures.

Summary

A formula, considering the main effective factors, is proposed for predicting the shear resistance of the studs used with sheeting perpendicular to the steel beams in this paper. This was done by analyzing the mechanical behaviour of the head stud connectors used with profiled steel sheeting. The proposed formula is applicable to both the stud connectors welded through holes in the sheeting and the stud connectors welded through the sheeting. The theoretical predictions are in good agreement with the test results.

1. Introduction

The use of mechanical connectors is essential for ensuring composite action in composite beams. The head stud is the most widely used type of connector in composite construction, especially in composite floor system with profiled steel sheeting. The direct shear strength of connectors may be evaluated by using a representative model test known as the push-out test. In 1970, Fisher[1] conducted through-deck push-out tests and found that specimens that included the profiled steel sheeting had reduced strength and stiffness of the connection for several profiles. He modeled the reduction in shear capacity by the following formula:

$$P_t = kP_s \tag{1}$$

where P_t is shear strength of a connector used with profiled steel sheeting; P_s is shear strength of a connector in a solid concrete slab; k is a reduction factor for resistance of the shear connector. Fisher's[1] reduction factor for sheeting that spans perpendicular to the beam, denoted by the symbol k_g, is

$$k_g = 0.35 b_a / h_p \tag{2}$$

where b_a is the breadth of the rib to be used in calculation , and taken as the mean rib breadth for open profiles, and the minimum breadth for re-entrant profiles; h_p is the over all depth of the

profiled sheeting.

Eq.(2) was modified by Grant, Fisher and Slutter[2] in 1977. They observed that besides the rib width-height radio b_a/h_p, the height of the rib and the embedment of the connector must be taken into account to correctly predict the resistance of the shear connectors used with profiled sheeting. The modified equation of k_g was given as follows:

$$k_g = (0.85/\sqrt{N_r})(b_a/h_p)[(h/h_p)-1] \leq 1 \tag{3}$$

where N_r is the number of studs per rib; h is the height of the stud connector.

Eq.(3) was adopted in many codes of practice. However, the evaluation of all the available tests revealed that the reduction factors given by Eq.(3) do not give safe results over the whole range of possible applications. Therefore the coefficient 0.85 in Eq.(3) was reduced to 0.7 in recently revised EC4[3] and limitations are given for the rib height, the rib breadth and the number of studs per rib. That is

$$k_g = (0.7/\sqrt{N_r})(b_a/h_p)[(h/h_p)-1] \leq k_{max} \tag{4}$$

with $h_p \leqslant 85$mm, $b_a \geqslant h_p$, $N_r \leqslant 2$, $k_{max}=1$ for $N_r=1$, and $k_{max}=0.8$ for $N_r=2$.

Several researchers[4-6] have shown that the reduction factor k_g given by Eq.(4) is unreliable and , in some conditions, it overestimates the strength of a ribbed-deck connection, although the coefficient 0.85 was reduced to 0.7. Besides, there are no such equations for the studs welded through holes in the sheeting in EC4. In this paper, the behaviour of the headed studs used with perpendicular profiled steel sheeting is analyzed, and main effects on the shear strength of the head stud connectors used with perpendicular profiled sheeting are identified. A formula is proposed to predict the shear strength of the stud connectors used with perpendicular profiled steel sheeting.

2. Development and Verification of Shear Strength Formula

2.1 Roik and Lungershausen's Formula

In composite beams with profiled steel sheeting, the horizontal shear is transferred from the steel beam to the concrete slab through the rib that can be taken as connecting members between the steel beam and the concrete slab. But in composite beams with solid slabs, the horizontal shear at the interface can be directly transmitted through the studs and the welding. Therefore the failure mechanisms of the shear studs in these two distinct types of composite beams are different. By analyzing the test data in Germany, a formula was given by Riok and Lungershausen for calculating the shear resistance of the studs used with perpendicular profiled steel sheeting (see Fig.1)[7]. According to Fig. 1 the ultimate shear resistance of the studs used with Perpendicular profiled steel sheeting P_t can be obtained as follows:

$$P_t = 2M_u/a = 2M_u/(\alpha/d) \tag{5}$$

with

$$M_u = f_u d^3 / 6 \tag{6}$$

$$\alpha = a / d \tag{7}$$

where M_u is the plastic resistance moment of the stud cross-section, a is the distance between two plastic hinges, α is a/d ratio.

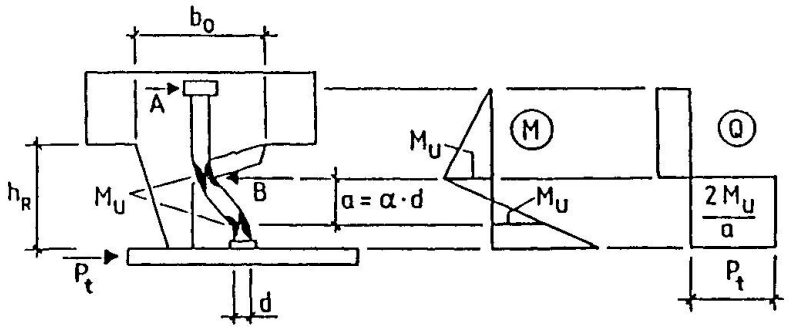

Fig.1 Failure Mechanism of stud used with profiled steel sheeting

Roik and Lungershausen have found that the coefficient α depends mainly on the geometry of the ribs. They proposed the following equation for α to take the effect of the geometry of the ribs into account:

$$\alpha = 0.6 + 0.8(h_p / b_o)^2 \tag{8}$$

where b_o is the top breadth of the rib.

In addition, they have introduced two coefficients β and $(N_r)^{-0.5}$, where β is taken as 1 for open profiles and 1.1 for re-entrant profiles and N_r is the number of studs per rib. Thus Eq.(5) becomes

$$P_t = \frac{\beta}{\sqrt{N_r}} \frac{f_u d^3}{0.6 + 0.8(h_p / b_o)^2} \tag{9}$$

2.2 Proposed Formula

There is a difference in the welding process of the studs used with profiled steel sheeting between in Germany and in USA, Canada, UK and some Member States of the European Union. In Germany, the holes are cut out in the decking before the studs are welded, and the stud connectors are welded through the holes to the beam underneath, while in USA, Canada, and UK the through-deck welding technique are usually used during the welding course of the stud connectors.

Test results have shown that the shear resistance of the studs welded through holes in the sheeting is lower relative to the studs welded through the sheeting to the steel beams[8]. In the push-out tests analyzed by Roik and Lungershausen, all studs were welded to the steel beams through holes in the sheeting, therefore, Roik and Lungershausen's formula is only suitable for the predictions of the stud connectors used with sheeting in which holes are cut out.

Test results of Roik and Lungerhausen[7] indicate that the resistance is independent of the cube strength of the concrete f_{cu}, but the dependence on f_{cu} is evident in the tests carried out by Bode and Künzel[8], Mattram and Johnson[9]. By analyzing the test data, it can be found that the shear resistance appears to be related to the tensile strength of the studs, the concrete strength and the geometry of the ribs. It is also to be noted that the stud weld transfers the partial shear force directly from the sheeting to the steel beam. This effect is obvious for studs welded through the sheeting.

According to the above analysis, the coefficient α in Roik and Lungershausen's formula should be reconsidered. To derive reasonable expression for the strength of the studs used with perpendicular profiled sheeting, the data from previous investigations which subjected to statistical analysis to determinate the importance of the variables involved, because a theoretical analysis considering the above effective factors is extremely difficult. From Eq.(5) α may be written as:

$$\alpha = (1/3) f_u d^2 / P_e \tag{10}$$

where P_e is the experimental shear resistance of the stud connectors used with perpendicular profiled steel sheeting. An alternative formula for calculating α is proposed through a multi-variable linear regression analysis on 69 push-out test specimens with one stud per rib reported in references [8]~[14].

$$\alpha = \left(0.424 + 0.775\sqrt{f_u d^2/(f_c b_m)}\sqrt{h_p/b_m}\right)/\alpha_t \tag{11}$$

where f_c is the cylinder compression strength of the concrete; b_m is the mean breadth of a rib of the profiled sheeting; α_t =1 for studs welded through holes in the sheeting, and α_t =1+0.6$b_u t/d^2$ for studs using through-deck welding technique; b_u is the bottom breadth of the rib, t is the thickness of the sheeting.

Additionally, the number of the studs in rib also affects the shear resistance. To consider this effect, the authors have carried out regression analysis using the test specimens with two studs per rib from references [8]~[14] and obtained an equation that fitted all sets of data well.

$$\alpha_n = 0.29[1 + (h - h_p)/d]/\sqrt{N_r} \tag{12}$$

Based on the above arguments, various cases are considered and the formula for calculating the shear resistance of the stud connectors can be written as follows:

$$P_t = \frac{A_s f_u}{1 + 1.82(d/b_m)\sqrt{f_u/f_c}\sqrt{h_p/b_m}}\alpha_t \alpha_n \tag{13}$$

where α_t and α_n are given by Eq.(11) and Eq.(12) , respectively. Eq.(13) is to be used with the following restrictions:

$d \le 22$ mm
$t = 0.75$~1.2 mm
h-$h_p \ge 50$ mm
$h_p \le 140$ mm
$N_r \le 2$

Fig.2 is a diagram to verify the accuracy of the proposed formula with respect to experimental data. A total of 91 test specimens were available in the literature to compare with the proposed theory. They were reported in [8]~[14]. Using the ratio of calculated shear strength to test shear resistance as an indicator, the mean and standard deviation of this ratio for 91 data were 1.006 and 0.096, respectively. The coefficient of correlation of experimental versus predicted results were 0.959.

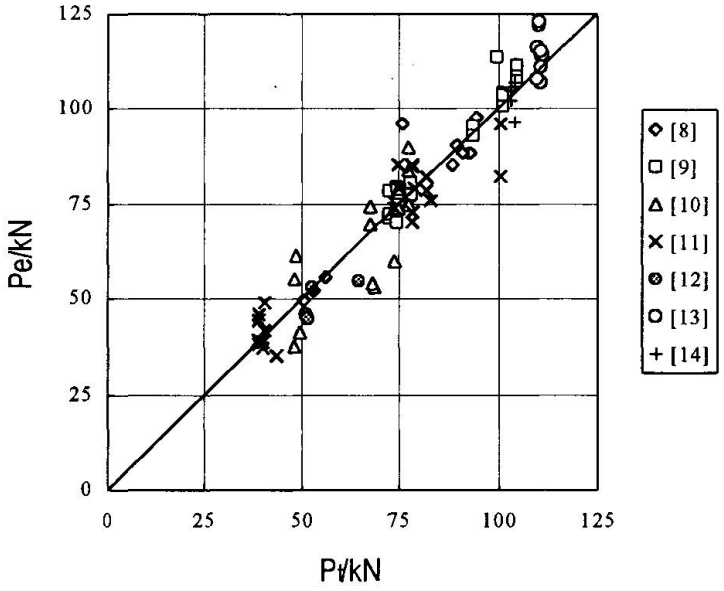

Fig.2 Comparison of calculated and experimental shear resistance

3. Conclusion

It is shown that the formula proposed in EC4 for calculating the shear strength of the head stud connectors used with perpendicular profiled steel sheeting can be unconservative, compared with the results of the push-out tests. In addition, the EC4 formula is not applicable to the specimens with studs welded through holes in the sheeting, because the shear strength of the studs with pre-holed deck is lower relative to the studs using through-deck welding technique.

Considering the main effective factors, a formula is proposed for predicting the shear resistance of the studs used with perpendicular profiled steel sheeting. This formula has taken the effects of the tensile strength of the stud material, the size of the stud, the compressive strength of the concrete, the geometry of the profiled sheeting and the welding process into account. The study has demonstrated that the proposed formula is applicable for modern composite beams with many different kinds of profiled steel sheeting and the different welding processes. Comparison of results indicates that the proposed calculation formula gives a much better fit to the test data.

References

1. Fisher, J. W.: Design of composite beams with formed metal deck. AISC Engineering Journal, Vol.7, No2, 1970, pp88~96
2. Grant, J. A.; Fisher, J. W.; Slutter, R. G.: Composite beams with formed metal deck. AISC Engineering Journal, Vol.14,No.1, 1977, pp24~42
3. Europäisches Komittee für Normung: Eurocode 4: Bemessung und Konstruktion von Verbundtragwerken aus Stahl und Beton-Teil 1-1: Allgemeine Bemessungsregeln, Bemessungsregeln für den Hochbau, Din V ENV 1994 Teil 1-1. Februar 1994
4. Lloyd, R. H.; Wright, H. D.: Shear connection between composite slabs and steel beams. Journal of constructional steel research. Vol.15, No14, 1990, pp255~287
5. Roik, K. H.; Hanswille, G.; Cunz, A.; Lanna, O.: Hintergrundbericht zu Eurocode 4 - Kopfbolzendübel. Bericht EC4/8/88, Univerität Bochum, März 1989
6. Bode, H.; Hu, X.: Untersuchungen zur Schubtragfähigkeit von Kopfbolzendübeln. Forschungsbericht, Univerität Kaiserslautern, August 1993
7. Roik, K.; Lungershausen, H.: Zur Tragfähigkeit von Kopfbolzendübeln in Verbundträgern mit unterbrochener Verbundfuge (Trapzeprofildecken). Der Stahlbau, B.58, H.9, 1989, pp269~273
8. Bode, H.; Künzel, R.: Zur Anwendung der Durchschweisstechnik im Verbundbau. Forschungsbericht 2/1991, Universität Kaiserslautern, März 1991
9. Mattram, J. T.; Johnson, R. P.: Push tests on studs welded through profiled steel sheeting. Research Report CE25, Department of Engineering, University of Warwick, May 1989
10. Roik, K.; Bürkner, K.-E.: Beitrag zur Tragfähigkeit von Kopfbolzendübeln in Verbundträgern mit Stahlprofilblechen. Der Stahlbau, B.56, H.2 , 1981, S.97-110
11. Roik, K.; Bürkner, K.-E.: Untersuchungen des Trägerverbundes unterverwendung von Stahlprofilblechen mit eine Höhe>80mm. Studiengesellschaft für Anwendungstechnik von Eisen und Stahl e.V., Projekt 40, Düsseldorf, 1980
12. Roik, K.; Lungershausen,H.: Verbundträger mit Stahlprofilblechen mit Rippen-höhe>80mm. Studiengesellschaft für Anweundungstechnik von Eisen und Stahl e.V. Projekt 99, Düsseldorf,1988
13. Bode, H.; Künzel, R.: Steifigkeit und Verformbarkeit von Vermitteln in Hochbau. International Symposium, Composite Steel Concrete Structures, Vol. I, Bratislava, 1987
14. Roik, K.; Hanswille, G.: Gutacten für die Holorib GmbH zur Frage der Tragfähigkeit von Kopfbolzendübeln bei auf dem Verbundträgerobergurt gestossenen Profilblechen. Bochum, Juli 1988

Flexural Behaviour of Two-Span Partially Continuous Prestressed Concrete Beam with External Tendons

Machida Atsuhiko
Professor
Saitama University
Saitama, Japan

Bamrungwong Chakree
Doctoral Student
Saitama University
Saitama, Japan

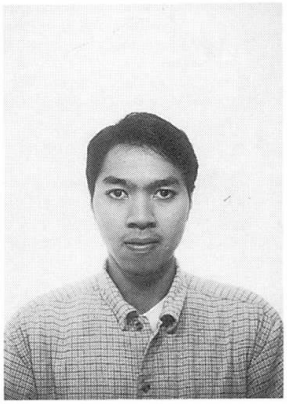

Machida Atsuhiko, Professor, received his B.Eng, M.Eng, and D.Eng degree from University of Tokyo, Japan.

Bamrungwong Chakree, received his B.Eng from SIIT, Thammasat University, Thailand, M.Eng(Civil Eng.) from Saitama University, Japan.

Summary

The objective of this study is mainly to experimentally and analytically investigate the flexural behaviour of the partially continuous PC beams to clarify the existing ambiguous characteristics. The flexural behaviour of two-span partially continuous PC beams is determined in comparison with single-span and two-span monolithically continuous PC beam having same internal prestressing force. The experimental results show that both monolithically and partially continuous PC beams have higher load carrying capacity than single-span PC beam. Nevertheless, compared to monolithically continuous PC beam, the load carrying capacity of all partially continuous PC beams is less, noting that the capacity is increased as the initial prestressing forces in external tendons become larger. Thereafter, a non-linear numerical analysis model is developed based on some basic assumptions to simulate the flexural behaviour of partially continuous PC beams. Satisfactory trends of flexural behaviour of partially continuous PC beams could be predicted by means of computer programming.

1. Introduction

As the existing highway bridges are getting older and higher load carrying capacity is necessary to serve an increasing transportation demand, the need of strengthening of these old bridges is initiated. In this paper the strengthening method for single-span prestressed concrete beams is described. The application of externally post-tensioned tendons is selected to build a continuity on two single-span PC beams owing to its less effort as well as cost effectiveness in construction. Besides, this method can also help improve the riding quality on the bridges, since single-span beams are connected to be continuous type. However, due to some encountered difficulties, for instance, member dependent characteristic of unbonded tendon stress and the rotation of the connection joint, so far, the flexural behaviour of single-span beams strengthened with using such a method is still not clearly understood. This research is, therefore, conducted so as to investigate the real flexural behaviour along with the analytical methodology for predicting the characteristic of strengthened beams. The comparative tests were conducted in order to observe the differences among behaviours of partially continuous, monolithically continuous, and single-span simply supported PC beam. Additionally, as it was expected that the magnitude of external prestressing force would affect the behaviour of partially continuous PC beam, the experimental program was, thus, set up for checking the influence of such a factor as well. In the analytical part, some basic assumptions, such as the beam theory, etc., were initially implemented to simulate the real flexural behaviours of partially continuous PC beams. Based on these assumptions, the flexural behaviour of the beams throughout loading steps until reaching the ultimate stage was analysed by means of computer programming. Lastly, the analytical predictions were brought into comparison with the data collected during conducting experiment and some discussions were then given in the view of load-displacement relationship and the characteristic of force in external tendon.

2. Experimental Methodology

Three partially continuous, one monolithically continuous, and one single-span PC beams having same T-shaped cross section were made in experiment as it was one of the major type of the existing beams. All beams have a similar sectional arrangement. However, for continuous specimens, at the centre support position the shape were altered to rectangular section. In preparation of the test specimens, six single-span PC beams were separately cast. After the main beams were internally prestressed with the force of magnitude equal to 250 kN, the reinforced concrete connection blocks between couples of single-span PC beams were then made. Finally, the coupled beams were firmly connected to each other with external tendons. The dimension of partially continuous PC specimens is shown in Fig.1. Within a group of partially continuous PC beams, the force introduced to external tendons were varied from 80, 160, and 210 kN for specimen number PCB1, PCB2, and PCB3, respectively. The test variables and materials used in making the specimens are given in Table 1. All beam specimens were then tested with two-point loading system of which loading span was set to be 1.3 m. During test, the forces and displacements were measured and collected through the data logger at every 5 kN loading step.

No.	Specimen Description	Reinforcements		Tendon Type	Tendon Force (kN)	Concrete Strength (MPa)
		Longitudinal Bars	Stirrups			
PCB1	Partially Continuous PC Beam I	2D13+2D6(top) 2D13(bottom)	D6@50 D6@90	2-SWPR7A 1-SWPR19	80(ext) 250(int)	31
PCB2	Partially Continuous PC Beam II				160(ext) 250(int)	36
PCB3	Partially Continuous PC Beam III				210(ext) 250(int)	32
MCB	Monolithically Continuous PC Beam			1-SWPR19	250(int)	35
SSB	Single Span PC Beam			1-SWPR19	250(int)	32

Table 1 Materials used and test variables

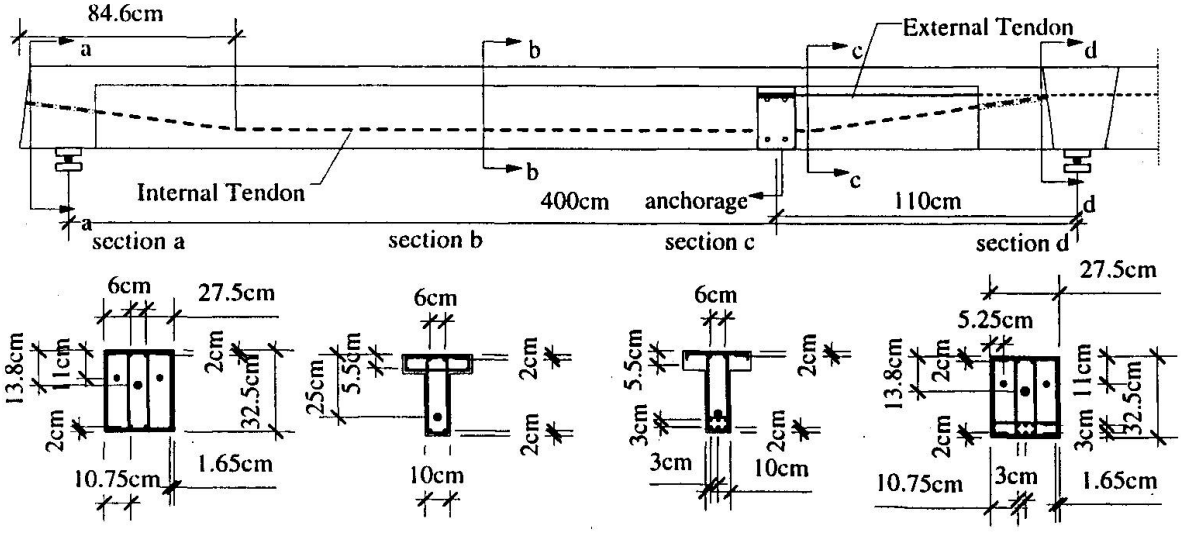

Fig.1 Detailed Design of Partially Continuous PC Beam(Connected Single-Span PC Beams)

3. Experimental Results and Discussions

Having experimentally investigated the flexural behaviour of single-span, monolithically, and partially continuous beams, the relationships between load and displacement at mid-span are plotted as in Fig.2, while the characteristic of force in external tendons of partially continuous PC beams are given in Fig.3. The crushing of concrete in compressive zone had, eventually, taken place at the mid-span section of the continuous beams, except for monolithically continuous case, where such a failure appeared simultaneously at mid-span as well as at centre support.

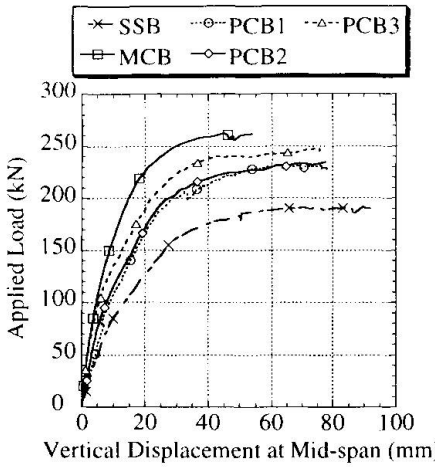

Fig.2 Load-Displacement

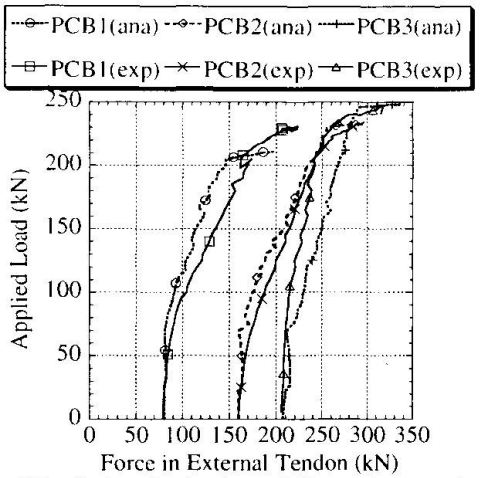

Fig.3 Analytical and Experimental Characteristic of Tendon Force

3.1 Load-Displacement Relationship of Partially Continuous PC Beams

From Fig.2, the relationship between applied load and the vertical displacement at mid-span of partially continuous PC beams, the conclusion could be drawn that specimen PCB3(with initial prestressing force equal to 210 kN) responded the load in stiffer manner than PCB2(with 160 kN prestress) and PCB1(with 80 kN prestress). The rate of change in applied load with respect to displacement response was varied from high to medium, and finally to low for all specimens. The first change in gradient of load-displacement curve could be noticed at the point where applied load was nearly equal to the cracking load of all specimens simultaneously with the opening of joint. That means after cracking the stiffness of beam had been lowered. After the load was further applied, a while later, it was found that the stiffness, again, began to decrease. At this loading stage, the strain in concrete at internal tendon level had been increased until reaching the values that was capable to yield the internal prestressed tendon which led to the yielding of the whole beam. Small increment of applied load caused large deflection to beam compared to a much smaller deflection generated by the same loading increment before tendon was yielded. Finally, from the investigation of load-displacement curves, notice was given that the ultimate strength of specimen PCB3 was higher than PCB2, and PCB1 showed the lowest ultimate load resisting capacity. It should also be noted that though the first crushing had already taken place, the beams still could withstand slightly increasing load in a very ductile manner. Conclusively, the resistance to applied load beyond the point where covering concrete reached its ultimate compressive strength (crushing of concrete in compressive zone), was due to the effect of confining reinforcements which were equally provided in all test specimens.

3.2 Behaviour of Force in External Tendons

The characteristics of forces in external tendons throughout the loading until the ultimate stage are as shown in Fig.3. From the plot, it is noticed that the differences in tendon forces between ultimate and initial stage for specimen PCB1, PCB2, and PCB3 are 142.2, 120.8, and 107.4 kN respectively. Considering these differences in tendon forces, it can be clearly seen that when the force applied initially into tendons is higher, the increment up to the ultimate stage are lower. From Fig.3, the forces in external tendons are, at first, slightly increased. Then at the point where the connection joint starts to open widely, the forces in tendons become progressively intensified. At the same load where internal tendon starts to yield, the forces in external tendons are sharply increased until arriving at ultimate stage.

3.3 Comparative Results on Flexural Behaviour of Partially Continuous PC Beams with Single-Span and Monolithically Continuous PC Beams

It is obvious that the monolithically continuous PC beam has the highest ultimate load carrying capacity followed by set of partially continuous PC beams, and single-span PC beam orderly. The percentage increase in ultimate strength, compared to single-span beam, of PCB1, PCB2, PCB3, and MCB are 21.6, 23.7, 28.9, and 37.4 percent, respectively. From Fig.2, load-

displacement relationships of PCB, MCB, and SSB, it can be deduced that monolithically continuous PC beam shows the stiffest behaviour in resisting load but the lowest ductility. The single-span PC beam behaves in the most ductile manner, however, the least load resisting capacity is provided by this beam. An intermediate behaviour between monolithically continuous and single-span PC beams can be obtained within the group of partially continuous PC beams. As magnitude of prestress in external tendons are increased, the behaviour of partially continuous PC beam will be rather like the monolithically continuous PC beam.

4. Analytical Methodology

Due to the unavailability of the accurate prediction methodology for the flexural behaviour of partially continuous PC beams, an analytical program was developed. The influences of secondary moment, member-dependency characteristics of stress in unbonded tendons, the effect of tendon eccentricity, and the joint rotation at the connection had been incorporated in the analytical procedure. Meanwhile, the non-linear material properties of concrete, steel and tendons were also taken into account to create a reliable model for predicting the flexural behaviour up to the ultimate stage, of partially continuous PC beams. The load-deformation characteristics, and change of stress in unbonded tendons were primarily simulated with the analytical models and later compared with the experimental results.

4.1 Basic Assumptions

A non-linear analysis model based on the fundamental assumptions used for flexural member, was adopted to establish the comprehensive analytical procedure. The assumptions imposed in the analytical model are given as follows,

1. Based on the beam theory, plane sections will remain plane after bending, thus the linear distribution of strain is assumed across the concrete section.
2. The increase of strain in external tendons is uniformly distributed along the entire length of tendon.
3. The deformation of concrete located at external tendon level plus amount of opening at the joint, is equal to the total elongation of the external tendon.
4. Concrete at the joint between main beam and connection block has no resistance to tensile force (dry joint).

4.2 Modelling of Partially Continuous PC Beams

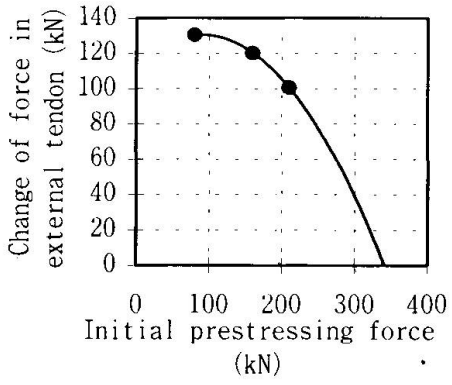

Fig.4 Relationship between Change in Tendon Force and Initial Prestress

Accordingly to the intermediate flexural behaviour of partially continuous PC beams observed in experiment, the model is presumably constructed in order to simulate the corresponding real characteristics. As the load is symmetrically applied on both spans, only left span is extracted out for analysis. At the centre support, unlike the monolithically continuous case, the boundary condition is assumed to be partially fixed, where, $M_{free\text{-}end} < M_{partailly\text{-}fixed} < M_{fixed\text{-}end}$. Along with this assumption, at centre support, the beam is also allowed to rotate to some degree. Since only a range of moment at partially fixed end is not adequate for analysing behaviour of the structure, a more specific value of moment is, therefore, assumed to be a function of fixed-end moment($M_{fixed\text{-}end}$) multiplied by one reduction factor called degree of continuity(D_{cont}). The degree of continuity is proposed as the ratio of initial prestressing force($Pps_{(initial)}$) to the ideal prestressing force($Pps_{(ideal)}$). The latter is presumably considered as the force that is sufficient to make no rotation at centre support, or the prestressing force which can make the flexural behaviour of partially continuous PC beam resemble to that of monolithically continuous one. Therefore,

$$M_{partially\text{-}fixed} = D_{cont}\, M_{fixed\text{-}end}$$

$$D_{cont} = Pps_{(initial)} / Pps_{(ideal)}$$

The change of force in external tendon is assumed to be a function of size of opening at connection joint. Thus if the partially continuous PC beam is prestressed with the ideal prestressing force, as assumed, the change of force in external tendon from initial to the ultimate stage should be approximately equal to zero. From the plot of experimental data in Fig.4, the ideal prestressing force is determined to be equal to 360 kN. After having defined the analytical model, the behaviour of partially continuous PC beam through loading steps until reaching the ultimate stage(crushing of concrete in compressive zone) is consecutively analysed by means of computer program developed in FORTRAN language. The main contents of the program are algorithmically explained in the following flowchart.

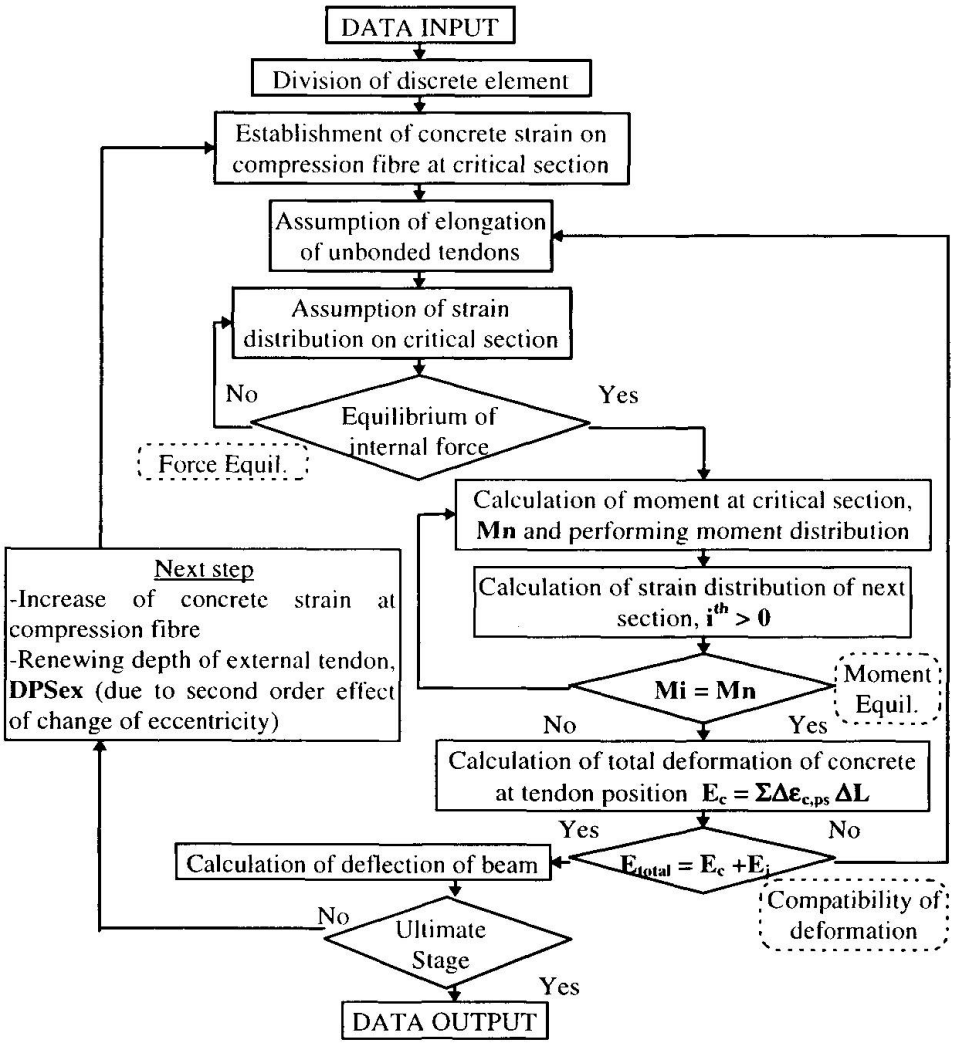

5 Comparison between Experimental Results and Analytical Predictions

To the flexural behaviour of partially continuous PC beams observed in the experiment, the analytical results which are based on some assumptions mentioned previously are compared, and discussed in the view of load-displacement characteristic along with the behaviour of forces in external tendons.

5.1 Load-Displacement Characteristics

From the comparative plots in Fig.5, conclusion can be drawn that, the analytical results show good agreement with the experimental ones up to a certain loading stage, which in all cases of partially continuous PC beams is the loading stage before the occurrence of joint opening. It is because before reaching such a loading stage, the beams still behave elastically. The assumptions used in defining the boundary conditions of partially continuous PC beams are correlatively

applicable. However, beyond the elastic stage, the whole beam looses its stiffness. Strain in external tendons is no longer only dependent on size of opening at joint but also on the deflection of beam. The calculation of moment at centre support is, therefore, not fully correct.

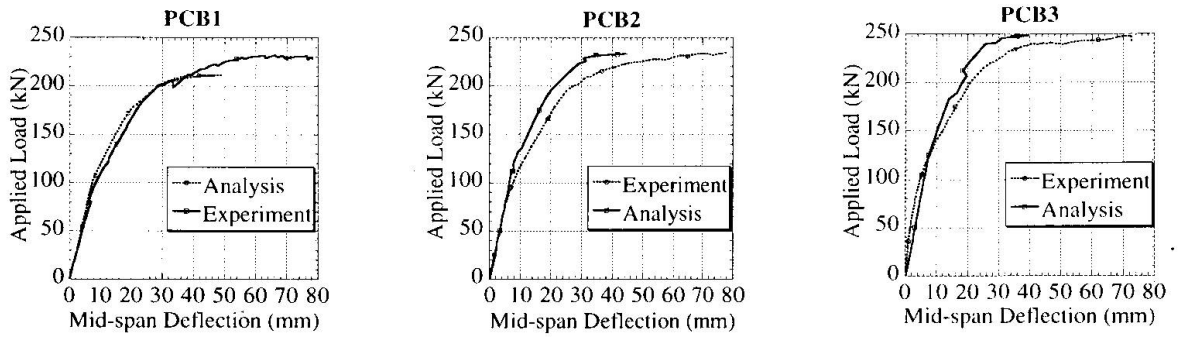

Fig.5 Comparison between Experimental and Analytical Load-Displacement Relationships

5.2 Behaviour of Force in External Tendons

It can be deduced from Fig.3 that, with using the developed program, the trend of change of forces in external tendon are almost correlated with those obtained from the tests. Within the elastic range, the analysed characteristics of force in external tendon show good agreement with the experimental results. Nevertheless, apart from this stage, the forces in external tendons are underestimated for specimen PCB1 and PCB2. But for specimen PCB3 the predicted force is overestimated. The largest errors produced in analysis compared to experimental data along this inelastic stage are 17.2, 7.3, and 11.1 percent in specimens PCB1, PCB2, and PCB2, respectively. The potential reason is also because of the deduction of the applicability of the assumption stating that the change of force in external tendon is a function of the opening size only.

6. Conclusion

Having carried out the experiments and developed the analytical methodology for predicting the flexural behaviour of partially continuous PC beams, the following conclusions could be drawn from the results of this experimental and analytical investigation :

1. As can be observed in experiment, partially continuous PC beams have an intermediate flexural behaviour between those of monolithically continuous and single-span simply supported PC beam.
2. The more intensively the external tendons are prestressed, the more the flexural behaviour of partially continuous PC beam will become closed to that of monolithically continuous PC beam.
3. The degree of continuity (D_{cont}) can be used to determine the specific value of moment at centre support in analysis with a fairly good agreement especially within elastic range.
4. The analytical program is applicable only to this specific type of partially continuous PC beams, since the degree of continuity is derived based on this particular set of experimental results.

References

[1] Songkiat M., "Flexural Behaviour of Externally Prestressed Concrete Beams", D.Eng. Dissertation, 1995, Saitama University, Saitama, Japan
[2] R.J.G. MacGregor, M.E. Kreger, and J.E. Breen, "Strength and Ductility of a Three-Span Externally Post-Tensioned Segmental Box Girder Bridge Model", External Prestressing in Bridges, ACI, sp120-15
[3] Chakree B., "Flexural Behaviour of Two-Span Partially Continuous Prestressed Concrete Beams with External Tendons", Master Thesis, 1998, Saitama University, Saitama, Japan

Performance of Plain Concrete Columns Bonded with Glass Fiber Wraps

Kiang-Hwee TAN
Associate Professor
National University of Singapore
Kent Ridge, Singapore

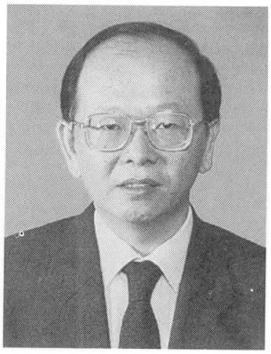

Kiang-Hwee Tan, born 1955, received his doctorate degree in civil engineering from the University of Tokyo in 1985. His research interests include external prestressing and fibre-reinforced polymer (FRP) reinforcement.

Qingqing Shen
Research Engineer
National University of Singapore
Kent Ridge, Singapore

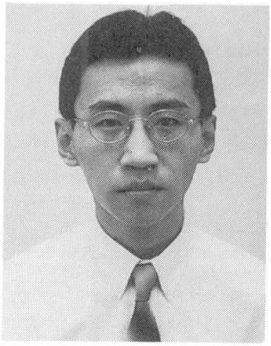

Qingqing Shen, born 1967, received his civil engineering degree from Tongji University, PRC, in 1989.

Summary

A test program was carried out to examine the effect of bonding unidirectional glass fiber wraps on the strength and ductility of circular and square plain concrete columns. Twenty-four specimens, bonded with up to three plies of the material in orientations varying from 0 to 90 degrees to the specimen axis, were tested to failure. The corners of the square columns were not rounded off intentionally. Test results indicated that both the strength and ductility of the columns increased with increasing plies of wraps with the same fiber orientation. For circular columns, bonding the wraps with the fibers orientated at 90 degrees to the specimen axis led to higher strength than when they were orientated otherwise. For square columns, placing the wraps with fibers orientated at between 30 to 45 degrees to the specimen axis resulted in comparable axial strength but considerably higher ductility than when the fibers were at 0 and 90 degrees.

1. Introduction

Fiber-reinforced polymer (FRP) materials utilizing high-performance fibers such as carbon, aramid and glass, are increasingly being used to strengthen and confine concrete columns due to their low unit weight, easy handling and low maintenance costs. They are also preferred over other strengthening methods using steel plates and enlarged sections, as they do not lead to significant change in the size of the member that is being strengthened.

Several studies had been carried out on the use of FRP composites in the repair and strengthening of concrete columns (Ramirez, 1996; Saadatmanesh, et al., 1994; Hosotani, et al., 1997; Tan and

Shen, 1997). They have so far demonstrated the potential of bonded external FRP sheets or wraps in improving both the compressive strength and ductility of the repaired columns by strengthening the potential plastic hinge regions or the entire height of the columns. However, most of the studies dealt with circular columns only and the behavior of square concrete columns bonded with external FRP composites have not been investigated adequately. Furthermore, the effect of varying the fiber orientation in both circular and square columns has not been examined.

The purpose of this study is to examine the effect of bonding unidirectional glass fiber wraps on the strength and ductility of circular and square plain concrete columns. Twenty-four plain concrete columns, bonded externally with up to three plies of glass fiber wraps at orientation varying from 0 to 90 degrees to the specimen axis, were tested to failure under uniaxial compression. The effects of fiber orientation on the compressive stress-strain response and failure characteristics of the strengthened column specimens are discussed.

2. Test Program

Two series of column specimens, consisting of twelve circular and twelve square plain concrete columns respectively, were prepared. The circular specimens measured 150-mm in diameter and 600-mm in height while the square ones measured 100-mm by 100-mm in cross-section and 500-mm in height. The specimens were designated as CO-ab and SO-ab for circular and square columns respectively. Symbol "a" indicates the number of plies of glass fiber wraps and "b" represents the angle at which the fibers of the wraps were orientated to the longitudinal axis of the specimen, with H, D, X and V indicating orientations at 90, 45, 30 and 0 degrees, respectively. For specimens bonded with two wraps, the second layer was wrapped symmetrically with respect to the first layer. For specimens bonded with three wraps, the interior two wraps were the same as those with two wraps, and the exterior third wrap was bonded with fibers orientated horizontally.

The concrete mix proportion was 1:2:4 by weight of cement, sand and aggregates of 10-mm nominal size, with a water-to-cement ratio of 0.62. The average cylinder and cube compressive strengths of concrete at the time of testing were 28 MPa and 35 MPa respectively. Circular specimens were cast in paperboard molds while square ones in steel molds. All specimens were de-molded one day after casting and moist-cured for the next three days.

About one month after casting, the specimens were bonded with glass fiber wraps with a two-part epoxy using manual placement procedure. The glass fiber wrap measured 1.27-mm in thickness, with an average tensile strength of 450 MPa and an average modulus of elasticity of 22460 MPa, according to the supplier's data. For square columns, the corners were not rounded off intentionally. The bonded glass fiber wraps were cured at room temperature for several days.

Columns CO-0 and SO-0 were not wrapped and served as reference columns. For each column, four strain gauges, equally spaced along the perimeter at the mid-height section, were placed in the longitudinal direction on the surface of the bonded glass fiber wrap. To avoid bursting of the end sections and ensure that failure occurred at the middle portion, the columns were strengthened with one or two steel straps at each end. All circular specimens were tested on a 2000 kN capacity compression-testing machine while all square ones on a 1000 kN capacity machine.

3. Test Results and Discussion

3.1 Failure characteristics

The specimens failed by crushing of concrete, accompanied by bulging of the section and de-bonding of the fiber wraps. For circular specimens, the glass fiber wraps that were orientated

horizontally generally ruptured at failure, while those fiber wraps that were orientated diagonally or vertically were sheared through along the fiber direction.

For square specimens, tearing of the wraps occurred along corners of the columns in which the wraps were placed with fibers orientated vertically, and along the fiber direction on the side face of SO-2X. Rupture of fibers was observed generally in specimens with a horizontal wrap and in specimen SO-2D.

3.2 Compressive stress-strain response

The compressive stress-strain curves of the circular and square columns are compared in Figs.1 and 2, respectively. It is observed that all the curves are characterized by three portions: an initial linear elastic portion up to the proportional limit, followed by a non-linear portion with gradually decreasing slope and a final descending portion. Before the proportional limit, the curves are almost identical, indicating that there was little effect due to the external glass fiber wraps. Both the ultimate axial strength and ductility of the columns, however, increased with an increase in the plies of glass fiber wraps.

For circular columns, Fig. 1 indicates that for the same amount of fiber wraps, specimens bonded with the fibers orientated at 90 degrees to the specimen axis (that is, horizontally) exhibited a significantly higher compressive strength than when they were orientated otherwise. For square columns, however, Fig. 2 shows that the ultimate compressive strength is almost the same, regardless of the angle of orientation of fibers. In addition, specimens bonded with the fibers orientated at between 30 to 45 degrees to the specimen axis had a considerably longer descending branch, indicating a more ductile form of failure.

3.3 Effect of fibre orientation on compressive strength

The ultimate compressive strength of the glass fiber wrapped specimens expressed as a ratio of that of the reference column are summarized in Figs. 3(a) and (b) for circular and square columns, respectively. It can be noted that the ultimate compressive strength of the specimens increased with increasing plies of bonded glass fiber wraps with the same fiber orientation.

For circular columns, the strengthening effect is more noticeable for specimens CO-1H, CO-2H and CO-3H. Their compressive strengths are respectively 1.47, 2.04 and 2.94 times that of the reference column CO-0. Although specimens CO-1D and CO-1V were bonded with one ply of glass fiber wrap as in specimen CO-1H, their strengths were relatively less and were about 0.74 and 1.03 times respectively of the strength of the reference column. Similarly, the compressive strengths of specimens CO-2D, CO-2X and CO-2V were also less than that of specimen CO-2H, and varied from 1.17 to 1.35 times that of the reference specimen CO-0. For specimens CO-3D, CO-3X and CO-3V, the compressive strengths were between 1.89 to 1.94 times that of CO-0.

In the case of square columns, the increase in compressive strength of specimens bonded with the same plies of glass fiber wraps did not differ much, even though the fiber orientation varied from 0 to 90 degrees. The compressive strengths ranged from 1.37 to 1.40, 1.37 to 1.67 and 1.71 to 1.81 times that of the reference specimen SO-0 for specimens bonded with one, two and three piles of glass fiber wraps respectively.

3.4 Effect of fibre orientation on strain at peak compressive strength

The compressive strains at which the peak compressive stresses were attained, expressed as ratios of that of the reference column, are shown in Figs. 4(a) and (b) respectively, for circular and square columns. These strains were found to increase with the plies of fiber wraps. For circular columns, it is noted from Fig. 4(a) that the strain at peak compressive strength increased with increasing angle of fiber orientation, for the same ply of wraps. However, for square columns, the peak compressive stress occurred at almost the same longitudinal strain for the same ply of wraps.

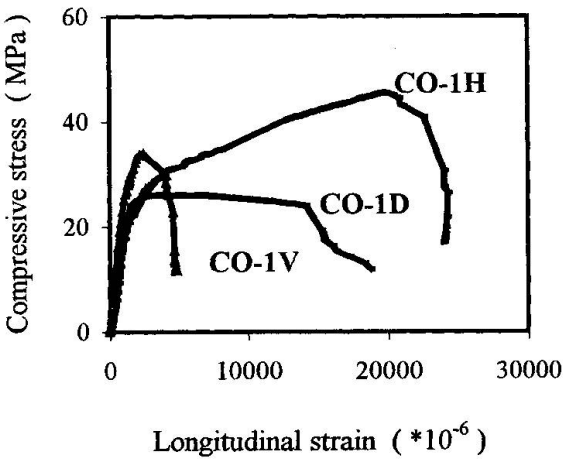

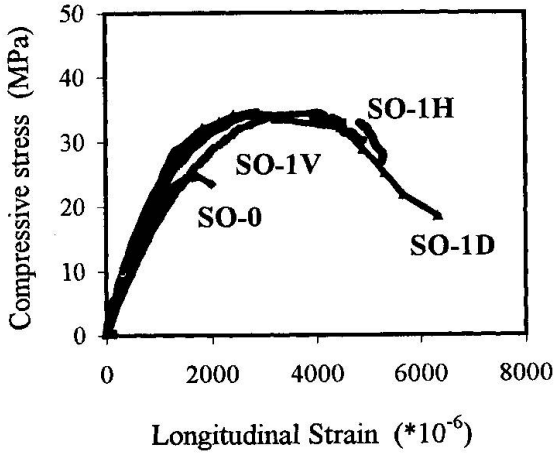

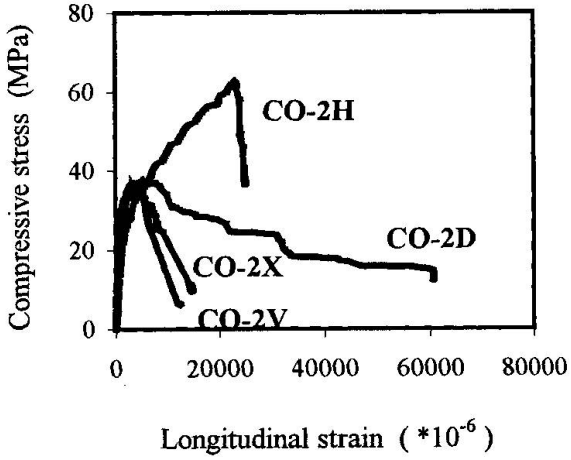

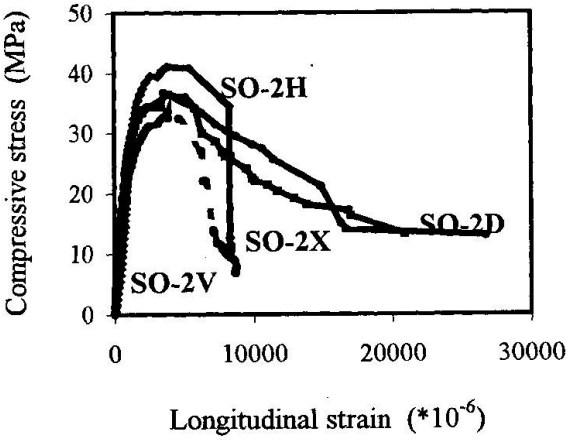

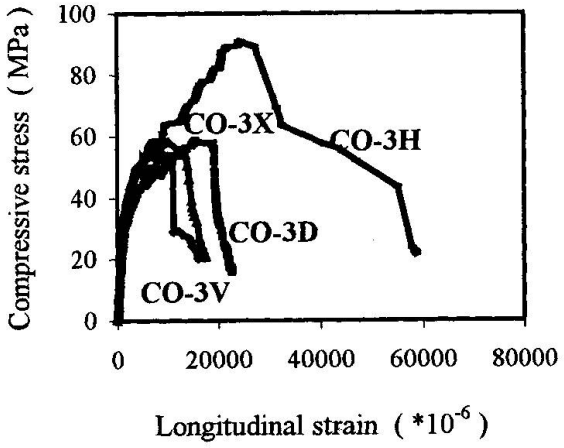

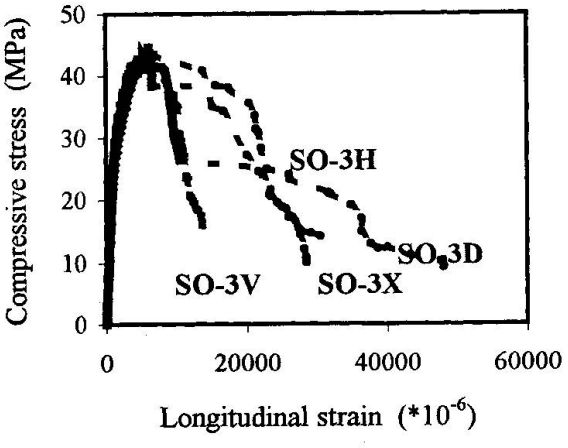

Fig. 1 Compressive stress-strain curves for circular columns

Fig. 2 Compressive stress-strain curves for square columns

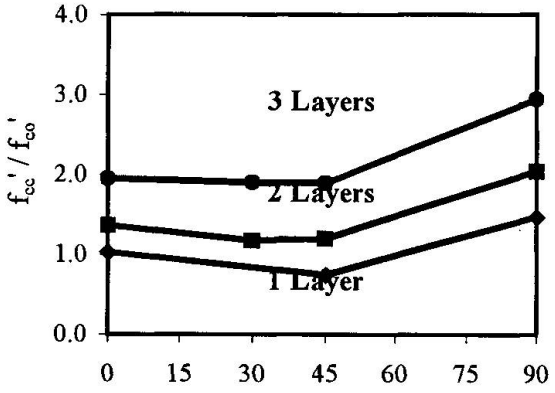

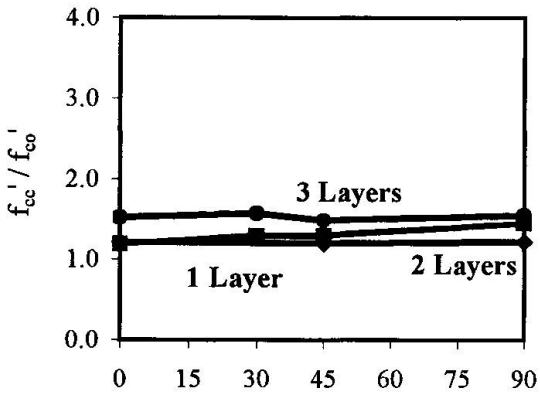

(a) Circular columns *(b) Square columns*

Fig. 3 Effect of fibre orientation on compressive strength

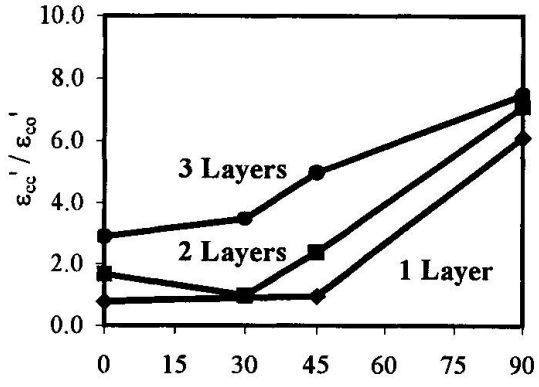

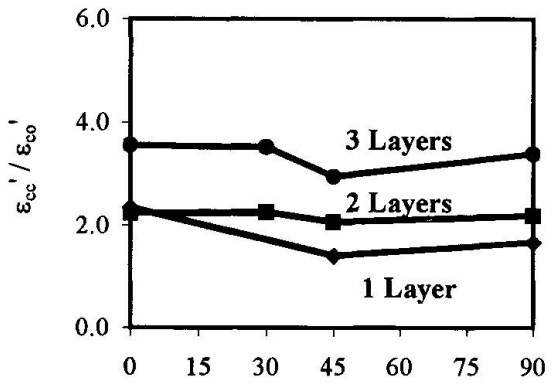

(a) Circular columns *(b) Square columns*

Fig. 4 Effect of fibre orientation on strain at peak compressive stress

3.5 Implications for effective application of glass fiber wraps

The above results indicated that to maximize the effectiveness of glass fiber wraps in confining and strengthening columns, the wraps should be bonded with fibers orientated at 90 degrees to the member axis (that is, horizontally) for circular columns. In the case of square columns, the fiber wraps may be placed with fibers at between 30 to 45 degrees to the member axis to achieve the confinement and strengthening effects without having to round off the corners of the columns. Where the fiber wraps are placed horizontally, the corners of the square columns should be rounded off so as to avert stress concentration and hence rupture of the fibers at failure.

4. Conclusions

The experimental study on circular and square plain concrete columns bonded with external glass fiber composite wraps indicates that as a result of the confinement provided by the external wraps, the concrete columns will have a higher load-carrying capacity and fail at a larger strain than if they were unconfined. Depending on the degree of confinement, significant increase in strength and ductility can be achieved.

It was further concluded that in general, increasing the plies of bonded glass fiber wraps with the same fiber orientation led to an increase in ultimate axial compressive strength and ductility for both circular and square sections. With the same piles of external glass fiber wraps, test results showed that for circular columns, bonding the fiber wraps with the fibers orientated at 90 degrees to the member axis leads to higher strength than when they were orientated otherwise. For square columns, placing the wraps with fibers orientated at between 30 to 45 degrees to the specimen axis resulted in comparable axial strength but considerably higher ductility than when the fibers were orientated at 0 or 90 degrees. Therefore, to maximize the effectiveness of the material, it is suggested that the fibers should be orientated horizontally for circular columns and at between 30 to 45 degrees to the member axis for square columns.

Acknowledgment

This study forms part of a research project funded by The National University of Singapore under Research Grant No. RP950683. The support is gratefully acknowledged.

References

1. Hosotani, M., Kawashima, K. and Hoshikuma, J. (1997). "A Study on Confinement Effect of Concrete Cylinders by Carbon Fiber Sheets." Non-Metallic (FRP) Reinforcement for Concrete Structures, *Proceedings of the Third International Symposium*, Sapporo, Japan, October 14-16, Vol. 1, pp. 209-216.
2. Ramirez, J.L. (1996). "Ten Concrete Column Repair Methods." *Construction and Building Materials*, Vol. 10, No. 3, pp. 195-202.
3. Saadatmanesh, H., Ehsani, M.R. and Li, M.W. (1994). "Strength and Ductility of Concrete Columns Externally Reinforced with Fiber Composite Straps." ACI *Structural Journal*, Vol. 91, No. 4, July-August, pp. 434-447.
4. Tan, K.H. and Shen, Q.Q. (1997). "Strengthening and Stiffening of Circular RC Columns with Glass Fibre Straps." *Fifth International Conference on Structural Failure, Durability and Retrofitting*, Singapore, November 27-28, pp. 396-401.